

ปริมาณรังสีที่ผู้ป่วยได้รับจากการตรวจเอกซเรย์คอมพิวเตอร์หลอดเลือดและการตรวจเอกซเรย์  
หลอดเลือดของสมอง



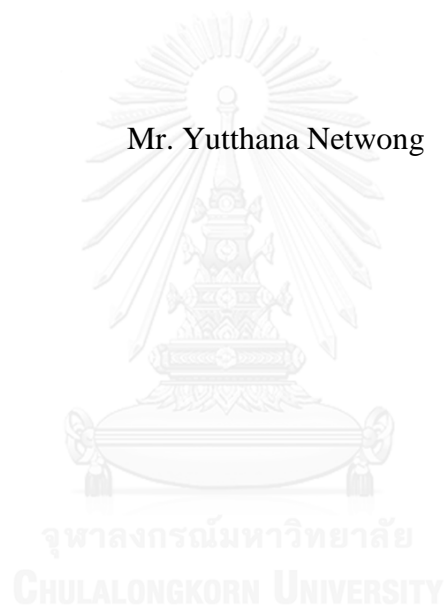
บทคัดย่อและแฟ้มข้อมูลฉบับเต็มของวิทยานิพนธ์ตั้งแต่ปีการศึกษา 2554 ที่ให้บริการในคลังปัญญาจุฬาฯ (CUIR)  
เป็นแฟ้มข้อมูลของนิสิตเจ้าของวิทยานิพนธ์ ที่ส่งผ่านทางบัณฑิตวิทยาลัย

The abstract and full text of theses from the academic year 2011 in Chulalongkorn University Intellectual Repository (CUIR)  
are the thesis authors' files submitted through the University Graduate School.

วิทยานิพนธ์นี้เป็นส่วนหนึ่งของการศึกษาตามหลักสูตรปริญญาวิทยาศาสตรมหาบัณฑิต  
สาขาวิชาอายุเวชศาสตร์ ภาควิชารังสีวิทยา  
คณะแพทยศาสตร์ จุฬาลงกรณ์มหาวิทยาลัย  
ปีการศึกษา 2558  
ลิขสิทธิ์ของจุฬาลงกรณ์มหาวิทยาลัย

PATIENT RADIATION DOSE FROM COMPUTED TOMOGRAPHY  
ANGIOGRAPHY AND DIGITAL SUBTRACTION ANGIOGRAPHY  
OF THE BRAIN

Mr. Yutthana Netwong



A Thesis Submitted in Partial Fulfillment of the Requirements  
for the Degree of Master of Science Program in Medical Imaging  
Department of Radiology  
Faculty of Medicine  
Chulalongkorn University  
Academic Year 2015  
Copyright of Chulalongkorn University



ยุทธนา เนตรวงศ์ : ปริมาณรังสีที่ผู้ป่วยได้รับจากการตรวจเอกซเรย์คอมพิวเตอร์หลอดเลือดและการตรวจเอกซเรย์หลอดเลือดของสมอง (PATIENT RADIATION DOSE FROM COMPUTED TOMOGRAPHY ANGIOGRAPHY AND DIGITAL SUBTRACTION ANGIOGRAPHY OF THE BRAIN) อ.ที่ปรึกษาวิทยานิพนธ์หลัก: รศ. ดร.อัญชลี กฤษณจินดา, 125 หน้า.

การตรวจเอกซเรย์คอมพิวเตอร์หลอดเลือดและการตรวจเอกซเรย์ระบบฟลูออโรสโคปี หลอดเลือดเป็นวิธีการตรวจหาความผิดปกติของหลอดเลือดสมองโดยที่คุณภาพของภาพสำหรับการวินิจฉัยโรคจากทั้งสองวิธีนี้มีความใกล้เคียงกัน แต่จากการศึกษาในหุ่นจำลองพบว่าปริมาณรังสีซึ่งผลจากการตรวจหลอดเลือดสมองด้วยเอกซเรย์คอมพิวเตอร์จะต่ำกว่าการตรวจเอกซเรย์ระบบฟลูออโรสโคปี หลอดเลือดถึง 1 ใน 5 การศึกษานี้มีวัตถุประสงค์เพื่อหาค่าปริมาณรังสีซึ่งผลในผู้ป่วยที่ได้รับการตรวจด้วยเอกซเรย์คอมพิวเตอร์หลอดเลือดและการตรวจเอกซเรย์ระบบฟลูออโรสโคปี หลอดเลือดของสมอง

ในการศึกษานี้ ปริมาณรังสีซึ่งผลจากการตรวจเอกซเรย์คอมพิวเตอร์หลอดเลือดสมองคำนวณโดยใช้ค่า DLP จากเครื่องเอกซเรย์คอมพิวเตอร์คูณกับค่า k-factor 0.0019 มิลลิซีเวิร์ตต่อมิลลิเกรย์เซ็นติเมตร ในผู้ป่วย 30 ราย เป็นผู้ป่วยชาย 15 ราย และ ผู้ป่วยหญิง 15 ราย มีอายุตั้งแต่ 23 – 89 ปี อายุเฉลี่ย 49 ปี คำนีมวลกายเฉลี่ย 24 กิโลกรัมต่อตารางเมตร และปริมาณรังสีซึ่งผลจากการตรวจด้วยเอกซเรย์หลอดเลือดของสมองคำนวณโดยใช้ค่า DAP ที่ได้จากเครื่องเอกซเรย์ระบบฟลูออโรสโคปี คูณกับค่า dose conversion coefficient 0.087 มิลลิซีเวิร์ตต่อมิลลิเกรย์ตารางเซ็นติเมตร โดยประเมินจากผู้ป่วย 30 ราย เป็นผู้ป่วยชาย 14 ราย และ ผู้ป่วยหญิง 16 ราย มีอายุตั้งแต่ 24 – 81 ปี อายุเฉลี่ย 47 ปี คำนีมวลกายเฉลี่ย 23 กิโลกรัมต่อตารางเมตร

ผลการศึกษาพบว่าปริมาณรังสีซึ่งผลจากผู้ป่วยที่ได้รับการตรวจเอกซเรย์คอมพิวเตอร์หลอดเลือดสมอง มีค่าตั้งแต่ 2.82 – 5.19 มิลลิซีเวิร์ต ค่าเฉลี่ย 3.70 มิลลิซีเวิร์ต โดยปัจจัยที่มีผลต่อปริมาณรังสีซึ่งผลในผู้ป่วยประกอบด้วย ลักษณะเฉพาะของผู้ป่วย ได้แก่ น้ำหนัก ส่วนสูง และคำนีมวลกาย และค่าพารามิเตอร์ในการเอกซเรย์ ได้แก่ ค่ากระแสหลอด-เวลา (มิลลิแอมแปร์-วินาที) ความต่างศักย์หลอด (กิโลโวลต์) และ ระยะเวลาของการแสกน ค่าความหนาสไลด์ระยะทางที่เตียงเคลื่อนที่ต่อหลอดเอกซเรย์หมุนหนึ่งรอบและเวลาที่หลอดเอกซเรย์หมุนคงที่หนึ่งรอบ

ในการตรวจหลอดเลือดสมองด้วยเครื่องเอกซเรย์ระบบฟลูออโรสโคปี พบว่า ปริมาณรังสีซึ่งผลมีค่าตั้งแต่ 3.30 - 10.06 มิลลิซีเวิร์ตค่าเฉลี่ย 5.94 มิลลิซีเวิร์ต สูงกว่าการตรวจด้วยเอกซเรย์คอมพิวเตอร์ 1.5 เท่า โดยปัจจัยหลักที่มีผลต่อปริมาณรังสี คือ การถ่ายภาพรังสีระบบ 2 มิติ และ 3 มิติ อีกทั้งการเพิ่มขึ้นของจำนวนหลอดเลือดสมองที่ทำการตรวจและระยะเวลาของการฟลูออโรสโคปี ก็มีผลต่อปริมาณรังสีซึ่งผล แต่ในการศึกษานี้พบว่าลักษณะเฉพาะของผู้ป่วยและประสบการณ์ของรังสีแพทย์ไม่มีความสัมพันธ์กับปริมาณรังสีที่ผู้ป่วยได้รับ

ภาควิชา รังสีวิทยา

ลายมือชื่อนิติต .....

สาขาวิชา ฉายาเวชศาสตร์

ลายมือชื่อ อ.ที่ปรึกษาหลัก .....

ปีการศึกษา 2558

# # 5774071830 : MAJOR MEDICAL IMAGING

KEYWORDS: CEREBROVASCULAR EXAMINATION / EFFECTIVE DOSE / COMPUTED TOMOGRAPHY ANGIOGRAPHY (CTA) / DIGITAL SUBTRACTION ANGIOGRAPHY (DSA)

YUTTHANA NETWONG: PATIENT RADIATION DOSE FROM COMPUTED TOMOGRAPHY ANGIOGRAPHY AND DIGITAL SUBTRACTION ANGIOGRAPHY OF THE BRAIN. ADVISOR: ASSOC. PROF. ANCHALI KRISANACHINDA, Ph.D., 125 pp.

Computed Tomography Angiography (CTA) and Digital Subtraction Angiography (DSA) are the types of cerebrovascular disorders examination. The 64-row multidetector CTA (64-MDCTA) provides vascular image quality of the brain similar to the DSA, but the effective dose of CTA is 1/5 lower than DSA studied in phantom. The purpose of this study was to evaluate patient effective dose from 64-MDCTA and DSA examination.

In this study, the effective dose according to ICRP 103 received by 30 patients (15 male, 15 female, mean age 49 yrs, range 23-89 yrs, mean BMI 24 kg/m<sup>2</sup>) underwent CTA examination of the brain were determined by the Dose Length Product (DLP) values in the unit of mGy.cm from a 64-row MDCT (Somatom Definition AS; Siemens, Erlangen, Germany) multiplied by the k-factor of 0.0019 mSv/mGy.cm. The effective dose from 30 patients (14 male and 16 female, mean age 47 yrs, range 24-81 yrs, mean BMI 23 kg/m<sup>2</sup>) from diagnostic cerebral DSA procedure calculated by using Dose Area Product (DAP) values displayed from DAP meter attached in a biplane angiography equipment (Axiom Artis; Siemens, Erlangen, Germany) multiplied by dose conversion coefficient of 0.087 mSv/mGy.cm<sup>2</sup>.

For CTA, the mean effective dose was 3.70 (2.82- 5.19) mSv. The effective dose of CTA depends on patient characteristics (weight, height, and BMI), exposure technique (mAs and kVp) and scan length when fixing other parameters (slice collimation, slice acquisition, pitch, and tube rotation time).

In DSA procedure, the mean effective dose was 5.94 (3.30-10.06) mSv. A number of 2D radiography and a number of 3-Dimensional rotational angiography were the key factors affecting the effective dose. The number of vessels selective catheterization and fluoroscopic time were moderate affects the effective dose. The experience of radiologist was no significant correlation with the effective dose.

The mean effective dose from DSA procedure was 1.5 time of CTA examination of the brain.

Department: Radiology  
Field of Study: Medical Imaging  
Academic Year: 2015

Student's Signature .....

Advisor's Signature .....

## ACKNOWLEDGEMENTS

I would like to express thankfulness and deepest appreciation to Associate Professor Anchali Krisanachinda, Ph.D., Division of Nuclear Medicine, Department of Radiology, Faculty of Medicine, Chulalongkorn University, my advisor for her helpful, suggestion, supervision, guidance, constructive direction and polishing of the thesis writing to improve the English expression.

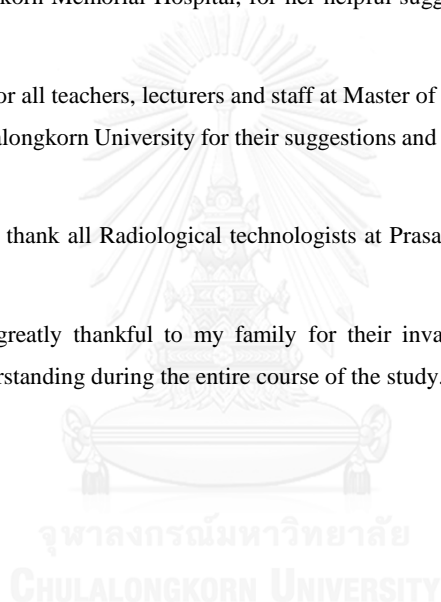
I would like to thank Professor Franco Milano, University of Florence Italy, who is the external examiner of the thesis defense for his constructive comments, recommendation and teaching of knowledge in Medical Imaging.

I would like to deeply thank Ms. Petcharleeya Suwanpradit, Department of Radiology, Faculty of Medicine, King Chulalongkorn Memorial Hospital, for her helpful suggestion and contribution in equipment QC part in this research.

I am thankful for all teachers, lecturers and staff at Master of Science Program in Medical Imaging, Faculty of Medicine, Chulalongkorn University for their suggestions and teaching knowledge during the course of Medical Imaging.

I would like to thank all Radiological technologists at Prasat Neurological Institute for their kind supports.

Finally, I am greatly thankful to my family for their invaluable encouragement, entirely care, financial support and understanding during the entire course of the study.



## CONTENTS

	Page
THAI ABSTRACT .....	iv
ENGLISH ABSTRACT.....	v
ACKNOWLEDGEMENTS .....	vi
CONTENTS.....	vii
LIST OF TABLES .....	xi
LIST OF FIGURES .....	xiii
LIST OF ABBREVIATIONS.....	xv
CHAPTER I.....	1
INTRODUCTION .....	1
1.1 Background and rationale .....	1
1.2 Research objective .....	3
CHAPTER II.....	4
REVIEW OF RELATED LITERATURE .....	4
2.1 Theory.....	4
2.2 Review of Related Literature .....	18
CHAPTER III .....	22
RESEARCH METHODOLOGY.....	22
3.1 Research design .....	22
3.2 Research design model .....	22
3.3 Conceptual framework.....	23
3.4 Research question .....	24
3.5 Sample .....	24
3.5.1 Target population .....	24
3.5.2 Sample population.....	24
3.5.3 Eligible criteria .....	24
3.5.3.1 Inclusion criteria.....	24
3.5.3.2 Exclusion criteria.....	24
3.5.4 Sample size determination.....	28

	Page
3.6 Materials .....	28
3.6.1 Research Equipment.....	28
3.6.1.1 CT scanner.....	28
3.6.1.2 DSA system.....	29
3.6.2 Quality Control materials .....	29
3.6.2.1 PMMA Phantom.....	29
3.6.2.2 Catphan® 600 phantom.....	30
3.6.2.3 Copper sheets .....	31
3.6.2.4 Unfors Ray Safe Xi Pencil ionization chamber, 10 cm active length .....	31
3.6.2.5 UnforsRaySafe Xi R/F dosimeter.....	32
3.7 Methods .....	33
3.7.1 Perform the quality control of Siemens Somatom Definition AS 64- MDCT .....	33
3.7.2 Verification of CTDI <sub>vol</sub> and DLP.....	33
3.7.3 Perform the quality control of Siemens Axiom Artis Biplane Flat panel detector .....	34
3.7.4 Data Collection.....	34
3.7.4.1 Patient selection.....	34
3.7.4.2 Data recording .....	34
3.7.5 Effective dose calculation .....	34
3.8 Variables measurement.....	35
3.9 Statistical analysis.....	35
3.10 Data analysis .....	36
3.11 Outcomes .....	36
3.12 Expected benefits.....	36
3.13 Ethical consideration .....	36
CHAPTER IV .....	37
RESULT .....	37



	Page
4.1 Quality control of the CT scanner: Siemens Somatom Definition AS .....	37
4.2 Quality control of the DSA equipment: Siemens Axiom Artis .....	37
4.3 Patient data and radiation dose calculation from CTA examination .....	37
4.3.1 Patient characteristics of CTA examination and effective dose .....	37
4.3.2 The correlation between effective dose and patient characteristics of CTA examination .....	39
4.3.3 Scanning parameters of CTA examination and effective dose .....	40
4.3.4 The correlation between effective dose and scanning parameters of CTA examination .....	42
4.4 Patient radiation dose from DSA examination .....	44
4.4.1 Patient characteristics and effective dose .....	44
4.4.2 The correlation between effective dose and patient characteristics of DSA examination .....	46
4.4.3 The acquisition parameters of DSA examination and effective dose .....	48
4.4.4 The correlation between effective dose and acquisition parameters of DSA examination .....	49
4.5 Comparison of the effective dose from CTA and DSA examination .....	52
CHAPTER V .....	58
DISCUSSION AND CONCLUSION .....	58
5.1 Discussion .....	58
5.1.1 Patient effective dose from CTA of the brain .....	58
5.1.2 Factors affecting the effective dose of CTA examination .....	62
5.1.2.1 Patient characteristics .....	62
5.1.2.2 Scanning parameters .....	63
5.1.3 Patient effective dose from cerebral DSA examination .....	63
5.1.4 Factors affecting the effective dose of DSA examination .....	65
5.1.4.1 Patient characteristics .....	65
5.1.4.2 Imaging parameters .....	65
5.2 Conclusion .....	67

	Page
5.2.1 Patient radiation dose from CTA examination .....	67
5.2.2 Patient radiation dose from DSA procedure.....	67
REFERENCES .....	69
Appendix A: Case Record Form.....	75
Case record form: CTA .....	75
Case record form: DSA .....	76
Appendix B: Quality Control of research equipment .....	77
Equipment performance for CT system.....	77
VITA.....	125



## LIST OF TABLES

<b>Table 3. 1</b> Routine CTA examination parameters 1. ....	25
<b>Table 3. 2</b> Routine CTA examination parameters 2. ....	26
<b>Table 3. 3</b> Parameters of DSA examination. ....	27
<b>Table 3. 4</b> Characteristics of Unfors model Xi platinum dosimeter. ....	32
<b>Table 4. 1</b> Patient characteristics of 30 cases from CTA examination. ....	38
<b>Table 4. 2</b> Patient characteristics from CTA examination. ....	39
<b>Table 4. 3</b> The correlations between effective dose and patient characteristics of CTA examination. ....	39
<b>Table 4. 4</b> Scanning parameters, DLP and effective dose from CTA of 30 patients. ....	41
<b>Table 4. 5</b> Scanning parameters from CTA examination. ....	42
<b>Table 4. 6</b> The correlations between effective dose and scanning parameters of CTA examination. ....	42
<b>Table 4. 7</b> Patient characteristics and effective dose from DSA examination in 30 patients. ....	45
<b>Table 4. 8</b> Patient characteristics from DSA examination. ....	46
<b>Table 4. 9</b> The correlations between effective dose and patient characteristics of DSA examination. ....	46
<b>Table 4. 10</b> The acquisition parameters and effective dose from DSA of 30 patients. ....	48
<b>Table 4. 11</b> The acquisition parameters of DSA examination (Factors affecting the effective dose). ....	49
<b>Table 4. 12</b> The correlation between effective dose and acquisition parameters of DSA examination. ....	49
<b>Table 4. 13</b> Effective dose and patient characteristics for CTA and DSA. ....	52
<b>Table 4. 14</b> The range of effective dose for CTA and DSA examination. ....	53
<b>Table 4. 15</b> The statistical profiles of CTA examination. ....	55
<b>Table 4. 16</b> The statistical profiles of DSA examination. ....	56

<b>Table 5. 1</b> Effective dose of CTA procedures compared with other studies....	59
<b>Table 5. 2</b> Parameters setting between our study and previous studies.....	61
<b>Table 5. 3</b> DLP to effective dose conversion factor (k-factor) for CT brain in adult .....	62
<b>Table 5. 4</b> Effective dose of DSA procedure compare with other studies.....	64



## LIST OF FIGURES

<b>Figure 2. 1</b> Four scanner generations were promoted in the 1970s.....	5
<b>Figure 2. 2</b> Diagram of CT scanner .....	6
<b>Figure 2. 3</b> CT scanner X ray beam and detector (a) approximately to scan (b) Schematic diagram.....	6
<b>Figure 2. 4</b> Technological advances in CT scanner, 1985-2007. ....	7
<b>Figure 2. 5</b> Effect of detector array on number of rotations and scan time.....	8
<b>Figure 2. 6</b> The attenuated intensity I of the X-ray beams .....	9
<b>Figure 2. 7</b> A very simplified example explains how image reconstruction works. ....	10
<b>Figure 2. 8</b> DSA images. ....	14
<b>Figure 2. 9</b> Photograph shows a large FPD fluoroscopy system. A- Flat- panel image receptor. B- X-ray tube. ....	15
<b>Figure 2. 10</b> Construction of an FPD array.....	15
<b>Figure 3. 1</b> 64-MDCT Siemens Somatom Definition AS. ....	29
<b>Figure 3. 2</b> DSA Biplane Flat panel detector Siemens Axiom Artis.....	29
<b>Figure 3. 3</b> Cylindrical PMMA phantom of 16 cm diameter. ....	30
<b>Figure 3. 4</b> Catphan® 600 Phantom. ....	30
<b>Figure 3. 5</b> Copper sheets. ....	31
<b>Figure 3. 6</b> Unfors Xi CT Detector 10 cm length of the pencil-type ionization. ....	32
<b>Figure 3. 7</b> Unfors Ray Safe Xi R/F dosimeter. ....	33
<b>Figure 4. 1</b> Scatter plots of correlations between the effective dose and; (a) weight, (b), BMI (c) height and (d) age from CTA.....	40
<b>Figure 4. 2</b> Scatter plot of correlation between the effective dose and; (a) mAs, (b) kVp and (c) scan length from CTA.....	43
<b>Figure 4. 3</b> Bar chart of the effective dose from CTA examination of the brain. ....	44

<b>Figure 4. 4</b> Scatter plots of correlations between the effective dose and; (a) age, (b) weight, (c) height, (d) BMI from cerebral angiogram examination ....	47
<b>Figure 4. 5</b> Scatter plots of correlations between the effective dose and; (a) number of 2D radiography, (b) number of 3D RA, (c) number of vessel, (d) fluoroscopic time and (e) experience of Radiologist from cerebral angiogram examination .....	51
<b>Figure 4. 6</b> The effective dose from DSA examination. ....	51
<b>Figure 4. 7</b> Box plots show the distribution of effective dose for the CTA 30 cases and DSA 30 cases .....	54
<b>Figure 4. 8</b> Distribution of effective dose for the CTA 30 cases.....	57
<b>Figure 4. 9</b> Distribution of effective dose for the DSA 30 cases.....	57
<b>Figure 5. 1</b> Protocol for brain pre-contrast, CTA brain and brain post contrast. ....	59
<b>Figure 5. 2</b> Protocol for brain pre-contrast, CTA brain and CTV.....	59
<b>Figure 5. 3</b> The effect between direct and indirect methods. ....	60
<b>Figure 5. 4</b> Examination parameters between 2D radiography and 3D RA.....	66
<b>Figure 5. 5</b> kVp, mAs, sequence time, frame rate and DAP of 2D radiography (1) and 3D RA (2). ....	66

## LIST OF ABBREVIATIONS

<b>Abbreviation</b>	<b>Terms</b>
2D	Two dimensions
3D RA	Three dimensions rotational angiography
AAPM	American association of physicist in medicine
ADC	Analog to digital converter
AICA	Anterior internal cerebral artery
BMI	Body mass index
cm	Centimeter
CTA	Computed tomography angiography
CTDI	Computed tomography dose index
CTDI <sub>vol</sub>	Volume computed tomography dose index
CTV	Computed tomography venography
DAP	Dose area product
DCCE	Dose conversion coefficient
DEL	Detector element
DLP	Dose length product
DRLs	Dose reference levels
DSA	Digital subtraction angiography
MDCT	Multi-detector computed tomography
MSCT	Multi-slice computed tomography
E	Effective dose
ESD	Entrance surface dose
FDA	Food and drug administration
FPD	Flat panel detector
f/s	Flame per second
Gy	Gray
ICA	Internal cerebral artery
ICRP	International commission on radiological protection
in	Inch
<i>k</i>	Conversion Coefficient
KERMA	Kinetic energy released per unit mass
kg	kilogram
kg/ m <sup>2</sup>	Kilogram per meter square
kPa	Kilopascal
kV	Kilovoltage
kVp	Kilovoltage peak
mAs	Milliampere-second
mGy	Milligray
mGy.cm	Milligray-centimeter

<b>Abbreviation</b>	<b>Terms</b>
mGy.cm <sup>2</sup>	Milligray-centimeter square
mm	Millimeter
mR	Milliroentgen
MRI	Magnetic resonance imaging
ms	Millisecond
mSv	Millisievert
NRPB	National radiological protection board
oz	Ounce
PACS	Picture archiving and communication system
PCA	Posterior cerebral artery
PMMA	Polymethylmethacrylate
p/s	Pulse per second
QC	Quality control
RPLD	Radiophotoluminescence dosimeter
s	Second
TLD	Thermoluminescent dosimeter
μGy	Microgray
μGy.cm <sup>2</sup>	Microgray-centimeter square
VA	Vertebral artery



## CHAPTER I

### INTRODUCTION

#### 1.1 Background and rationale

Cerebrovascular disorders can create the clinical problem to the brain. The most common types are Stroke, Aneurysm and Arteriovenous malformations (AVMs). Computed Tomography Angiography (CTA), Magnetic Resonance Angiography (MRA) and Digital Subtraction Angiography (DSA) are procedures used to diagnose the diseases.

Computed Tomography (CT) is a method which X-rays and computers produce the medical images for analyses. Beams of x-rays pass from tube through patient's body at different angles to the detectors, and then the images are reconstructed by the computer. CTA is a combined CT scan with injection of contrast media through the venous vessel produce image of blood vessels and tissues.

Angiography is a medical imaging technique used to visualize the blood vessels and organs of the body, with particular interest in the arteries, veins, and the heart chambers. This is traditionally done by injecting a contrast agent into the blood vessel and imaging using X-ray fluoroscopy based techniques. DSA is type of fluoroscopic technique to clearly visualize blood vessels and has been the “gold standard” for many vascular and cerebrovascular imaging studies. Images are produced using contrast media by subtracting pre-contrast image (mask) from contrast images.

The effective dose, absorbed and organ doses are important for the procedures that either involve high doses or include sensitive tissues in the primary radiation beam. Effective dose provides an approximate indicator of potential detriment from ionizing radiation and should be used as one parameter in evaluating the appropriateness of examinations involving ionizing radiation.  
[1]

Modern CT scanners provide two dose parameters that both became available by the scanner manufacturers around 2001: the Volume CTDI (CTDI<sub>vol</sub>) measured in mGy, and the dose-length product (DLP) measured in mGy.cm. CTDI<sub>vol</sub> is a measure of the average dose within the scan volume to a standardized phantom. The total amount of radiation delivered to a standardized phantom is represented by the DLP, which is the product of CTDI<sub>vol</sub> and the

scan length. Organ doses in CT are well below the threshold for the induction of deterministic effects (e.g., erythema, epilation). Patient radiation risks in CT are related to carcinogenesis. An estimate of effective dose ( $E$ ), which is related to the carcinogenic risk, may be obtained by use of  $E/DLP$  conversion factors. [2]

The most direct way of estimating doses to patients undergoing CT examinations is to measure organ doses in patient-like phantoms. Another way of obtaining the pattern of energy deposition in patients undergoing CT examinations is by calculation. This type of calculation assumes that the patient resembles the phantom used for measurements or Monte Carlo simulation. Effective dose values calculated from DLP values for the corresponding clinical exams to determine a set of coefficients  $k$ , where the values of  $k$  are dependent on the region of the body being scanned. Using this methodology,  $E$  can be estimated from the DLP, which is reported on most CT systems. [3]

The most convenient and widely used method for indirect monitoring in DSA is the dose-area product (DAP) meter. The DAP measurements using a flat x-ray transition ionization chamber have been accepted as a suitable dosimetric technique for angiographic examination. DAP measurements are commonly used to assess the effective dose for evaluation of stochastic risk. Modern devices are designed for the simultaneous measurement of DAP and air kerma diagnostic radiology during fluoroscopy and exposure. DAP has the advantage of being constant at any distance from the tube focus, so wherever DAP is measured; it reflects the air kerma radiation field size at the patient's skin. The DAP is also useful in estimating the effective dose via calculation of the total energy imparted to the patient, which can be used to calculate the stochastic risk. [4]

In this study, the patient effective dose (according to ICRP 103) from CTA and DSA performed in the cerebrovascular region of the brain is evaluated by indirect methods. Effective dose was calculated by DLP (mGycm) from 64-MDCTA and DAP (mGycm<sup>2</sup>) from DSA flat panel detector.

## 1.2 Research objective

The purpose of this study is to evaluate the patient effective dose from CTA and DSA of the brain.



## CHAPTER II

### REVIEW OF RELATED LITERATURE

#### 2.1 Theory

##### 2.1.1 The introduction of Computed Tomography (CT) [5]

The CT is an imaging technique that produces cross-sectional images, representing in each pixel the local X-ray attenuation properties of the body. The first experimental set-up of Hounsfield in 1970 worked with the so-called translation/rotation principle. A thin beam of X-rays was generated through the use of a collimator and a single detector element was used to measure the attenuated intensity. By translating this set-up, different positions were measured. After an entire set of parallel measurements had been acquired, the set-up was rotated to acquire the next parallel projection. This principle is the first generation of CT scanner.

The second generation of CT scanners differed only slightly from that initial design in that a small number of measurement values could be obtained simultaneously. In Hounsfield's first scanner a total of 180 projections were obtained in steps of  $1^\circ$  with 160 measurement values each. The acquisition of those 28,800 measurement values took five minutes. From that data an image of  $80 \times 80$  pixels was reconstructed. With such a scanner, a head examination requiring six slices took about half an hour. Therefore, physicists were aiming at shortening the examination times. This was achieved with the introduction of the third generation CT scanners: a 1D array of detector elements positioned on an arc covers the entire measurement field and acquires a complete 'fan-beam' projection. This not only avoided the slow translation movements, but also improved the efficiency of using the output of the X-ray tube.

The third generation CT scanner consisted of a donut-shaped gantry with a big hole. Head, body, arms or legs were in the middle of the gantry to make a cross-sectional image. The patient is moved in and out on a motor-controlled table. The slice thickness is usually 0.5 to several mm and the spatial resolution, in the cross section, is roughly 1 mm at  $512 \times 512$  pixels per slice.

Within the gantry of the CT scanner, an X-ray tube is placed opposite a detector array with up to 1200 detecting elements receiving the photons that passing through the patient. If one measurement has been done this way, the

source and detector rotate over a small angle (roughly  $1^\circ$ ) and a new measurement is taken. The scanner repeats this procedure until a rotation of  $180^\circ$  has been reached. Then all thousands of measurements for reconstructing one slice have been done. The table on which the patient lies can then move a little further through the gantry for measuring a new slice.

Later scanners followed with stationary detectors fully encircling the patient so that only the x-ray tube rotated; it was termed the ‘Fourth generation’. Rotatory systems were quickly accepted, and translation–rotation systems meanwhile disappeared completely. The third generation has prevailed and constitutes the standard approach in clinical scanners today.

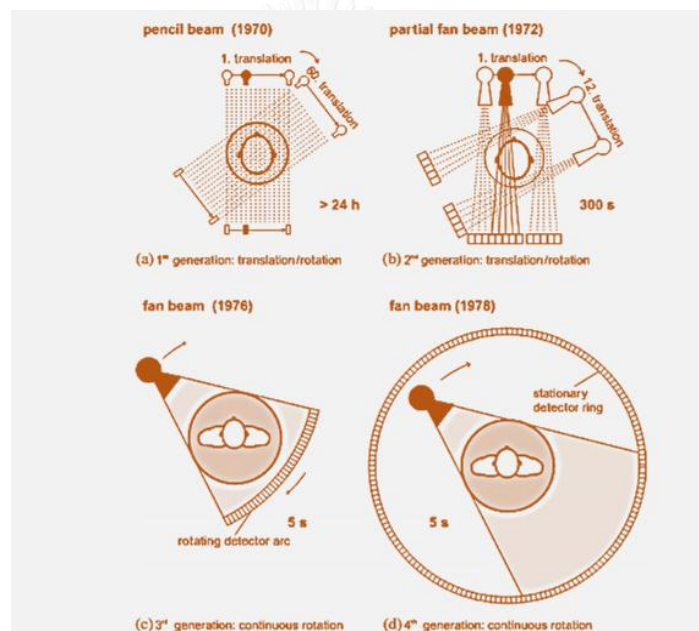


**Figure 2. 1** Four scanner generations were promoted in the 1970s. Head scanners, which scanned the patient by translation and rotation of the measurement system with a pencil beam (a) or a small fan beam (b), and fan beam systems, in which all body sections can be scanned with a continuous  $360^\circ$  rotation. The ‘3<sup>rd</sup> generation’, featuring a rotating detector (c), has clearly outdistanced the ‘4<sup>th</sup> generation’, utilizes stationary detector rings (d).

The basic components of CT scanner are an x-ray tube and arch of detectors, mounted on a gantry with a circular aperture (Figure 2.2a). Along the patient long axis, there are many rows of these arches of detectors, multi-slice CT (MSCT) or multidetector CT (MDCT) (Figure 2.3). The extent of area coverage by the detector rows currently ranges from 12 mm to 160 mm in length

(Figure 2.3b) depends on scanner model. The patient lies on an integral couch, the x-ray tube and detectors rotate, continuously monitoring the absorption of x-rays as their path through the body changes. Image data can be acquired in sequential mode or in helical mode (Figure 2.2b). In sequential mode, axial mode or step and shoot mode, the couch is stationary during one rotation, and then steps through the gantry to the next position in order to acquire another set of data. [6]

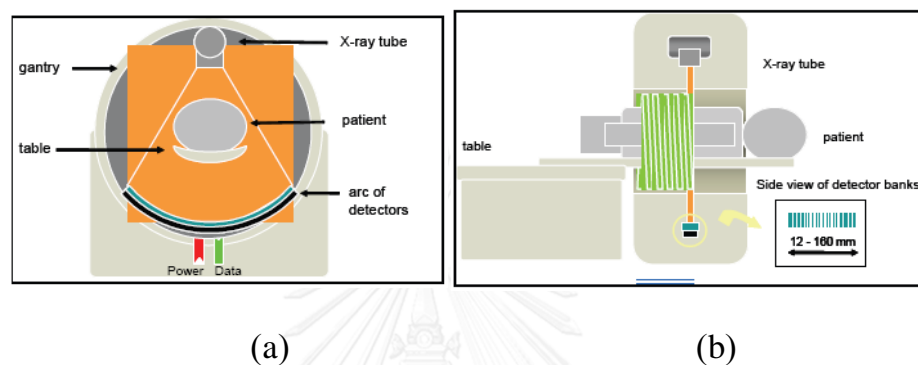


**Figure 2. 2** Diagram of CT scanner (a) 'End view', (b) 'Side view' in helical acquisition mode.

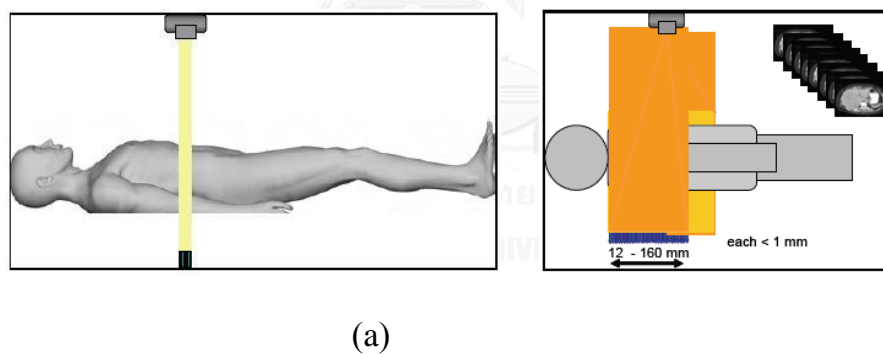


**Figure 2. 3** CT scanner X ray beam and detector (a) approximately to scan (b) Schematic diagram.

### 2.1.2 Spiral CT [5]

In 1987 continuously rotating gantries were introduced to shorten examination times even more: Spiral or Helical CT. Initially, power supply to the rotating gantry and data transmission out of the gantry was performed via cables. Therefore, the direction of rotation had to be reversed after each scan, substantially slowing down the acquisition of a series of images and making the system rather vulnerable for mechanical cable damages. These drawbacks were overcome with the introduction of slip ring technology for the power supply and

optical transfer for data transmission. The patient couch is moving slowly (1-3 mm/s) and continuously while the scanner rotates constantly at about 1-3 rotations/s. Spiral CT has the important advantage to be fast: modern scanners can collect and reconstruct a high-resolution slice of  $512 \times 512$  pixels within half a second.

### 2.1.3 Multi-Detector CT (MDCT) [5]

To achieve more substantial volume coverage, faster and/or with improved z-axis resolution, are the concurrent acquisition of more than one slice, and a decrease in gantry rotation time. Beginning in 1998, CT manufacturers introduced 4-channel MDCT systems, which provided a considerable reduction in scan time, the ability to acquire thinner images with the same scan time, or more efficient utilization of the available x-ray beam. This began the current revolution in CT technology that has been the basis of a dramatic increase in the number and utility of CT clinical application. Two essential advances toward modern MDCT systems were the fabrication of x-ray detectors that were physically and electrically separated along the z-axis, and the ability to flexibly combine the data from the individual detector elements by assigning the output of more than one detector to a single data channel. The resulting decrease in scan time was of tremendous clinical advantage.

Figure 2.4 illustrates the rapid pace of developments in scanner technology over the last twenty years, and especially the acceleration of development in last ten years from four to 320-slice scanner.

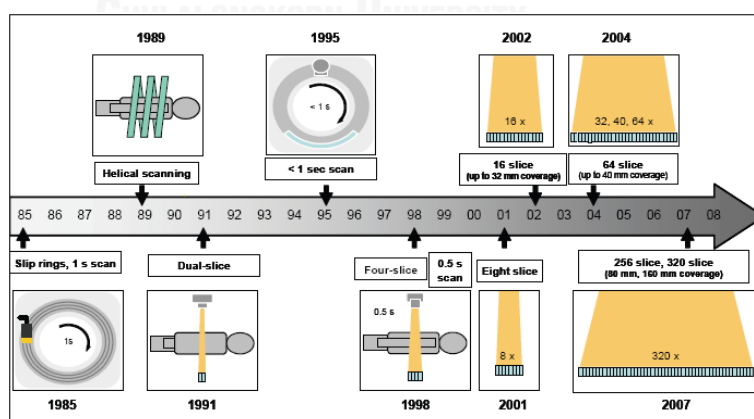


Figure 2. 4 Technological advances in CT scanner, 1985-2007.

### 2.1.4 Scan time and scan length [5]

The maximum scan length is an important factor in scanner performance, and may limit the ability to perform certain procedures, for example when scanning peripheral angiography ‘run-off’. Another aspect of maximum scan length that may need to be considered is the coverage available in dynamic studies such as CT perfusion scanning, where the same volume of patient is repeatedly scanned in quick succession. The maximum scan length is governed by the z-axis detector array design, and the x-ray tube heat characteristics. With the large volume of data generated with a 64 slice scanner, for example, the total scan length may also be limited by computer memory capacity.

### 2.1.5 Gantry rotation time [5]

The rotation time of the tube and the detectors around the patient, gantry rotation time, has a direct effect on total scan time. Image quality will be improved with faster rotation times, as there will be reduced misregistration of data (both in-plane and along the patient) arising from patient movement (whether from heartbeat, breathing, peristalsis, or restlessness). This misregistration of data introduces artifacts in image. Scanners can now achieve rotation times of less than 0.3 seconds, but the fastest rotations are generally reserved for specialist applications such as cardiac scanning in order to minimize image artifacts due to motion of heart.

### 2.1.6 Detector array length [5]

The length of detector array will determine the number of rotations needed to cover the total scan length, and thus the overall scan time. The example in figure 2.5 shows how the total scan time will be halved by doubling the array length. The ability to scan a given length with fewer rotations also helps to minimize heat load on the x-ray tube, thereby allowing the scanning of longer lengths.

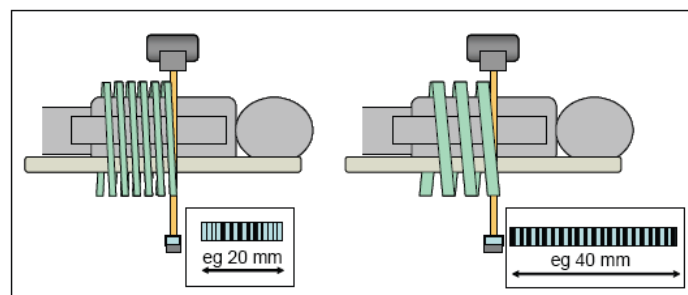


**Figure 2. 5** Effect of detector array on number of rotations and scan time.



Detector arrays are divided into two types; fix and variable, or known as matrix and hybrid. Fixed arrays have detectors of equal z-axis dimension over the full extent of the array, whereas on variable arrays, the central portion comprises finer detectors. With variable arrays, the total scan time for a given length, the finest slice acquisition, will be longer, because the z-axis coverage is reduced.

Complete coverage of an organ, such as the brain or heart, offers advantages for both dynamic perfusion and cardiac studies. The z-axis detector array lengths on the 64-slice scanners, of up to 40 mm, are adequate to cover these organs in only few rotations. A coverage length of 160 mm usually allows complete organ coverage in a single rotation, so the function of the whole organ can be monitored over time.

### 2.1.7 Image reconstruction [7]

Imagine splitting up a piece of different tissues into many mini-cubes and sending X-ray beams through them at different angles. Detector elements receive signals depending on the different attenuation coefficients  $\mu$  in each cube along the distance they have to travel. The line of cubes consists of different tissues with different atomic densities (Figure 2.6).

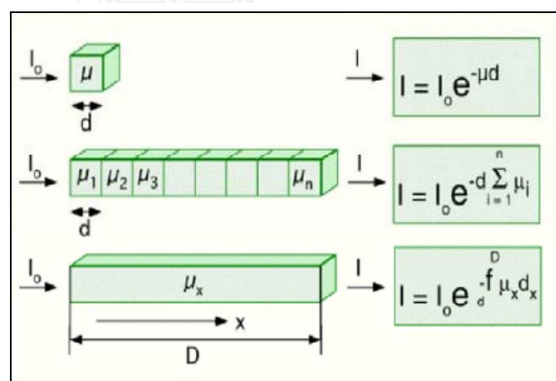


**Figure 2. 6** The attenuated intensity  $I$  of the X-ray beams at the detector depends on the intensity  $I_0$  at the source, the attenuation coefficients  $\mu$  of the different tissues and the path length  $d$ .

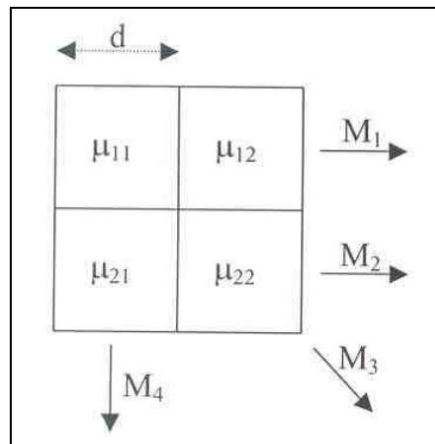


**Figure 2. 7** A very simplified example explains how image reconstruction works.

Suppose our patient slice contains only four pixels. In such a case we are dealing with four unknown attenuation coefficients ( $\mu_{11}$  to  $\mu_{22}$ ).

Of this four-pixel object four transmission intensities ( $I_1$  to  $I_4$ ) are measured. Assume that every pixel has a uniformly distributed absorption coefficient. The size of the pixels is given by  $d$ . To calculate the absorption coefficients of the four pixels, we have four equations with four unknowns:

$$I_1 = I_0 e^{-(\mu_{11}d + \mu_{12}d)}$$

$$I_2 = I_0 e^{-(\mu_{21}d + \mu_{22}d)}$$

$$I_3 = I_0 e^{-(\mu_{11}d\sqrt{2} + \mu_{22}d\sqrt{2})}$$

$$I_4 = I_0 e^{-(\mu_{11}d + \mu_{21}d)}$$

This simple problem of four equations with four unknowns can easily be solved, but one can imagine that larger images as used in daily clinical routine ( $512 \times 512$  pixels = 262144 unknown  $\mu$  values) need highly sophisticated algorithms to solve so many equations. The most widely used algorithm is the filtered back-projection method, using Fourier transform. Scientists are still searching for better algorithms nowadays.

### 2.1.8 Hounsfield units [7]

To honor Hounsfield for his work the mean X-ray attenuation within one pixel (also known as CT number) is expressed in Hounsfield units (HU). Measured values of attenuation are transformed into CT numbers using the international Hounsfield scale:

$$\text{CT number} = [(\mu - \mu_{\text{water}})/\mu_{\text{water}}] \times 1000$$

In this expression  $\mu$  is the effective linear attenuation coefficient for the X-ray beam. This scale is so defined that air and water respectively have the following CT numbers:  $-1000$  and  $0$  HU.

### **2.1.9 Computed Tomography Angiography (CTA) definition [8]**

CTA is a combined CT scan with injection of contrast media through the venous vessel in arm to produce image of blood vessels and tissues. CTA is primarily performed for assessing the heart, arteries, or veins. It requires at a minimum a thin section helical (spiral) CT acquisition coupled with a power injection of intravenous iodinated contrast medium. Three-dimensional rendering and multi-planar reformations are important components of many CTA examinations.

### **2.1.10 CTA indication [8]**

Indications for CTA of the head and neck vessels include the diagnosis, characterization, and/or surveillance of: arterial and venous aneurysms or pseudo aneurysms, stroke and vasospasm, atherosclerotic occlusive disease, non-atherosclerotic, non-inflammatory vasculopathy, traumatic injuries to arteries and veins, arterial dissection and intramural hematoma, venous and dural sinus thrombosis, congenital vascular anomalies, vascular anatomic variants, vascular interventions (percutaneous and surgical, vasculitis and collagen vascular diseases, vascular infection, head and neck tumors of vascular origin, with rich vascular supply or invading vascular structures.

### **2.1.11 CTA examination technique [8]**

Prior to acquiring the CTA, an unenhanced helical CT acquisition may be necessary for detecting mural or extra-vascular hemorrhage, mapping of arterial calcification, or localization of the anatomy of interest. The section thickness for this preliminary CT acquisition is application dependent. Ideally, it should be the same thickness as the CTA but definitely should not exceed  $5$  mm. The radiation exposure to the patient should be minimized within the limits of acceptable image quality, including optimization of kVp and mAs. If infants and children are being imaged, there should be written guidelines for acceptable CT radiation exposure, including weight-appropriate or age-appropriate guidelines to reflect the ALARA principle. Dose modulation approaches can be used, with appropriate targeted signal-to-noise ratio.

### **2.1.12 Ionizing radiation and patient dose [8]**

Doses from CT examinations are generally significantly higher than those from conventional X-rays, although a CT scan provides more diagnostic information. Recent UK surveys reported conventional X-ray examinations with

average doses of 0.04 mSv for head examinations, 0.02 mSv for chest and 0.7 mSv for abdomen examinations. A similar survey for CT examinations gave values of 1.5, 5, and 6 mSv respectively for the head, chest and abdomen regions. These figures represent average values from the use of a wide range of operational parameters, such as tube current and voltage, however they can be used as a guide.

The standard reference parameters used to describe dose in CT are the volume computed tomography dose index ( $CTDI_{vol}$ ) and the dose length product (DLP). The  $CTDI_{vol}$  is calculated from measurements, made with a 100 mm long pencil ion chamber, in standard sized polymethyl methacrylate (PMMA) head and body phantoms which have been irradiated at the halfway position, along the length, with a single beam rotation. However, as a dose descriptor, it is important to think of the  $CTDI_{vol}$  as representing the average dose in a slice of tissue, halfway along a 100 mm irradiated length.

The DLP represents the total amount of irradiation given, and as such gives an indicator of risk (without taking into account the radiosensitivity of particular organs). The  $CTDI_{vol}$  is a very useful dose descriptor for comparing dose from different protocols or different scanners. However, comparisons should only be done for scans undertaken on standard size patients. The  $CTDI_{vol}$  and DLP values are displayed on the scanner console. It is always invaluable to look at these figures when reviewing patient images for an assessment of the image quality and dose performance of a scanner. Both the  $CTDI_{vol}$  and the DLP are used when comparing with dose reference levels (DRLs). MDCT scanners have the potential to give higher radiation doses compared to single slice scanners. Their flexibility in scanning lengths with high mAs values, and the ease with which they perform dual and even triple-phase contrast studies, can lead to high patient doses. In addition, there are some intrinsic features of current MDCT design which can give rise to slightly higher doses.

To minimize controversy over differences in effective dose values that are purely the result of calculation methodology and data sources, a generic estimation method was proposed by the European Working Group for Guidelines on Quality Criteria in Computed Tomography. Effective dose values calculated from the NRPB Monte Carlo organ coefficients were compared to DLP values for the corresponding clinical exams to determine a set of coefficients  $k$ , where the values of  $k$  are dependent only on the region of the body being scanned (head, neck, thorax, abdomen, or pelvis). Using this methodology,  $E$  can be estimated from the DLP, which is reported on most CT systems. [1]

### **2.1.13 Introduction of Digital Subtraction Angiography (DSA) system [9]**

Diagnostic cerebral and peripheral angiography utilizes modified techniques that are extensions of those used in the coronary arterial system. Visualization of a vascular bed is made possible under fluoroscopy by injecting radio opaque contrast into the proximal vessel. These images allow two-dimensional visual assessment if orthogonal views are taken. Characteristics of contrast flow through a vessel and pressure measurements allow acquisition of hemodynamic data that represent functional competence of an artery. DSA has become an imaging standard for evaluation of vascular anatomy. First introduced in 1970s, it is highly effective in contrasting arterial structures with their surrounding bone and soft tissue. DSA was first used in humans in 1978 and was made commercially available in 1980.

### **2.1.14 Digital Fluoroscopy [10]**

Digital fluoroscopy is most commonly configured as a conventional fluoroscopy system (tube, table, image intensifier, video system) in which the analog video signal has been digitized with an ADC. Alternatively, digitization may be accomplished with a digital video camera (e.g., a charge-coupled device) or via direct capture of x-rays with a flat panel detector. For digital fluoroscopy system in which the analog video signal is digitized with an ADC, the resolution is limited by the resolution of the video camera, which is typically 1–2 line pairs per millimeter.

For the typical system, the ADC samples the analog video signal at discrete time points and converts the value of the signal to a binary number for storage. The maximum and minimum analog video signal values will be scaled to the maximum and minimum digital values according to the bit depth of the ADC. An 8-bit ADC will convert the video signal to a maximum of 256 different values. Improved representation of the analog video signal will occur as the bit depth of the ADC is increased and the sampling frequency of the discrete time points increases.

The digital image data from digital fluoroscopy may be processed by using many useful image processing techniques. These techniques may serve to decrease radiation exposure to the patient and medical imaging staff or improve visualization of anatomy. Processing options include last image hold, gray-scale processing, temporal frame averaging, and edge enhancement. Additional processing is available when digital fluoroscopy data are used to perform DSA.

### 2.1.15 DSA acquisition [10]

The acquisition of digital fluoroscopic images can be combined with injection of contrast material and real-time subtraction of pre and post-contrast images to perform examinations that are generally referred to as digital subtraction angiography (Figure 2.8).

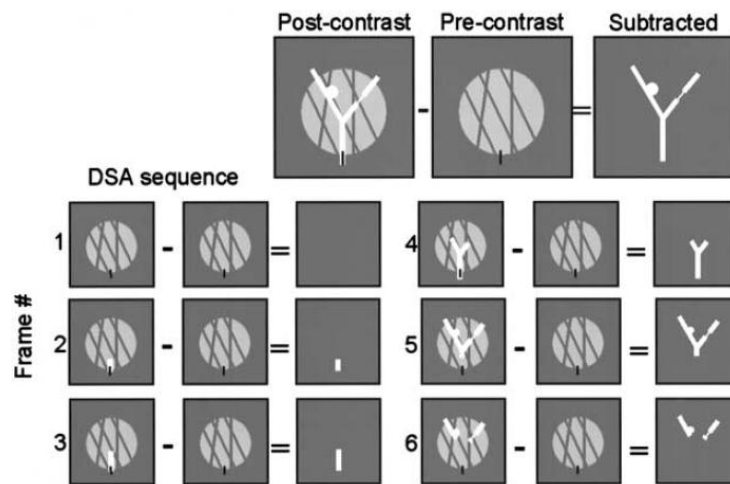


**Figure 2. 8** DSA images.

A pre-contrast mask image (which shows a distracting background structure and the tip of a catheter) is subtracted from a post-contrast image obtained at the same location (which shows contrast material-filled vessels). The result is an image of only the contrast material-filled vessels. During the actual imaging sequence, the subtraction process may begin slightly prior to contrast material injection, with each frame capturing a different phase of the injection. The sequence of subtracted frames can then be reviewed in cine mode or as still frames. The unsubtracted original digital fluoroscopic images are generally not reviewed.

### 2.1.16 Flat panel detector (FPD) fluoroscopy systems [10]

FPD fluoroscopy systems have begun to dominate angiography and cardiac catheterization laboratories (Figure 2.9). Currently, only their high purchase cost is preventing their utilization with low-end fluoroscopy equipment such as gastrointestinal fluoroscopy systems and C-arm mobile units. The smaller size of the FPD imaging chain allows for more flexible movement during patient examinations. Moreover, FPD systems do not require a television camera to produce an electronic signal for the display monitor.



**Figure 2. 9** Photograph shows a large FPD fluoroscopy system. A- Flat-panel image receptor. B- X-ray tube.

By its design, the FPD produces a digital electronic signal, which represents the intensity of the x-rays that impinge on each detector element (DEL) in the solid-state FPD array. Moreover, the entire process is digital, which reduces image noise caused by electronic components.

The FPD consists of an array of individual DELs (Figure 2.10a). The typical size of those in fluoroscopy systems ranges from 200  $\mu\text{m}$  to about 140  $\mu\text{m}$  per side, depending on the manufacturer and model. The size of the entire array ranges from 25  $\times$  25 cm to 40  $\times$  40 cm. However, some manufacturers specify the size of the FPD by providing a diagonal measurement, and others quote the edge dimension. A FPD may contain 1.5–5.0 million individual DELs; a challenge of manufacturing is to make a uniform array with few defective or degraded DELs.

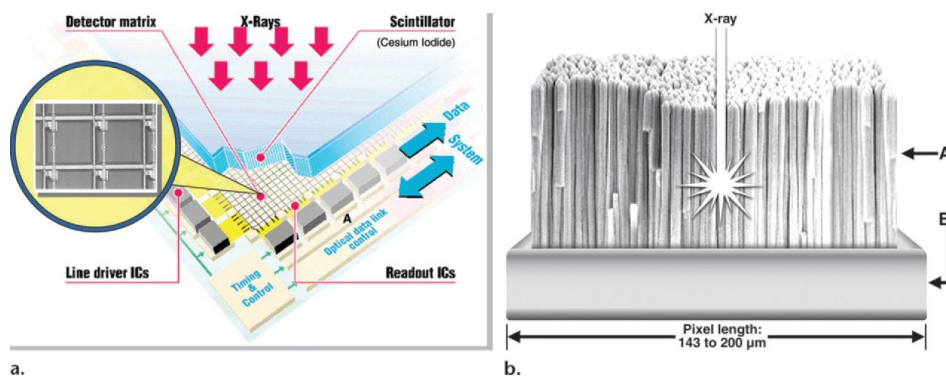


**Figure 2. 10** Construction of an FPD array. (a) Drawing shows a section of the FPD and many individual DELs. A - 14-bit A/Ds, IC - integrated circuit. (b) Drawing shows one DEL in the FPD array. A - CsI needle scintillator layer, B - photodiode and transistor layer.

Currently, most FPD arrays are indirect solid-state systems, meaning that the x-ray energy is first converted to light and then to an electronic signal. An individual DEL consists of a scintillation layer, which usually is composed of thallium-activated CsI (Figure 2.10b). The scintillation layer attenuates the incident x-rays and produces light. The CsI scintillation layer is composed of many needle-like crystals, which are grouped together to cover the surface of the DEL. These needle-like structures help direct light toward the photodiode located below. The amount of light produced is directly related to the amount of x-ray flux that is incident on the DEL. When light hits the surface of the low-noise photodiode and transistor below, it acts like a switch, allowing the diode to conduct electricity. In the absence of light on its surface, the photodiode acts like an insulator, preventing the flow of electrons.

Each DEL is able to quantify the amount of x-ray radiation incident upon its surface. First, an electronic switch is closed and the capacitor is charged. Next, the electronic switch is opened. Because no light is incident upon the surface of the DEL, the charge remains on the capacitor, which stores the initial charge, similar to the way a bank stores money. The interaction of x-rays with the scintillator produces light in proportion to the x-ray flux. This light causes the photodiode to conduct to different degrees, depending on the intensity of the light. As more light is produced, more charge is drained from the capacitor, like a bank withdrawal of money. Finally, another electronic switch is closed and the remnant charge is withdrawn from the storage capacitor and sent to the display system. The loss in charge is related to the amount of x-ray radiation incident upon the DEL. By reading each DEL in the FPD array row by row, an electronic image of the distribution of x-rays that are incident upon the FPD can be formed. In this way, an FPD array is used to create an image without the use of a television camera.

### **2.1.17 Diagnostic DSA examination [11]**

Diagnostic cervicocerebral catheter angiography is a process by which the intracranial and extra-cranial head and neck circulation is evaluated. It consists of placement of a catheter selectively into extra-cranial cervical vessels using imaging guidance, followed by contrast injection to delineate anatomy. The catheter is usually inserted via a common femoral arterial access site, but other access sites may be used in selected cases. Aortic arch injections may be performed to delineate the origins and/or tortuosity of the extra-cranial cervical vessels prior to selective catheterization.



Injection of contrast medium must be at a rate and volume that safely and adequately opacifies the vascular territory of interest. Optimal positioning, magnification, and filming rates are necessary to provide sufficient information regarding the disease and vascular territory being studied. Several projections may be necessary to best demonstrate the targeted area, but a minimum of two orthogonal projections is essential. Findings are acquired and stored either on conventional film or digitally on computerized storage media. Imaging and image recording must be consistent with the ALARA radiation safety guidelines.

#### **2.1.18 Dose-area product (DAP) [12]**

Dose-area product (DAP) is defined as the KERMA to air multiplied by the area of the X-ray beam in the plane perpendicular to the beam axis. It is usually measured in  $\text{Gy}\cdot\text{cm}^2$  and radiation back-scattered from the patient is excluded. Provided that the cross sectional area of the beam lies completely with the detector, it may be shown by simple application of the inverse square law that the reading will not vary with the distance from the tube focus. Thus the DAP can measure at any point between the diaphragm housing on the X-ray tube and the patient, but not so close to the patient that there is significant back-scattered radiation.

DAP meters consist of flat, large area parallel plate ionization chambers connected to suitable electrometers which respond to the total charge collected over the whole area of the chamber. The meter is mounted close to the tube focus where the area of the X-ray beam is relatively small and dose rates are high. It is normally mounted on the diaphragm housing where it does not interfere with the examination and is usually transparent so that when fitted to an over-couch X-ray tube the light beam diaphragm device can still be used.

DAP measures of total energy fluence incident on the patient and related to the energy absorbed in the patient. Some studies for which DAP meters should be used include barium enemas, barium meals, micturatingcystograms, cardiac investigations and interventional techniques in neuroradiology and biliary procedures.

#### **2.1.19 Effective dose [13]**

The concept behind effective dose and its predecessor, effective dose equivalent, was proposed in 1975. The aim was to define a quantity that could be related to the probability of health detriment due to stochastic effects from exposure to low doses of ionizing radiation. Effective dose is a sum of the equivalent doses in tissues and organs of the body that are considered to be sensitive to radiation damage, weighted according to the risk of aggregated

health detriment. The weighting factors that are used for individual tissues are based predominantly on a statistical analysis of the increase in the long-term incidence and mortality for cancer determined from a life span study (LSS) of the survivors exposed to radiation when the atomic bombs were exploded over Japan, although account is taken of data from other groups of workers and patients who have received high radiation exposures, and of the possibility of hereditary effects.

The application of effective dose in its present form was recommended by the International Commission on Radiological Protection (ICRP) which stated that it was intended for use in radiation protection, including the assessment of risks in general terms. However, effective dose has been applied extensively to medical exposures, often to specific individuals of known gender and age. Effective dose can be used in both the generic justification and the optimization of medical exposures, but should not be used to predict absolute risk levels. Values have been derived for a variety of diagnostic procedures in radiology and nuclear medicine in order to provide a relative index of harm that can be considered in justification of medical exposures.

For medical exposures, conversion coefficients have been derived that allow values for effective dose to be calculated from measurable dose quantities, such as entrance surface dose (ESD) or DAP for radiology examinations and administered activity for nuclear medicine procedures.

#### **2.1.20 Effective dose conversion coefficients [13]**

The coefficients have been established from computer simulations for the exposure of anthropomorphic phantoms. The coefficients are quoted to two or three significant figures, but the uncertainties in these and in the tissue weighting factors are seldom considered. The conversion coefficients are derived from mathematical phantoms, which represent idealized anatomical forms in terms of size, shape and position of each tissue. Coefficients used currently for the assessment of effective dose have been based on a variety of models with differences in the positions and sizes of the tissues, although the geometry for a standard human body anthropomorphic phantom has now been specified, on which future computational phantoms should be based.

### **2.2 Review of Related Literature**

**Klingebiel R, et al. [14]** compared images quality of cervicocranial vasculature between a 64 multi-slice computed tomography angiography (MSCTA) and DSA by retrospective evaluation in patients with presumptive cervicocranial vascular disorders. Twenty-four 64-MSCTA studies (32 mm

detector width, slice thickness 0.5 mm, 120 kVp, 150 mAs, pitch 0.75) of patients with presumptive cervicocranial vascular pathology (13 men, 11 women, mean age 38.3 yrs, range 19-54 yrs) were assessed in comparison with DSA studies without abnormal findings in age-matched patients (11 men, 13 women, mean age 39.7 yrs, range 18-54 yrs). Study readings were performed in a blinded manner by two neuroradiologists with respect to image quality and accessibility of various cervicocranial vascular segments by using five-point scale. Radiation exposure was calculated for 64-MSCTA. Each reader assessed 384/528 different vessel segments (64-MSCTA/DSA). Superior image quality was attributed to DSA with respect to the C1 ICA-C6 ICA, A3 ACA, and P3 PCA segments as well as the AICA and SCA. The 64-MSCTA was scored superior for C7 ICA and V4 VA segments. A significantly increased number of non-assessable V2- and V3 VA segments in DSA studies were noted. The effective dose from 64-MSCTA amounted to 2.2 mSv. 64-MSCTA provides near equivalent diagnostic information of the cervicocranial vasculature as compared with DSA. The DSA should be considered primarily when peripheral vessels (A3/P3) or ICA segments close to the skull base (C2-5) are of interest.

**Cohnen M, et al. [15]** studied radiation exposure of patients in comprehensive computed tomography of the head in acute stroke. Effective doses were derived from measurements with the use of lithium-fluoride thermoluminescent dosimeters (LiF-TLD) at several organ sites using an Alderson-Rando phantom. The measurements resulted in effective doses of 1.7 mSv for CT brain, 1.9 mSv for CTA of intracranial vessels, and 2.8 mSv for CTA of cervical vessels, respectively. Depending on examination parameters, effective doses varied between 1.1 and 5.0 mSv for cerebral CT perfusion (CTP). For CTP, local doses in the area of the primary beam ranged between 114 and 444 mGy.

**Mnyusiwalla A, et al. [16]** determined the radiation dose delivered during comprehensive computed tomography (CT) imaging for acute stroke. All CT examinations performed over 18 months using our acute stroke protocol were included. Protocol includes an unenhanced CT head, CT angiography from the arch to vertex, CT perfusion/permeability, and an enhanced CT head. All imaging was acquired with a 64-MDCT. Examinations where any element of the protocol was repeated or omitted due to mistimed injection or patient motion were excluded. Dose-length products (DLP) for all components of each examination were obtained from dose reports generated at the time of acquisition, separating neck, and head calculations. Effective doses for each examination were calculated using the DLP and normalized values of effective dose per DLP appropriate for the body regions imaged. Ninety-five examinations were included. Mean DLP was 6,790.0 mGy·cm. Effective doses ranged from

11.8 to 27.3 mSv, mean effective dose of 16.4 mSv. Mean effective dose for acquisition of the unenhanced head was 2.7 mSv. Largest contribution to effective dose was the CTA with a mean effective dose of 5.4 mSv. Mean effective dose for the CT perfusion was 4.9 mSv. A comprehensive CT acute stroke protocol delivered a mean effective dose of 16.4 mSv, which is approximately six times the dose of an unenhanced CT head. These high-dose results must be balanced with the benefits of the detailed anatomic and physiologic data obtained. Centers should implement aggressive dose reduction strategies and freely use MRI as a substitute.

**Manninen AL, et al. [17]** compared radiation exposure between diagnostic CTA and DSA examinations of cerebral and cervicocerebral vessels by exposed anthropomorphic phantom using typical diagnostic CTA and DSA setups and imaging parameters. For both imaging techniques, the imaging area of cerebral vessels included intracranial vessels only, while the imaging area of cervicocerebral vessels included both cervical and intracranial vessels from the aortic arch to the vertex. The effective dose was determined by using radiophotoluminescence dosimeter (RPLD). The DSA examination was simulated by using a biplane angiography system, and the CTA examination, by using a 64-row multidetector CT scanner. For the imaging of cerebral vessels, the effective dose according to ICRP 103 was 0.67 mSv for CTA and 2.71 mSv for DSA. For the imaging of cervicocerebral vessels, the effective dose was 4.85 mSv for CTA and 3.6 mSv for DSA. The effective dose for CTA assessment of cerebral vessels was approximately 1/5 the dose compared with DSA. In the imaging of cervicocerebral vessels, the effective dose for CTA was approximately 1/3 higher compared with DSA.

**Marshall NW, et al. [18]** reported patient radiation doses received during interventional radiological procedures. Patient dose survey has been conducted of such procedures. A total of 288 non-coronary procedures (177 classified as diagnostic and 111 as therapeutic) were accrued into the study. For each procedure, the fluoroscopic screening time and the fluoroscopic and digital radiographic dose–area products were recorded in a computer database. For example, median dose–area product values (due to fluoroscopy and digital radiography combined) of 24.2, 27.9, 69.6 and 74.7 Gy.cm<sup>2</sup> were obtained for nephrostomy, biliary stent removal/insertion, cerebral angiography and percutaneous transhepatic cholangiography procedures. While the effective dose is not an accurate measure of patient risk, it is convenient for comparing the radiological risks associated with various procedures. Effective doses were estimated from the total dose–area products. The respective median estimated effective dose values for the four procedures noted above were 3.9, 4.5, 7.0 and 12.0 mSv. While an infrequently performed procedure at this institution

(n=4 during this survey), the transjugular intrahepatic portosystemic shunt (TIPS) procedure had the greatest median dose–area product and effective dose values: 347 Gy cm<sup>2</sup> and 55.5 mSv, respectively.

**Deak PD, et al. [19]** determined conversion factors for the new ICRP publication 103 recommendations for adult and pediatric patients and to compare the effective doses derived from Monte Carlo calculations with those derived from DLP for different body regions and CT scanning protocols. Effective dose values for the Oak Ridge National Laboratory phantom series, including phantoms for newborns; 1, 5 and 10-year-old children and adults were determined by using Monte Carlo methods for a 64-section multi-detector CT scanner. For each phantom, five anatomic regions (head, neck, chest, abdomen, and pelvis) were considered. Monte Carlo simulations were performed for spiral scanning protocols with different voltages. Effective dose was computed by using ICRP publication 60 and 103 recommendations. The calculated effective doses were compared with those derived from the DLP by using previously published conversion factors. In general, conversion factors determined on the basis of Monte Carlo calculations led to lower values for adults with both ICRP publications. Values up to 33% and 32% lower than previously published data were found for ICRP publication 60 and ICRP publication 103, respectively. For pediatric individuals, effective doses based on the Monte Carlo calculations were higher than those obtained from DLP and previously published conversion factors (e.g., for chest CT scanning in 5-year-old children, an increase of about 76% would be expected). For children, a variation in conversion factors of up to 15% was observed when the tube voltage was varied. For adult individuals, no dependence on voltage was observed. Conversion factors from DLP to effective dose should be specified separately for both sexes and should reflect the new ICRP recommendations. For pediatric patients, new conversion factors specific for the spectrum used should be established.

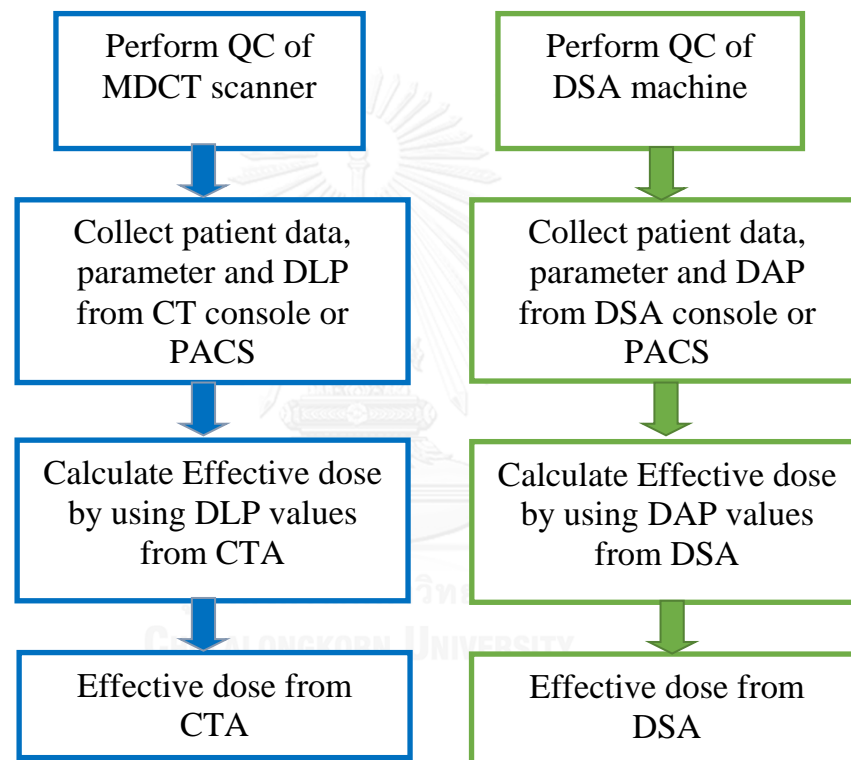
## CHAPTER III

### RESEARCH METHODOLOGY

#### 3.1 Research design

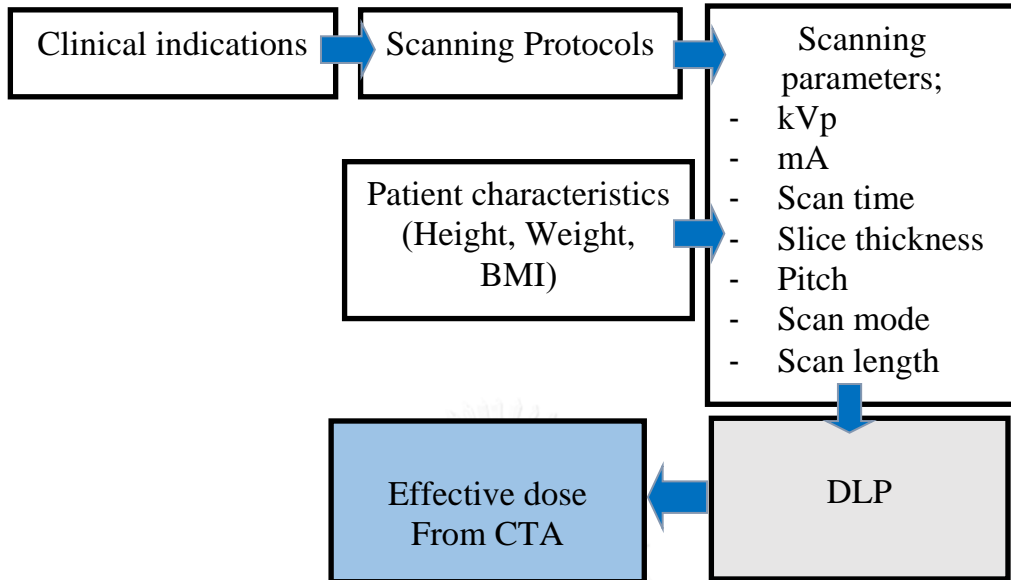
This study is an observational analytical research (retrospective study).

#### 3.2 Research design model

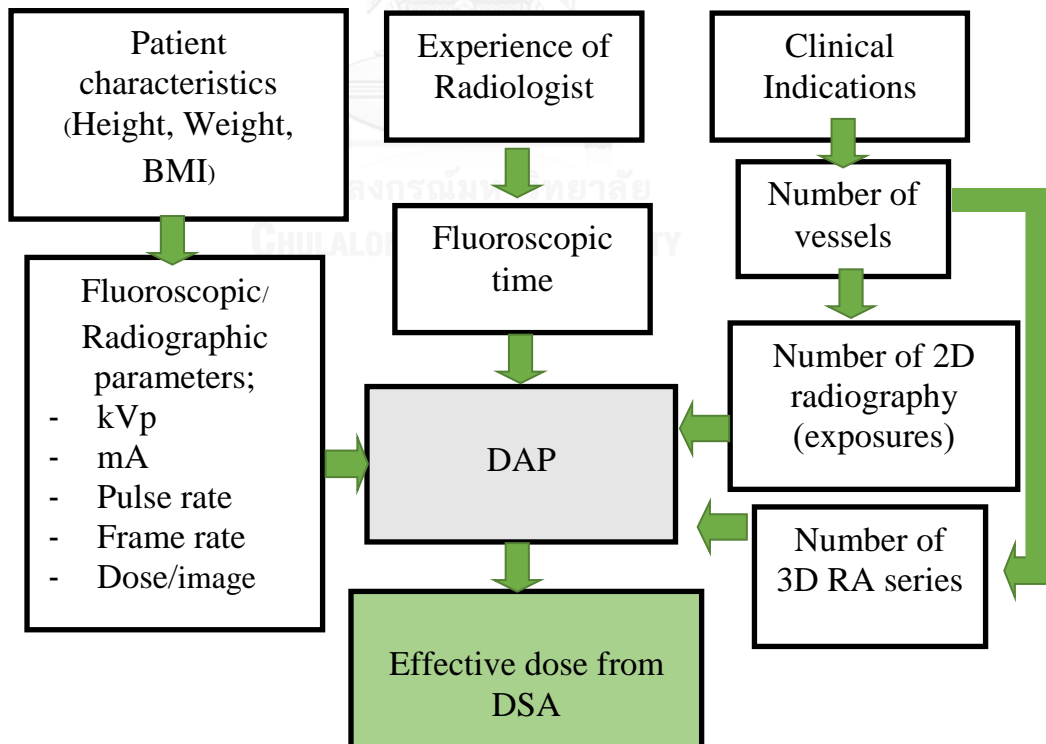


### 3.3 Conceptual framework

#### - CTA



#### - DSA



### **3.4 Research question**

What is the patient radiation doses received from CTA and DSA examination of the brain study?

### **3.5 Sample**

#### **3.5.1 Target population**

- The patients underwent CTA at Department of Neuroradiology, Prasat Neurological Institute.
- The patients underwent DSA at Department of Neuroradiology, Prasat Neurological Institute.

#### **3.5.2 Sample population**

The data will be recorded on 30 patients who underwent the CTA examination and 30 patients who underwent the DSA examination at Department of Neuroradiology, Prasat Neurological Institute.

#### **3.5.3 Eligible criteria**

##### **3.5.3.1 Inclusion criteria**

- Patients age >18 years old.
- CTA and DSA performed by using routine protocol.
- Diagnostic DSA procedure.
- Follow up case, at least 3 vessels have been selected.

##### **3.5.3.2 Exclusion criteria**

- Patients performed CTA of the brain and neck.
- Patients performed CTA of the brain with CT perfusion for stroke fast track protocols.
- Interventional radiology procedure.



**Table 3. 1** Routine CTA examination parameters 1.

- Routine protocols 1; CTA+ Brain post contrast enhancement.  
Indication: for investigation of vascular and parenchyma diseases (Headache, Subarachnoid hemorrhage, Moya-moya diseases).

<b>Parameters for CTA examination</b>				
	kVp	reference mAs	Pitch Factor	TI (s)
Topogram	120	35		4.0
Control scan	120	450		1.0
Non Contrast	120	450	0.55	1.0
Premonitoring	120	20		0.33
Monitoring	120	20		0.33
Head Angiogram	120	158	1.4	0.33
Brain Post contrast	120	400	1.4	0.33
Slice acquisition	64x0.6 mm			
Slice collimation	0.6 mm			

**Note:** TI = Tube rotation time.

Slice acquisition = number of detector row × detector thickness.

**Table 3. 2** Routine CTA examination parameters 2.

- Routine protocols 2; CTA+ CTV  
Indications: for investigation of vascular disorder (Stroke, Arteriovenous malformation, Carotid-Cavernous fistula, Arteriovenous fistula, Aneurysm, Vascular stenosis).

<b>Parameters for CTA examination</b>				
	kVp	reference mAs	Pitch Factor	TI (s)
Topogram	120	35		4.0
Control scan	120	450		1.0
Non Contrast	120	450	0.55	1.0
Premonitoring	120	20		0.33
Monitoring	120	20		0.33
Head Angiogram	100	175	1.4	0.33
Head CTV	100	175	1.4	0.33
Slice acquisition	64×0.6 mm			
Slice collimation	0.6 mm			

**Note:** TI = Tube rotation time.

Slice acquisition = number of detector row × detector thickness.

**Table 3. 3** Parameters of DSA examination.

<b>Parameters for DSA examinations</b>			
	<b>Fluoroscopy</b>	<b>2D mode</b>	<b>3D mode</b>
kVp	77	77	70
Pulse width (ms)		40	12.5
kVp filter		81	OFF
kVp mask		96	
Pulse rate	10 pulse/s		
Dose ( $\mu$ Gy/image)		3.6	0.36
Phase 1		4 frame/s	4 s
Phase2		1 frame /s	16 s
Mask		30 frame /s	5 s
Fill		30 frame /s	5 s
Washout		0.5 frame /s	2 s

### 3.5.4 Sample size determination

The sample population in each group is independent and will be determined by formula,

$$N = \frac{2(Z_{\alpha/2} + Z_{\beta})^2 \sigma^2}{(x_1 - x_2)^2} \quad \text{where; } \alpha = 0.05, Z_{\alpha/2} = 1.96, 90\% \beta = 0.1, Z_{\beta} = 1.28$$

$$\begin{aligned} \sigma^2 &= S_p^2 = \frac{SD_1^2 + SD_2^2}{2} ; n_1 = n_2 \\ &= \frac{0.64^2 + 1.21^2}{2} ; n_1 = n_2 \quad (\text{from pilot study}) \\ &= 0.937 \\ (x_1 - x_2)^2 &= (3.68 - 4.49)^2 \\ &= 0.656 \end{aligned}$$

$$\begin{aligned} N &= \frac{2(1.96 + 1.28)^2 0.937}{0.656} \\ &= 30 \text{ cases.} \end{aligned}$$

## 3.6 Materials

### 3.6.1 Research Equipment

#### 3.6.1.1 CT scanner

The 64-MDCT scanner manufacturer Siemens Healthcare, Model Somatom Definition AS installed at Department of Neuroradiology, Prasat Neurological Institute in 2010 as shown in figure 3.1.



**Figure 3. 1** 64-MDCT Siemens Somatom Definition AS.

### **3.6.1.2 DSA system**

Biplane Flat panel detector angiography system manufacturer Siemens Healthcare, Model Axiom Artis installed at Department of Neuroradiology, Prasat Neurological Institute in 2007 as shown in figure 3.2.



**Figure 3. 2** DSA Biplane Flat panel detector Siemens Axiom Artis.

## **3.6.2 Quality Control materials**

### **3.6.2.1 PMMA Phantom**

The CT phantom is manufactured to comply with the FDA performance standard for diagnostic x-ray systems. The cylindrical phantom of two 14 cm lengths is made of solid Polymethyl Methacrylate (PMMA) disks measuring 16 cm (head) diameter as shown in figure 3.3 and 32 cm (body) in diameter.

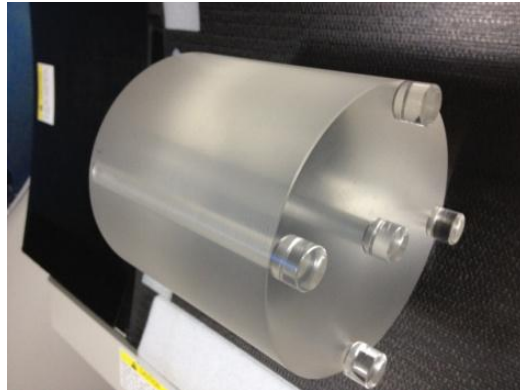


**Figure 3. 3** Cylindrical PMMA phantom of 16 cm diameter.

There are 5 holes with acrylic rods to plug the holes for the phantoms when not in use. Through holes are 1.31 cm in diameter and 14 cm length to accommodate standard CT probes. One is at center and four are around the perimeter, 90° apart and 1 cm hole center to the outside edge of each phantom.

### 3.6.2.2 Catphan® 600 phantom

Catphan® 600 phantom was used for the performance study of the CT scanner as shown in Figure 3.4.

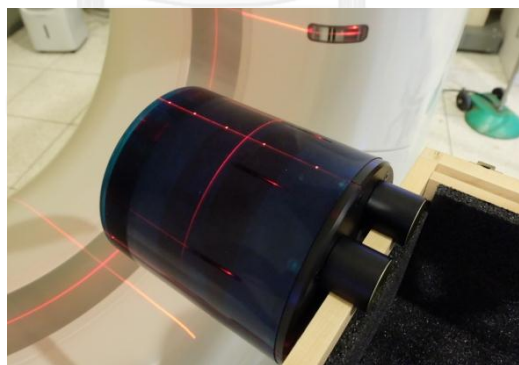


**Figure 3. 4** Catphan® 600 Phantom.

The Catphan® phantom was positioned in the CT scanner by mounting on the case placed directly at the end of the table.

The Catphan® 600 phantom is all test sections located by precisely indexing the table from center of section 1 (CTP404) to the center of each

subsequence test module. The indexing distances from section 1 are Catphan® 600 test module locations:

Module	Distance from section 1 center
CTP404, Slice width, Sensitometer and pixel size	
CTP591, Bead geometry	32.5 mm
CTP528, 21-line pair high resolution	70.0 mm
CTP528, Point source	80.0 mm
CTP515, Sub-slice and supra-slice low contrast	110.0 mm
CTP486, Solid image uniformity module	150.0 mm

### 3.6.2.3 Copper sheets

Copper sheets; 0.5 mm (4 sheets) and 1 mm (2 sheets) thickness were used to drive kVp during QC of DSA system.

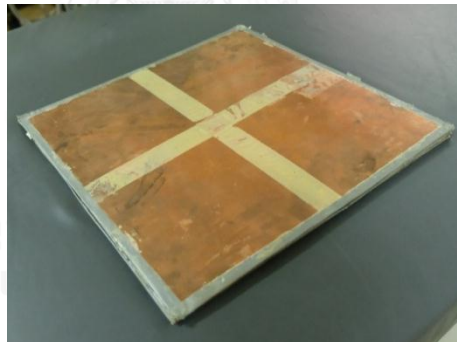


**Figure 3. 5** Copper sheets.

### 3.6.2.4 Unfors Ray Safe Xi Pencil ionization chamber, 10 cm active length

CT pencil-type ionization chamber of 4.9 cm<sup>3</sup> active volume, 10 cm total active length is shown in Figure 3.6. The Unfors Xi CT detector is a new hybrid ion chamber designed by Unfors. The ion chamber and electronics are combined into one unit making it possible to measure both temperature and pressure to actively compensate for this dependency. The temperature is actually measured inside the ion chamber giving very precise compensations both with and without

a CT phantom. With no baseline drift, this carbon fiber ion chamber is ready to use within one minute.



**Figure 3. 6** Unfors Xi CT Detector 10 cm length of the pencil-type ionization.

**Table 3. 4** Characteristics of Unfors model Xi platinum dosimeter.

Unfors Xi CT detector	
Unfors Xi base unit firmware	4.0 or higher
Size detector	200 x 20 x 12 mm (7.9 x 0.8 x 0.5 in)
Size diameter detector	7.5 mm (0.30 in)
Size diameter phantom adapter	12.5 mm (0.49 in)
Effective length	100 mm (3.94 in)
Weight	50 g (1.75 oz)
Range	10 $\mu$ Gy – 9999 Gy (1 mR – 9999 R) 20 $\mu$ Gy/s – 100 mGy/s (140 mR/min – 680 R/min)
Uncertainty	5% (at 80 kV-150 kV; RQR and RQA qualities)
Radial uniformity	$\pm 2\%$
Axial uniformity	$\pm 3\%$ , within rated length
Influence of relative humidity	< 0.3% (for RH < 80%) Uncertainty in Temp and pressure correction 2%
Pressure range	80.0 – 106.0 kPa
International standard	Fulfill requirements in IEC 61674

### 3.6.2.5 UnforsRaySafe Xi R/F dosimeter

The Unfors Xi dosimeter (Figure 3.7) is a complete system for multi-parameter measurements on all modalities. The detector is solid state type which is not affected by the temperature and pressure of the environment. The system



can be used for the calibration of the radiographic-fluoroscopic, mammography, dental and CT systems with and added option for luminance and illuminance measurements of medical monitors. All Unfors Xi detectors are interchangeable and function with any base unit.



**Figure 3. 7** Unfors Ray Safe Xi R/F dosimeter.

### 3.7 Methods

The study was carried on as the following steps

1. Quality control of MDCT scanner, verification of  $CTDI_{vol}$  and DLP.
2. Quality control of DSA system.
3. Patient data collection from CTA and DSA examination.
4. Patient effective dose calculation.

#### 3.7.1 Perform the quality control of Siemens Somatom Definition

##### AS 64-MDCT

The quality control of CT scanner was performed following the AAPM report No.39 (1993): specification and acceptance testing of CT scanner [20] in the part of performance evaluation and ImPACT information leaflet 1: CT scanner acceptance testing version 1.02. [21] The quality control program consists of the test of performance of electromechanical components, image quality and radiation dose.

#### 3.7.2 Verification of $CTDI_{vol}$ and DLP

The  $CTDI_{vol}$  and DLP values are displayed on the monitor of the console of Siemens Somatom Definition AS 64-MDCT. To make a confidence of using these values, the verification of  $CTDI_{vol}$  and DLP will be performed.

### **3.7.3 Perform the quality control of Siemens Axiom Artis Biplane Flat panel detector**

The performances of the DSA system will be evaluated for;

- Dose assessment
- Automatic brightness control test
- Maximum dose rate assessment
- Table attenuation
- Half value layer
- Image quality assessment

### **3.7.4 Data Collection**

#### **3.7.4.1 Patient selection**

Random select the patients that have already been performed CTA and DSA examinations in Neuroradiology department at Prasat Neurological Institute in November 2014 – June 2015 (6 months) for CTA 30 cases and DSA 30 cases. The cases selection is under the inclusion and exclusion criteria (3.5.3).

#### **3.7.4.2 Data recording**

Record data into case record form (Appendix A, page 91-92);

- Patient characteristics: age, gender, height, weight, body mass index (BMI).
- Parameters setting, Acquisition protocols, kVp and mAs.
- The DLP read out from CT monitor or PACS.
- The DAP read out from DSA monitor or PACS.

This data was collected at Computed Tomography unit and Digital Subtraction Angiography unit, Department of Neuroradiology, Prasat Neurological Institute, Bangkok Thailand, using 64-MDCT Siemens Somatom Definition AS 64 and Siemens Biplane Flat panel detector Axiom Artis.

#### **3.7.5 Effective dose calculation**

Calculate the effective dose by using equations;

- Effective dose (mSv) from CTA = DLP (mGy.cm)  $\times$  k-factor (mSv/mGy.cm) [3]; k-factor (Conversion factors) is 0.0019 mSv/mGy.cm for CTA brain. [19]
- Effective dose (mSv) from DSA = DAP (mGy.cm<sup>2</sup>)  $\times$  Dose conversion coefficient (DCCE; mSv/mGy.cm<sup>2</sup>) [3]; DCCE is 0.087 mSv/mGy.cm<sup>2</sup> for cerebral angiogram. [22]

MS excel was using for recorded the data and analyzed the mean, standard deviation, minimum and maximum of effective dose.

IBM SPSS statistics version 22 was using for analyzed;

- The independent sample t-test the effective dose between CTA and DSA.
- The Spearman's Correlation coefficient between effective dose and the factors affecting the dose from CTA and DSA.

### 3.8 Variables measurement

Measure independent and dependent variables;

**3.8.1** Independent variables: Scanning parameters of CTA, Acquisition protocols of DSA.

**3.8.2** Dependent variables: DLP (mGy.cm), DAP (mGy.cm<sup>2</sup>), Effective dose (mSv).

### 3.9 Statistical analysis

**3.9.1** The independent-samples t-test statistics was used for data analysis by SPSS (version 22) statistical analyzing program.

**3.9.2** Descriptive statistics: mean, median, mode, standard deviation, minimum, maximum and range of effective dose were determined with the excel program.

**3.9.3** Correlation coefficient between the effective dose and patient characteristics and protocols of CTA and DSA were determined by Spear's man correlation.

### **3.10 Data analysis**

The verification of  $CTDI_{vol}$  will be reported as percentage difference between the displayed and the measured for each kVp setting. After that the radiation dose data for specific parameter setting will be collected from the values of  $CTDI_{vol}$  and DLP displayed on the CT console in the unit of mGy and mGy.cm, respectively, presented in form of table and graph.

Data from patients will be reported as mean, median, mode, standard deviation, minimum, maximum and range presented in form of table.

The data of DLP displayed on CT monitor will be obtained for the calculation of the effective dose for CTA examination and DAP values displayed on DSA console will be obtained for the calculation of the effective dose for DSA examination presented in form of table and scatter plot, the comparisons of effective dose between CTA and DSA will be presented in form of table and box plots.

### **3.11 Outcomes**

The patient effective dose will be calculated by using the DLP from CTA examination and DAP from DSA in each patient.

### **3.12 Expected benefits**

The effective dose from CTA and DSA examinations are expected from this study. These would be beneficial to the patients and the radiologists in order to justify requesting the examination or further investigations. The patient dose reduction should be considered for the radiation safety for the patients.

### **3.13 Ethical consideration**

Although the patient data will be collected from the monitor or PACS system of the hospital, the patient radiation dose had been calculated retrospectively, without any direct contact to patients. The research proposal had been submitted and approved by the Ethic Committee of Faculty of Medicine, Chulalongkorn University and Ethic Committee of Prasat Neurological Institute.

## CHAPTER IV

### RESULT

#### 4.1 Quality control of the CT scanner: Siemens Somatom Definition AS

The quality control of CT scanner was performed following AAPM report No.39 [20] and ImPACT Information Leaflet [21]. It includes the test of electromechanical component, image quality and radiation dose. The detail of quality control of CT scanner is shown with the summarized report of CT scanner performance test in Appendix B (page 94).

#### 4.2 Quality control of the DSA equipment: Siemens Axiom Artis

The performance of the digital subtraction angiography equipment was evaluated including the test of electromechanical component, dose assessment, automatic brightness control test, maximum dose rate assessment, table attenuation, image size assessment, half value layer assessment and image quality assessment. The results are shown in Appendix B (page 108).

#### 4.3 Patient data and radiation dose calculation from CTA examination

The patient data and scanning parameters of CTA examination were recorded from CT console or PACS. The effective dose was calculated by using DLP (mGy.cm) values multiplied by k – factor 0.0019 mSv/mGy.cm for CTA the brain. [19]

##### 4.3.1 Patient characteristics of CTA examination and effective dose

Patient characteristics of 30 cases (15 male, 15 female) from CTA examination in Neuroradiology department at Prasat Neurological Institute in November 2014 – June 2015 (6 months) were recorded as show in Table 4.1. The mean age was  $49 \pm 17$  year (23-89 year). The mean of patient height and weight were  $161 \pm 10$  (140-180) cm and  $62 \pm 13$  (37-85) kg. The mean BMI patient was  $24 \pm 4$  (17-31)  $\text{kg/m}^2$ . The results are shown in Table 4.2.

**Table 4. 1** Patient characteristics of 30 cases from CTA examination.

Case No.	Gender (M, F)	Age (year)	Height (cm)	Weight (kg)	BMI (kg/m <sup>2</sup> )	Effective Dose (mSv)
1	F	48	158	70	28.04	3.47
2	M	39	165	85	31.22	5.19
3	F	89	140	37	18.88	2.82
4	F	31	170	50	17.30	3.10
5	M	51	176	85	27.44	4.26
6	M	39	165	74	27.18	3.93
7	F	50	155	56	23.31	2.96
8	M	45	160	70	27.34	4.23
9	M	45	160	70	27.34	4.14
10	M	23	180	70	21.60	3.72
11	M	63	162	68	25.91	3.46
12	M	24	172	76	25.69	4.65
13	M	23	168	85	30.12	5.13
14	M	54	154	57	24.03	3.32
15	M	42	179	63	19.66	3.28
16	F	33	150	45	20.00	4.13
17	M	57	161	60	23.15	3.46
18	M	45	178	65	20.52	3.49
19	F	43	153	48	20.50	2.85
20	F	57	152	49	21.21	3.24
21	F	48	156	60	24.65	3.03
22	F	38	160	56	21.88	3.14
23	F	62	159	75	29.67	3.78
24	M	32	165	60	22.04	4.34
25	F	82	150	41	18.22	2.87
26	F	86	149	54	24.32	4.35
27	F	74	155	75	31.22	3.17
28	F	47	156	65	26.71	3.99
29	M	55	165	62	22.77	4.37
30	F	61	150	42	18.67	3.22

**Table 4. 2** Patient characteristics from CTA examination.

Patient characteristics	Mean $\pm$ SD	Min	Max
Age (year)	49 $\pm$ 17	23	89
Height (cm)	161 $\pm$ 10	140	180
Weight (kg)	62 $\pm$ 13	37	85
BMI (kg/m <sup>2</sup> )	24 $\pm$ 4	17	31

#### 4.3.2 The correlation between effective dose and patient characteristics of CTA examination

The correlation between effective dose and patient characteristics for CTA examination has been investigated. The results show;

- A significant strong linear relationship between the effective dose and body weight ( $r = 0.642$ ,  $p < 0.001$ ).
- A significant moderate linear relationship between the effective dose and BMI ( $r = 0.552$ ,  $p = 0.002$ ) and height ( $r = 0.445$ ,  $p = 0.014$ ).
- Not significant weak linear relationship between the effective dose and patient age ( $r = -0.353$ ,  $p = 0.056$ ).

Table 4.3 shows the relationship by Spearman's correlation.

**Table 4. 3** The correlations between effective dose and patient characteristics of CTA examination.

Patient characteristics	Correlation coefficient (r)	p value
Weight	.642**	<.001
BMI	.552**	.002
Height	.445*	.014
Age	-.353	.056

\*\* . Correlation is significant at the 0.01 ( $p < 0.01$ ) level (2-tailed).

\* . Correlation is significant at the 0.05 ( $p < 0.05$ ) level (2-tailed).

The correlation between effective dose and patient characteristics for CTA examination are plotted separately as show in figure 4.1.

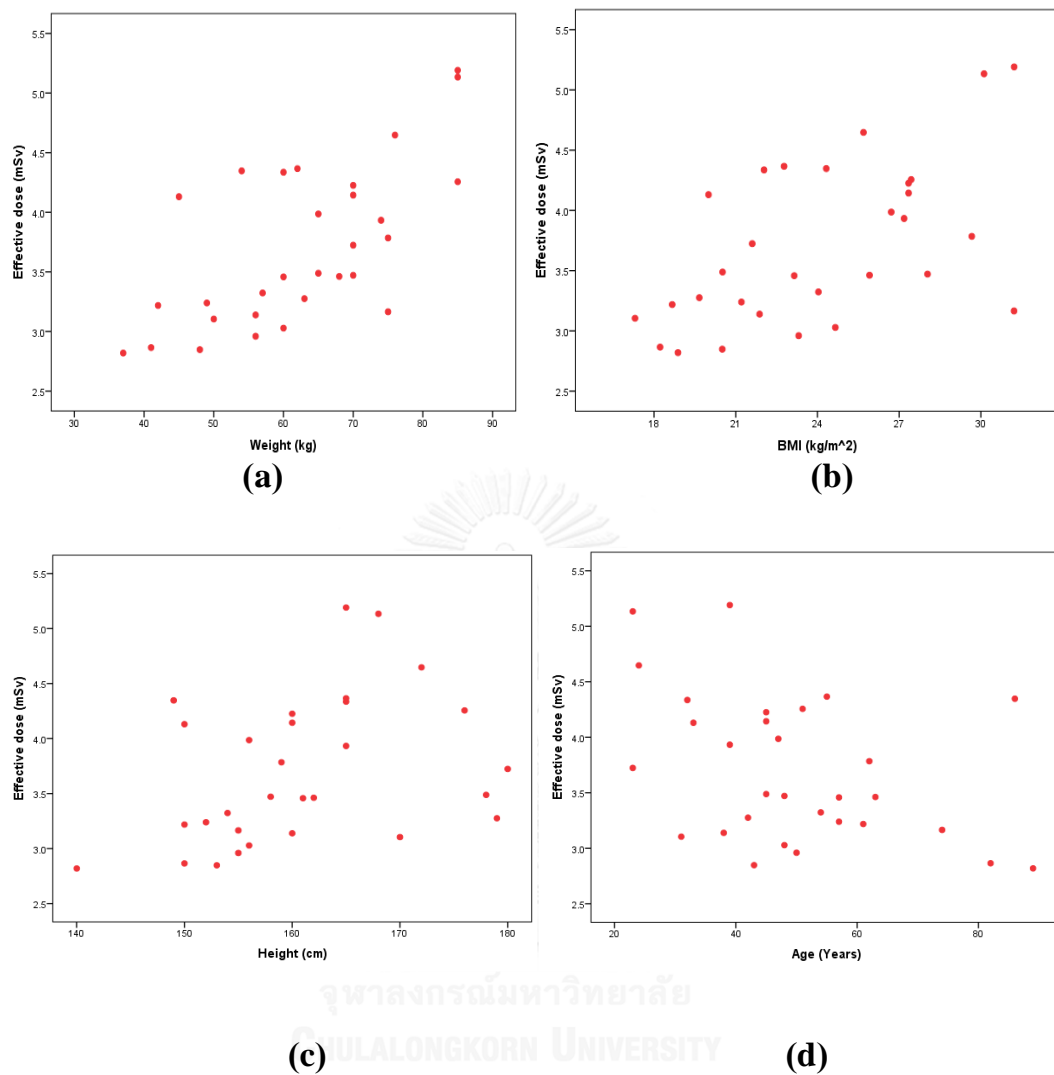


**Figure 4. 1** Scatter plots of correlations between the effective dose and; (a) weight, (b), BMI (c) height and (d) age from 30 patients who underwent CTA examination of the brain, respectively.

#### 4.3.3 Scanning parameters of CTA examination and effective dose

Scanning parameters affecting the effective dose of 30 patients from CTA examination were recorded. Slice collimation 0.6 mm, slice acquisition 64×0.6 mm had been set for all cases. The tube voltage 100 – 120 kVp, references tube current 158 – 450 mAs, pitch factor 0.55 – 1.4, tube rotation time 0.33-1 s and coverage (scan length) were varied by two protocols. The results of scanning parameters, DLP and calculated effective dose are shown in Table 4.4.



**Table 4. 4** Scanning parameters, DLP and effective dose from CTA of 30 patients.

Case No.	Tube voltage (kVp)	Tube current (total mAs)	Scan Length (cm)	DLP (mGy.cm)	Effective Dose (mSv)
1	120	7396	20.06	1827	3.47
2	120	9800	24.25	2732	5.19
3	100	6566	19.24	1484	2.82
4	100	7279	20.55	1634	3.10
5	120	9148	20.56	2240	4.26
6	120	8358	22.85	2070	3.93
7	100	6995	17.76	1558	2.96
8	120	8274	22.53	2224	4.23
9	120	8142	22.85	2181	4.14
10	100	8588	21.41	1960	3.72
11	100	8027	20.90	1822	3.46
12	120	9068	23.74	2446	4.65
13	120	9975	23.84	2702	5.13
14	120	7142	18.64	1749	3.32
15	100	7681	18.44	1724	3.28
16	120	8014	21.44	2174	4.13
17	100	8103	21.25	1820	3.46
18	120	7519	20.16	1836	3.49
19	100	6591	21.93	1499	2.85
20	100	7476	22.14	1705	3.24
21	100	7056	19.85	1594	3.03
22	120	6837	18.74	1652	3.14
23	120	7513	19.14	1992	3.78
24	120	8296	23.46	2282	4.34
25	100	6698	22.33	1508	2.87
26	120	8337	21.10	2288	4.35
27	100	7486	17.25	1666	3.17
28	120	7723	19.65	2098	3.99
29	120	9090	20.74	2298	4.37
30	120	6964	19.45	1694	3.22

**Table 4. 5** Scanning parameters from CTA examination.

Parameters	Mean $\pm$ SD	Min	Max
Tube voltage (kVp)	-	100	120
Tube current (total mAs)	7871 $\pm$ 908	6566	9975
Scan Length (cm)	20.76 $\pm$ 1.87	17.25	24.25
DLP (mGy.cm)	1948.63 $\pm$ 348	1484	2732

#### 4.3.4 The correlation between effective dose and scanning parameters of CTA examination

The correlation between effective dose and scanning parameters for CTA examination has been investigated. The results show;

- A significant very strong linear relationship between the effective dose and mAs ( $r = 0.931$ ,  $p < .001$ ).
- A significant strong linear relationship between the effective dose and kVp ( $r = 0.723$ ,  $p < .001$ ).
- A significant moderate relationship between the effective dose and scan length ( $r = 0.574$ ,  $p < .001$ ).

Table 4.6 shows the relationship by Spearman's correlation.

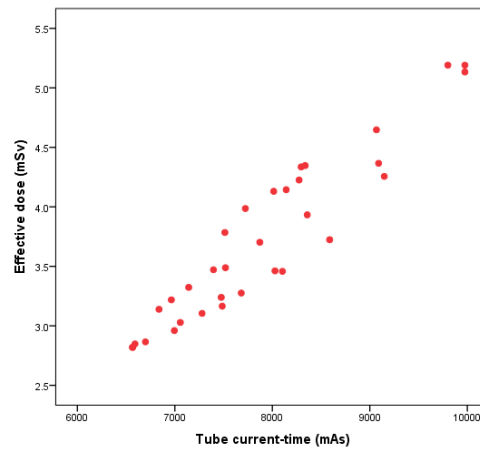
**Table 4. 6** The correlations between effective dose and scanning parameters of CTA examination.

Scanning parameters	Correlation coefficient (r)	p value
mAs	0.931**	<.001
kVp	0.723**	<.001
Scan length	0.574**	<.001

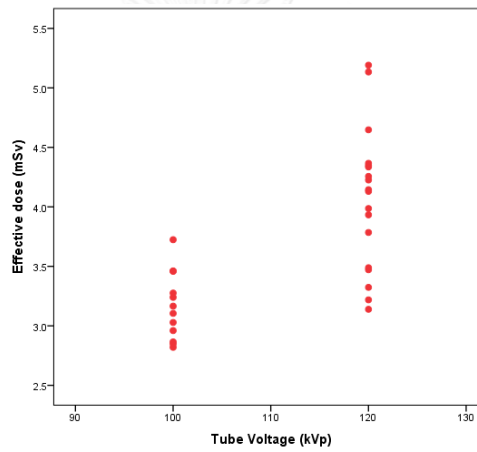
\*\* . Correlation is significant at the .01 ( $p < .01$ ) level (2-tailed).

\* . Correlation is significant at the .05 ( $p < .05$ ) level (2-tailed).

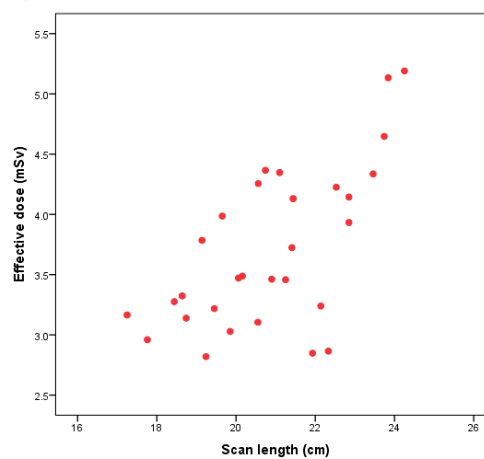
The correlation between effective dose and scanning parameters of CTA examination are plotted separately as show in figure 4.2.



(a)



(b)



(c)

**Figure 4. 2** Scatter plot of correlation between the effective dose and; (a) mAs, (b) kVp and (c) scan length from 30 patients who underwent CTA examination of the brain, respectively.

The effective dose from CTA examination in each patient is plotted against 30 cases as shown in figure 4.3.

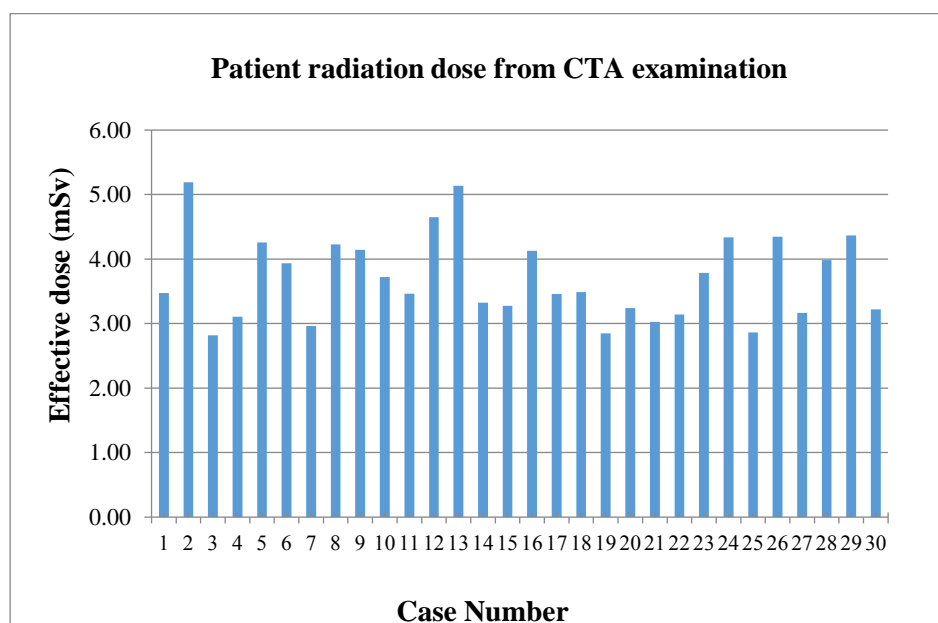


**Figure 4. 3** Bar chart of the effective dose from 30 patients who underwent CTA examination of the brain.

#### 4.4 Patient radiation dose from DSA examination

The patient data and parameters of DSA examination were recorded from DSA console or PACS. The effective dose was calculated by using DAP values ( $\text{mGy}\cdot\text{cm}^2$ ) multiplied by dose conversion coefficient of  $0.087 \text{ mSv}/\text{mGy}\cdot\text{cm}^2$  for cerebral angiogram. [22]

##### 4.4.1 Patient characteristics and effective dose

Patient characteristics of 30 cases (14 male, 16 female) from DSA examination in Neuroradiology department at Prasat Neurological Institute in November 2014 – June 2015 (6 months) were recorded as show in Table 4.7. The mean age was  $47\pm 16$  year (24-81 year). The mean of patient height and weight were  $162\pm 10$  (140-180) cm and  $60\pm 14$  (42-83) kg. The mean BMI patient was  $23\pm 4$  (17-36)  $\text{kg}/\text{m}^2$ . The results are shown in Table 4.8.

**Table 4. 7** Patient characteristics and effective dose from DSA examination in 30 patients.

Case No.	Gender (M, F)	Age (year)	Height (cm)	Weight (kg)	BMI (kg/m <sup>2</sup> )	Effective dose (mSv)
1	F	32	172	75	25.35	4.72
2	F	56	179	73	22.78	7.69
3	M	81	160	54	21.09	7.78
4	M	69	147	56	25.92	5.99
5	F	58	148	51	23.28	4.25
6	F	32	162	70	26.67	3.30
7	F	27	173	62	20.72	5.04
8	F	68	170	51	17.65	5.55
9	M	26	156	49	20.13	4.98
10	F	64	155	44	18.31	5.40
11	F	52	157	49	19.88	6.36
12	M	29	162	57	21.72	5.71
13	F	24	180	72	22.22	4.64
14	F	39	161	64	24.69	5.06
15	M	57	140	45	22.96	7.05
16	M	63	162	68	25.91	5.38
17	F	22	152	45	19.48	6.22
18	M	52	170	80	27.68	4.27
19	M	36	168	71	25.16	7.73
20	F	47	168	48	17.01	3.91
21	F	51	163	51	19.20	7.82
22	M	60	170	50	17.30	7.73
23	M	34	168	58	20.55	5.86
24	M	21	159	47	18.59	3.83
25	F	28	162	47	17.91	5.28
26	F	49	162	75	28.58	6.04
27	F	32	175	75	24.49	9.28
28	F	41	170	83	28.72	10.06
29	M	31	150	52	23.11	6.28
30	M	61	150	42	18.67	4.93

**Table 4. 8** Patient characteristics from DSA examination.

Patient characteristics	Mean $\pm$ SD	Min	Max
Age (year)	47 $\pm$ 16	24	81
Height (cm)	162 $\pm$ 10	140	180
Weight (kg)	60 $\pm$ 14	42	83
BMI (kg/m <sup>2</sup> )	23 $\pm$ 4	17	36

#### 4.4.2 The correlation between effective dose and patient characteristics of DSA examination

The correlation between effective dose and patient characteristics for DSA examination has been investigated. The results show not significant statistic ( $p > .05$ ) and weak linear relationship ( $r < 0.3$ ) between the effective dose and patient characteristics. Table 4.9 shows the relationship by Spearman's correlation.

**Table 4. 9** The correlations between effective dose and patient characteristics of DSA examination.

Patient characteristics	Correlation coefficient (r)	p value
Age	0.257	.170
Weight	0.132	.487
Height	0.077	.686
BMI	0.079	.680

\*\* . Correlation is significant at the .01 ( $p < .01$ ) level (2-tailed).

\* . Correlation is significant at the .05 ( $p < .05$ ) level (2-tailed).

The correlation between effective dose and parameters of DSA examination are plotted separately as shown in figure 4.4.

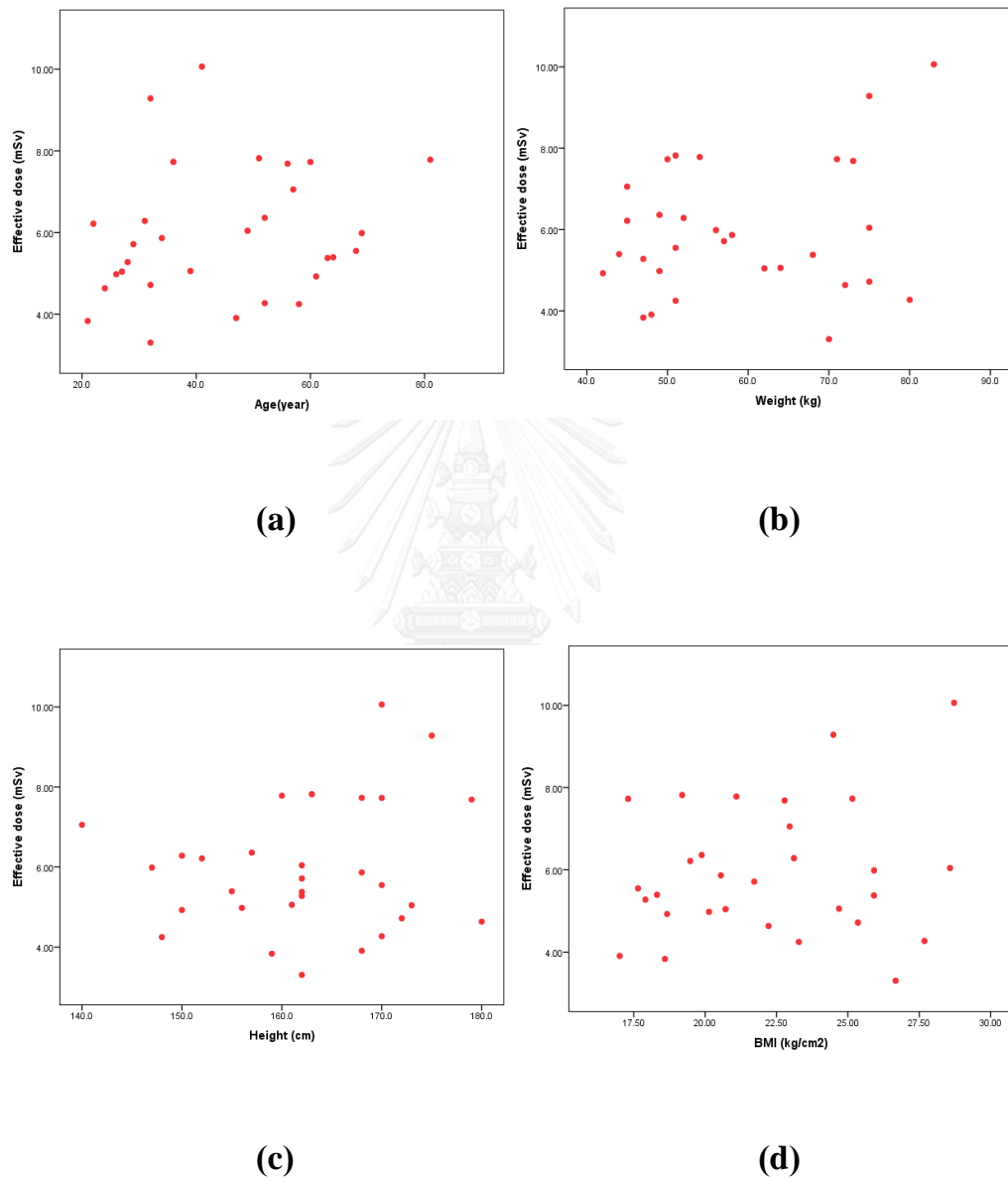


**Figure 4. 4** Scatter plots of correlations between the effective dose and; (a) age, (b) weight, (c) height, (d) BMI from 30 patients underwent cerebral angiogram examination, respectively.

#### 4.4.3 The acquisition parameters of DSA examination and effective dose

The acquisition parameters of DSA examination were recorded and the effective dose was calculated in each patient. The results show in Table 4.10.

**Table 4. 10** The acquisition parameters and effective dose from DSA of 30 patients.

Case No.	No. of vessels	No. of 2D radiography	No. of 3D RA	Flu. Time (minute)	Experience of Radiologist (year)	DAP (Gycm <sup>2</sup> )	Effective dose (mSv)
1	5	10	0	11.8	2	54.2	4.72
2	6	18	2	17.1	18	88.3	7.69
3	3	12	3	9.4	9	89.4	7.78
4	5	16	3	11.8	28	68.8	5.99
5	3	10	2	7.7	7	48.8	4.25
6	4	8	0	11.4	7	38.0	3.30
7	4	11	1	10.9	5	58.0	5.04
8	5	13	1	7.5	7	63.8	5.55
9	5	14	1	8.7	5	57.2	4.98
10	3	15	3	14.0	2	62.0	5.40
11	5	16	2	11.5	28	73.1	6.36
12	5	14	1	9.7	5	65.7	5.71
13	3	8	1	4.9	18	53.3	4.64
14	7	14	0	18.9	18	58.1	5.06
15	4	22	4	17.1	2	81.1	7.05
16	3	9	1	21.5	5	61.8	5.38
17	5	16	3	8.8	28	71.4	6.22
18	3	8	1	10.4	18	49.1	4.27
19	5	16	2	10.2	18	88.9	7.73
20	3	8	1	5.3	7	44.9	3.91
21	4	18	4	13.3	18	89.9	7.82
22	7	14	0	13.1	18	88.8	7.73
23	4	18	1	9.6	18	67.4	5.86
24	3	8	1	7.9	18	44.1	3.83
25	5	12	1	8.6	18	60.7	5.28
26	3	12	3	3.9	5	69.5	6.04
27	6	20	2	16.6	3	106.7	9.28
28	4	17	4	14.6	18	115.7	10.06
29	6	17	2	6.4	7	72.2	6.28
30	3	12	3	5.5	18	56.6	4.93



**Table 4. 11** The acquisition parameters of DSA examination (Factors affecting the effective dose).

Parameters	Mean $\pm$ SD	Min	Max
DAP (Gy.cm <sup>2</sup> )	6825.2 $\pm$ 1825.4	3797.8	11565
Number of Vessels	4 $\pm$ 1.25	3	7
No. of 2D Radiography	14 $\pm$ 3.89	8	22
Number of 3D RA	2 $\pm$ 1.22	0	4
Fluoroscopic time (minute)	11 $\pm$ 4.31	4	22
Experience of Radiologist (year)	13 $\pm$ 8.2	2	28

#### 4.4.4 The correlation between effective dose and acquisition parameters of DSA examination

The correlation between effective dose and acquisition parameters of DSA examination has been investigated. The results show;

- A significant very strong linear relationship between the effective dose and number of 2D radiography ( $r = 0.818$ ,  $p < .001$ ).
- A significant moderate linear relationship between the effective dose and, the number of 3D rotational angiography ( $r = 0.580$ ,  $p = .001$ ), the number of vessels ( $r = 0.427$ ,  $p = .019$ ) and fluoroscopic time ( $r = 0.407$ ,  $p = .026$ ).
- Not significant weak linear relationship between the effective dose and experience of Radiologist for 2-28 year ( $r = 0.337$ ,  $p = .451$ ).

Table 4.12 shows the relationship by Spearman's correlation.

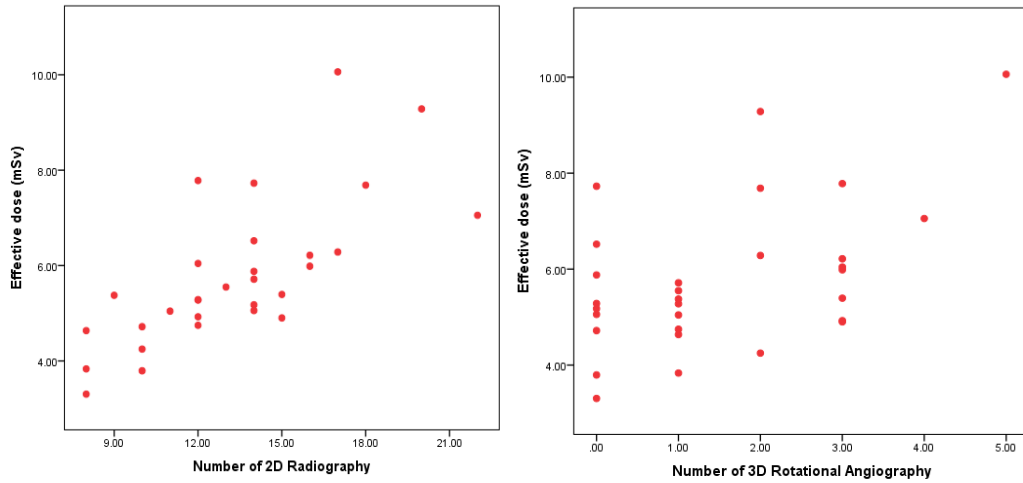
**Table 4. 12** The correlation between effective dose and acquisition parameters of DSA examination.

Parameters	Correlation coefficient (r)	p value
Number of 2D radiography	0.818**	<0.001
Number of 3D RA	0.580**	0.001
Number of Vessels	0.427*	0.019
Fluoroscopic time	0.407*	0.026
Experience of Radiologist	0.337	0.451

\*\* . Correlation is significant at the .01 ( $p < .01$ ) level (2-tailed).

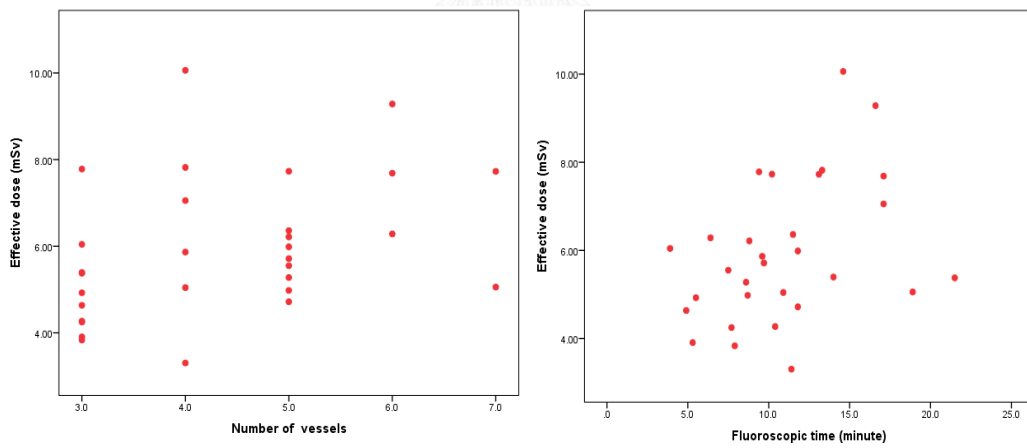
\* . Correlation is significant at the .05 ( $p < .05$ ) level (2-tailed).

The correlation between effective dose and parameters of DSA examination are plotted separately as shown in figure 4.5.



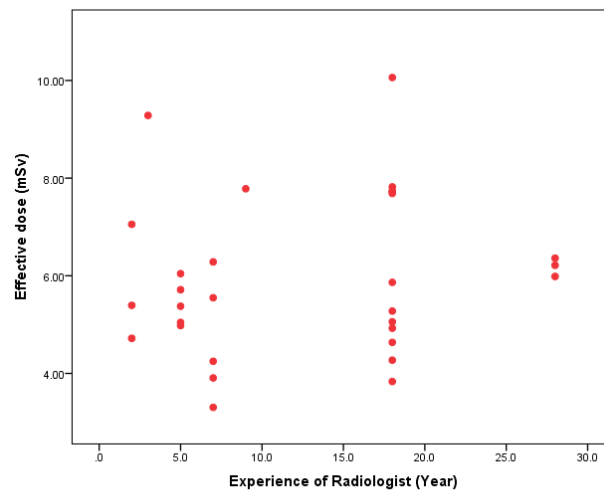
(a)

(b)



(c)

(d)



(e)

**Figure 4. 5** Scatter plots of correlations between the effective dose and; (a) number of 2D radiography, (b) number of 3D RA, (c) number of vessel, (d) fluoroscopic time and (e) experience of Radiologist from 30 patients underwent cerebral angiogram examination, respectively.

Effective dose from DSA examination in 30 patients is plotted in figure 4.6.

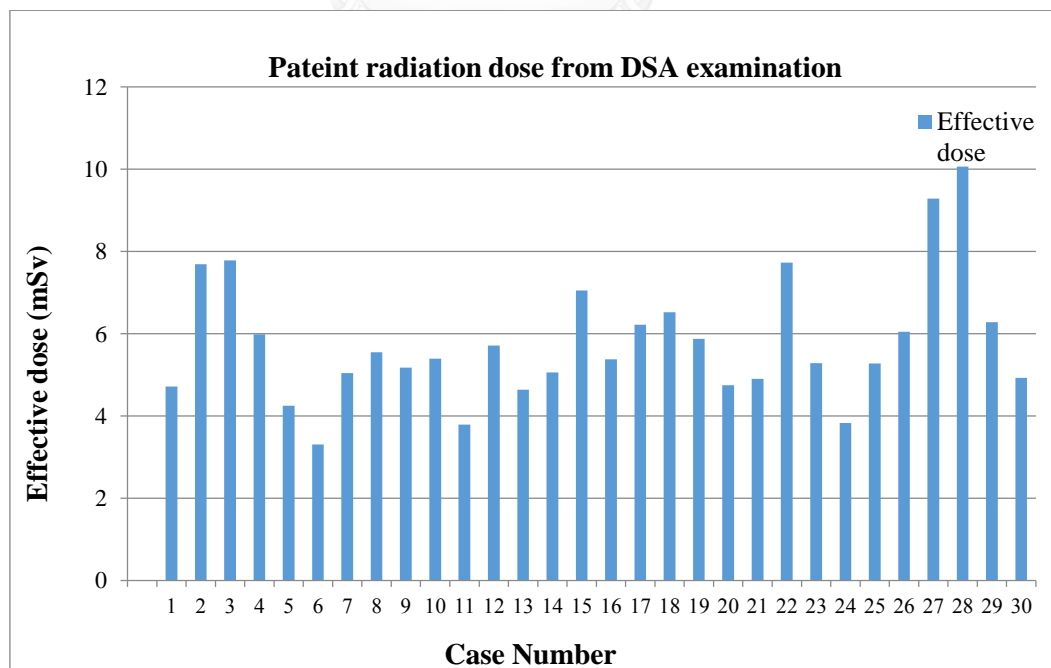


**Figure 4. 6** The effective dose from 30 patients underwent DSA examination.

#### 4.5 Comparison of the effective dose from CTA and DSA examination

The mean effective dose related to patient characteristic is 3.70 mSv range from 2.82 - 5.19 mSv for CTA (15 male, 15 female, 49 yrs. mean age and 24.02 kg/m<sup>2</sup> BMI). For DSA the mean effective dose was 5.94 mSv range from 3.30 – 10.06 mSv (14 male, 16 female, 47 yrs. mean age and 22.82 kg/m<sup>2</sup> BMI). The effective dose between CTA and DSA examinations was statistically significant difference ( $p < .001$ ). Patient characteristics between CTA and DSA examinations were not significant difference. The results are shown in Table 4.13.

**Table 4. 13** Effective dose and patient characteristics for CTA and DSA.

		<b>CTA</b>	<b>DSA</b>	<b>p value</b>
Effective dose (mSv)	Mean $\pm$ SD	3.70 $\pm$ 0.66	5.94 $\pm$ 1.61	< .001
	Min, Max	2.82, 5.19	3.30, 10.06	
Gender	Male	15 (50%)	14 (46.67%)	.800
	Female	15 (50%)	16 (53.33%)	
Age (year)	Mean $\pm$ SD	49 $\pm$ 17.30	47 $\pm$ 16.12	.529
	Min, Max	23, 89	24, 81	
BMI (kg/m <sup>2</sup> )	Mean $\pm$ SD	24.02 $\pm$ 4.01	22.82 $\pm$ 4.27	.265
	Min, Max	17.30, 31.22	17.01, 35.94	

**Table 4. 14** The range of effective dose for CTA and DSA examination.

No.	Examinations			
	CTA		DSA	
	Case number	Effective dose (mSv)	Case number	Effective dose (mSv)
1	3	2.82	6	3.30
2	19	2.85	24	3.83
3	25	2.87	20	3.91
4	7	2.96	5	4.25
5	21	3.03	18	4.27
6	4	3.10	13	4.64
7	22	3.14	1	4.72
8	27	3.17	30	4.93
9	30	3.22	9	4.98
10	20	3.24	7	5.04
11	15	3.28	14	5.06
12	14	3.32	25	5.28
13	17	3.46	16	5.38
14	11	3.46	10	5.40
15	1	3.47	8	5.55
16	18	3.49	12	5.71
17	10	3.72	23	5.86
18	23	3.78	4	5.99
19	6	3.93	26	6.04
20	28	3.99	17	6.22
21	16	4.13	29	6.28
22	9	4.14	11	6.36
23	8	4.23	15	7.05
24	5	4.26	2	7.69
25	24	4.34	22	7.73
26	26	4.35	19	7.73
27	29	4.37	3	7.78
28	12	4.65	21	7.82
29	13	5.13	27	9.28
30	2	5.19	28	10.06

The effective dose between examinations displayed as box plots is shown in Figure 4.7.

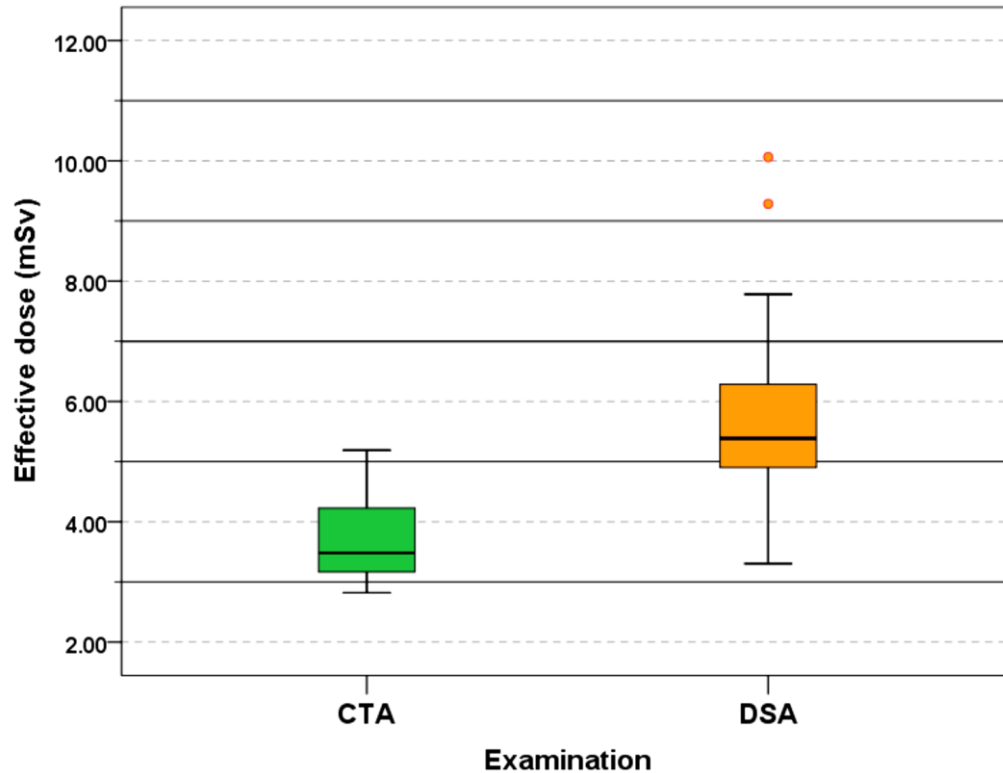


**Figure 4. 7** Box plots show the distribution of effective dose for the CTA 30 cases and DSA 30 cases. The bar indicates the range of effective dose, boxes contain all value of effective dose within 25<sup>th</sup> to 75<sup>th</sup> percentiles (interquartile range) and thick black lines represent the median.

**Table 4. 15** The statistical profiles of CTA examination.**Statistics**

Statistics		DLP (mGy.cm)	Effective dose (mSv)
N	Valid	30	30
Mean		1948.63	3.70
Median		1831.50	3.48
Mode		1484	2.82
Std. Deviation		348.07	0.66
Variance		121156.03	0.43
Range		1248	2.73
Minimum		1484	2.82
Maximum		2732	5.19
Percentiles	25 <sup>th</sup>	1662.50	3.16
	75 <sup>th</sup>	2228.00	4.23

**Table 4. 16** The statistical profiles of DSA examination.

**Statistics**

Statistics		DAP (Gy.cm <sup>2</sup> )	Effective dose (mSv)
N	Valid	30	30
Mean		68.25	5.93
Median		64.73	5.63
Mode		38.0	3.30
Std. Deviation		18.52	1.61
Variance		343.13	2.59
Range		77.7	6.75
Minimum		38.0	3.30
Maximum		115.7	10.06
Percentiles	25 <sup>th</sup>	56.02	4.87
	75 <sup>th</sup>	82.89	7.21



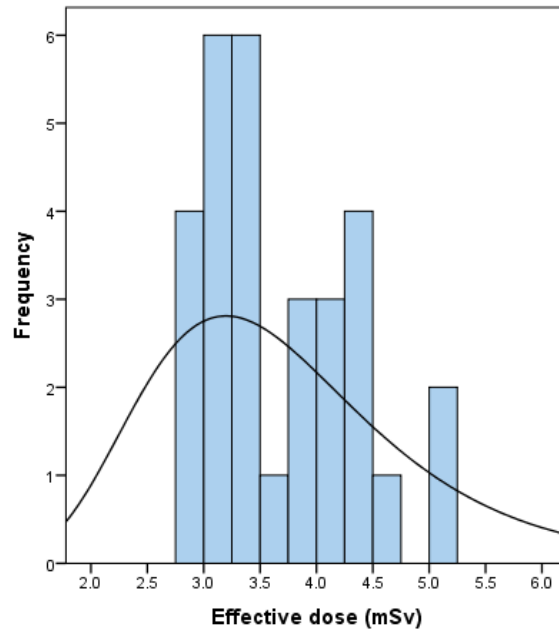


**Figure 4. 8** Distribution of effective dose for the CTA 30 cases.

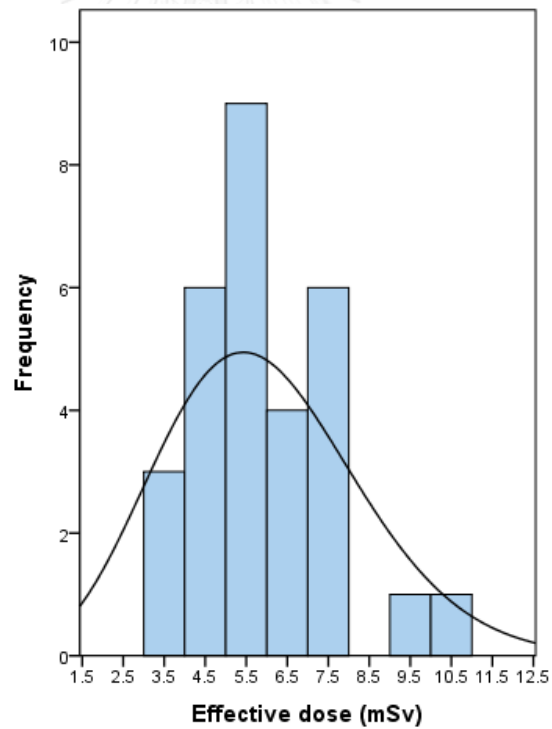


**Figure 4. 9** Distribution of effective dose for the DSA 30 cases.

## CHAPTER V

### DISCUSSION AND CONCLUSION

#### 5.1 Discussion

Although the DSA is the gold standard for vascular imaging, it is invasive technique that gives a risk to the patient. CT technology has been rapidly developed by many manufactures. The increasing of the detector row results in faster scanning. Some study concludes that the 64 -MDCTA provides diagnostic information similar to DSA of cervicocerebral vessels. CTA can replace DSA for vascular imaging in some part of the body [14]. An important principle guiding the diagnostic use of radiation is to keep the radiation exposure as low as reasonably achievable. Because DSA and CTA have different irradiation geometries and the radiation exposure is in different quantities, the effective dose is a useful means of comparing the stochastic risks, such as cancer induction, malignant disease or heritable effects caused by an exposure to ionization radiation [23]. In this study, the patient radiation dose in terms of effective dose from CTA and DSA of the brain was determined by using DLP and DAP values. The factors affecting patient dose were evaluated.

##### 5.1.1 Patient effective dose from CTA of the brain

Generally, the effective dose is computed by using Monte Carlo dose simulation tools for reference human phantoms. The practical method used in clinical routine is to estimate the effective dose from dose-length product (DLP) measurements. [19]

In this study, the effective dose was calculated by using conversion coefficient  $0.0019 \text{ mSv/mGy.cm}$  for CTA brain multiplied DLP value ( $\text{mGy.cm}$ ). The results demonstrated that the effective dose from CTA of brain examination of 30 patients ranged from 2.82-5.19 mSv, the average was 3.70 mSv. The comparison of patient effective dose from CTA examinations are shown in the Table 5.1.

At our institute, the two types of routine protocols for CTA of the brain had been chosen by radiologist which depends on clinical indication. First protocol was routine brain pre-contrast enhancement, CTA and routine brain post-contrast enhancement used for diagnosis of vascular disorder and parenchyma diseases. Second protocol is routine brain pre-contrast

enhancement, CTA and CTV of the brain used for diagnostic of vascular disorder. CTV of the brain and routine brain post-contrast enhancement were different in scanning parameters, tube voltage (kVp), tube current (mAs), tube rotation time and pitch. The examples of different parameters setting obtained from CT monitor are shown in Figure 5.1 and 5.2.

Total mAs 11214		Total DLP 3137 mGycm					
	Scan	KV	mAs / ref.	CTDIvol* mGy	DLP mGycm	TI s	cSL mm
Patient Position H-SP							
	1	120	35 mA	0.29 S	12	4.2	0.6
Topogram	2	120	392 / 450	49.63 S	25	1.0	5.0
Control Scan	3	120	376 / 450	61.39 S	1390	1.0	0.6
Non Contrast	4	120	20	2.51 S	3	0.33	10.0
PreMonitoring							
Contrast							
Monitoring	5	120	20	35.09 S	35	0.33	10.0
HeadAngio	19	120	119 / 158	19.40 S	480	0.33	0.6
Brain CE	20	120	306 / 400	49.96 S	1192	0.5	0.6

**Figure 5. 1** Protocol for brain pre-contrast, CTA brain and brain post contrast.

Total mAs 8588		Total DLP 1960 mGycm					
	Scan	KV	mAs / ref.	CTDIvol* mGy	DLP mGycm	TI s	cSL mm
Patient Position H-SP							
	1	120	35 mA	0.29 S	15	5.3	0.6
Topogram	2	120	494 / 450	62.54 S	31	1.0	5.0
Control Scan	3	120	374 / 450	61.09 S	1308	1.0	0.6
Non Contrast	4	120	20	2.42 S	2	0.33	10.0
PreMonitoring							
Contrast							
Monitoring	5	120	20	22.18 S	22	0.33	10.0
HeadAngio	14	100	130 / 175	12.85 S	291	0.33	0.6
HeadCTV	15	100	130 / 175	12.88 S	291	0.33	0.6

**Figure 5. 2** Protocol for brain pre-contrast, CTA brain and CTV.

The min, max and mean  $\pm$  SD of the effective dose from 5 patients who underwent CTA examination by the first protocol were 3.71, 5.19 and  $4.46 \pm 0.59$  mSv, respectively. The effective dose of 2.82, 4.37 and  $3.52 \pm 0.51$  mSv were the min, max and mean  $\pm$  SD of the effective dose from 25 patients who underwent CTA examination by the second protocol.

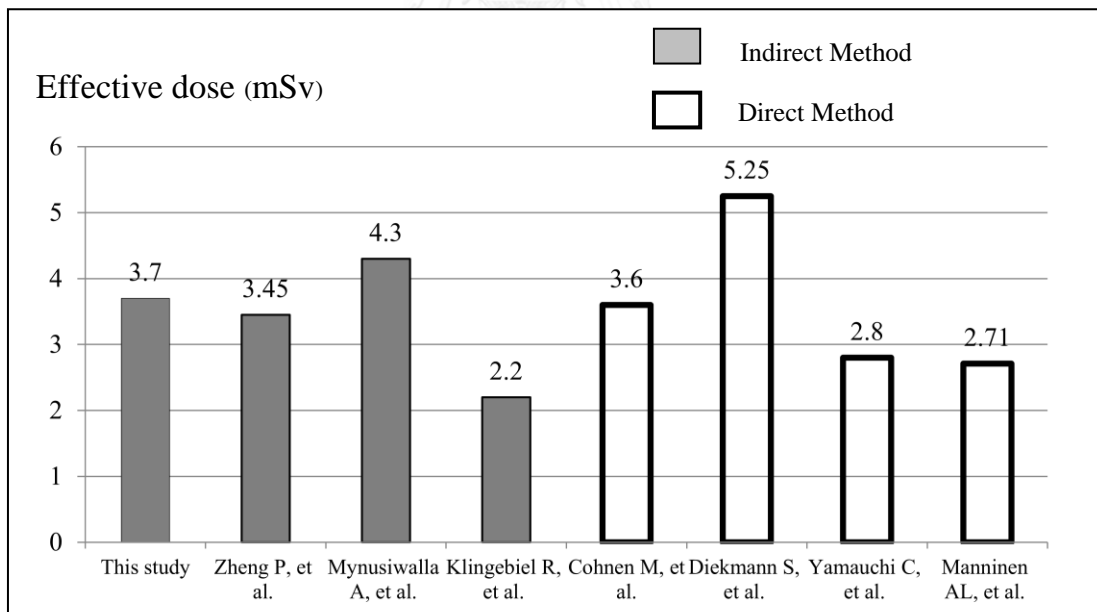
From the first protocol, 120 kVp, 400 reference mAs and 0.5 second tube rotation time set up of routine brain post-contrast enhancement result in higher CTDIvol, DLP and effective dose than CTV of the brain in the second protocol.

The difference between direct and indirect methods results in the difference of patient effective dose. Table 5.1 showed the results from other studies.

**Table 5. 1** Effective dose of CTA procedures compared with other studies.

Studies	Effective dose (mSv)		Measurement methods	Number of Cases
	Mean	Range		
This study	3.7	2.82-5.19	DLP×k-factor	30
Cohnen M, et al. (2006) [15]	3.6	N/A	LiF-TLD	Phantom
Klingebl R, et al. (2008) [14]	N/A	2.2-4.3	N/A	24
Mnyusiwalla A, et al. (2009) [16]	4.3	N/A	DLP×k-factor	95
Diekmann S, et al. (2010) [24]	5.25	N/A	LiF-TLD	Phantom
Yamauchi C, et al. (2010) [25]	2.8	N/A	Photodiode	Phantom
Manninen AL, at al. (2012) [17]	2.71	N/A	RPLDs*	Phantom
Zheng P, et al. (2012) [26]	3.45	N/A	DLP×k-factor	109

**Note:** \* Radiophotoluminescence dosimeter, N/A Not applicable

**Figure 5. 3** The effect dose between direct and indirect methods.

Our results can compare with other study. The mean effective dose mSv in this study is lower than Mnyusiwalla A, et al. but higher than Zheng P, et al.

The difference of CT scanner, scanning setup and imaging parameters results in the different patient effective dose of 3.7 mSv from our study, 4.3 mSv from Mnyusiwalla A, et al. and 3.45 mSv from Zheng P, et al.

The higher parameters setting of references mAs (500 mAs), tube rotation time (0.5 s), scan length (Aortic arch-circle of Willis) and lower pitch factor (0.75) in head CTA were found in Mnyusiwalla A, et al. study.

The 140 kVp setting in Zheng P, et al. study was higher than our study, the effective dose should be higher. But the lower references mAs (320 mAs) and scan length (base skull – vertex) were used. So the effective dose in this study is higher.

The different parameters setting of CTA protocol between our study and previous studies in patient show as table 5.2.

**Table 5. 2** Parameters setting between our study and previous studies.

	Studies	MDCT Scanner	kVp	References mAs	Tube rotation time (s)	Scanning slice thickness (mm)	Pitch	Scan area
Head unenhanced	This study	S-64	120	450	1	0.6	0.55	C4-vertex
	[16]	GE-128	120	420	1	0.6	0.55	N/A
	[26]	S-128	140	320	1	0.625	N/A	Base skull-vertex
Head CTA	This study	S-64	100/ 120	175	0.33	0.6	1.4	C4-vertex
	[16]	GE-128	100	500	0.5	0.6	0.75	Aortic arch-circle of Willis
	[26]	S-128	140	Auto mA	0.5	0.625	0.75	Aortic arch-vertex
Head enhanced	This study	S-64	120	400	1	0.6	0.55	C4-vertex
	[16]	GE-128	N/A	N/A	N/A	N/A	N/A	N/A
	[26]	S-128	140	320	1	0.625	N/A	Base skull-vertex

**Note:** **S-64:** Siemens 64 slices, **S-128:** Siemens 128 slices, **GE-64:** General Electric 64 slices, [16] - Mnyusiwalla A, et al. (2009), [26] - Zheng P, et al. (2012), **C** = Cervical spine, **N/A** Not applicable

In case of the indirect methods, the different k-factor from different studies results in the different effective dose. The k-factor (mSv/mGy.cm) of 0.0019 is used in this study, 0.0021 was used by Mynusiwalla A, et al and 0.0022 was used in Zheng P, et al. Table 5.3 shows the differences of k-factor from different studies.

**Table 5. 3** DLP to effective dose conversion factor (k-factor) for CT brain in adult.

Studies	Journal	Year	MDCT	kVp setting	k-factor (mSv/mGy.cm)
Jessen K.A, Shimpton P. C [27]	Applied Radiation and isotopes	1999	4-row	120, 125, 130, 133, 140	0.0021
Huda W, et al. [28]	Radiology	2008	16-row	120	0.0022
Huda W, Magill D. [29]	AAPM	2010	N/A	N/A	0.0024
Deak P.D, Kalender W.A [19]	Radiology	2010	64-row	80, 100, 120, 140	0.0019

## 5.1.2 Factors affecting the effective dose of CTA examination

### 5.1.2.1 Patient characteristics

Patient weight, height and BMI are the factors affecting the effective dose but patient age is not significant correlation with the effective dose. In this study, the patient received the lowest effective dose of 2.82 mSv was female, 89 yrs. (oldest), 37 kg (lowest) and 140 cm (shortest) while a man, 39 yrs., 85 kg (highest) and 31.22 kg/m<sup>2</sup>(highest BMI) received the highest effective dose of

5.19 mSv, respectively. Similarly Huda W, et al. [30] showed that, increasing of patient dose resulted from increasing of patient size.

In our institute, the tube current modulation (Siemens: CARE dose 4D) has been used in all of CT examination protocols which the adjusted mAs depends on the patient size, Z- axis and tube angle. Using the tube current modulation can reduce the dose to the patient. Kalender WA, et al. [31] and Greess H, et al. [32] indicated that the tube current modulation allowed for significant dose reduction without any impairment of image quality by mean dose reduction was 18% and 11% in the skull base, respectively.

### 5.1.2.2 Scanning parameters

Tube current-time (mAs), tube voltage (kVp) and scan length are the factors affecting the effective dose in this study. There are many studies reported about dose reduction for CT examination i.e. Smith AB et al. [33] indicated that the CT parameters such as tube current, tube rotation time, peak voltage, pitch, and collimation are major contributor to the radiation dose received during CT study.

Previous studies, Waaijer A, et al. [34] recommended that for evaluation of the circle of Willis in patients, using of 90 kVp can give the superior image quality compared with the image quality achieved with 120 kVp and the patient dose is reduced by approximately 30%. Peterson A, et al. [35] showed the increasing pitch from 1.0 to 1.5 would decrease the radiation dose by 33%. Zheng P, et al. reported the reducing the mAs from 500 mAs to 200 mAs and increasing pitch from 0.75 to 0.8 results in decreasing the effective dose for the CTA phase by 62% in routine CT Perfusion examination.

### 5.1.3 Patient effective dose from cerebral DSA examination

The most convenient and widely use method for indirect monitoring is the dose-area product (DAP) values. The DAP measurement is a function of the x-ray field size and the x-ray exposure at the collimator; thus, the measurement is expressed as either the dose-area product or the air-kerma-area product. The measured DAP is independent of distance from the focal spot. The distance factor cancels because the exposure rate varies inversely and the x-ray field area varies inversely as the square of the distance from the focal spot to the point of measurement. [1]

In this study, the effective dose was calculated by using DAP values ( $\text{mGy.cm}^2$ ) multiplied by dose conversion coefficient of 0.087  $\text{mSv/mGy.cm}^2$  for cerebral angiogram [22]. The results demonstrated that the effective dose

from cerebral DSA examination of 30 patients ranged from 3.30-10.06 mSv, the average was 5.94 mSv.

The effective dose to the patients from DSA procedure in this study is compared with other study as shown in Table 5.4.

**Table 5. 4** Effective dose of DSA procedure compare with other studies.

Studies	Effective dose (mSv)		Measurement methods	Number of cases
	Mean	Range		
This study	5.94	3.3-10.06	DAP value	30
Feygelman VM, et al. (1992) [36]	6.2	1.6-14	DAP value	10
Marshall NW, et al. (1994) [18]	3.2	-	TLD	Phantom
McParland BJ, et al. (1998) [37]	7.0	2.1-19.6	DAP value	28
Manninen AL, at al. (2012) [17]	2.71	-	RPLDs	Phantom

**Note:** TLD Thermoluminescent dosimeter, RPLDs Radiophotoluminescence dosimeter.

The table 5.4 shows the different patient effective dose from cerebral angiogram procedures. The tendency of mean and range of effective dose in this study is similar to Feygelman VM, et al. and McParland BJ, et al. which effective dose calculated from DAP values. The mean effective dose of 5.94 mSv in our study is lower than Feygelman VM, et al. (6.2 mSv) and McParland BJ, et al. (7.0 mSv). Many factors from different study can cause the variation of effective dose from DSA procedure such as kVp, mA, pulserate and framerate setting.

There is evidence of a wider variation in patient radiation dose due to clinical technique differences, statistical sampling and the types of x-ray equipment used. [38]



## **5.1.4 Factors affecting the effective dose of DSA examination**

### **5.1.4.1 Patient characteristics**

The results in this study showed no significant correlation between the effective dose and patient characteristics (weight, height, BMI and age).

International Atomic Energy Agency (IAEA) -TECDOC-1641 [39] reported that coronary angiography and percutaneous transluminal coronary angioplasty were lack of statistical significant between maximum skin dose and BMI and concluded that BMI is not a strong predictor of high skin dose risk to patients from fluoroscopy but did not report the correlation between patient characteristics and effective dose.

### **5.1.4.2 Imaging parameters**

The number of 2D radiography and the number of 3-Dimensional rotational angiography (3D RA) were the key factors affecting the effective dose from DSA procedure. The results show significant correlation between effective dose and 2D radiography and 3D RA ( $p < .001$ ). The number of vessels selective catheterization and fluoroscopic time were the statistical significant correlation with the effective dose to the patients who underwent cerebral angiography ( $p < .05$ ). The complexity of procedure could not be analyzed because of retrospective study. From published study, Gkanatsios NA, et al. [40] concluded that in DSA procedure, the patient dose increased for a more complex procedure, as a result of radiographic (DSA) exposures and less for fluoroscopy related.

The kVp, pulse width and dose per image in 2D radiographic mode are higher than 3D RA mode, thus radiation dose from 2D is higher than 3D mode. This parameters have been set by manufacturer to maintain image quality of radiographic images. The pulse rate 10 pulse per second (normal mode) in fluoroscopic mode can reduce radiation dose to the patient from DSA procedure.

In fact, a 2D radiographic sequences were the first priority given high dose per image to the patient when compared with 3D RA because of imaging parameters but the number of images in 3D RA sequences were more than 2D radiographic sequences at least 5 times, thus the DAP values of 3D sequences were greater than 2D radiographic sequences. The parameters between 2D and 3D sequences shown in Figure 5.4 and Figure 5.5 showed DAP values.

Parameters for DSA examinations			
	Fluoroscopy	2D mode	3D mode
kV	77	77	70
Pulse width (ms)		40	12.5
kV filter		81	OFF
kV mask		96	
Pulse rate	10p/s		
Dose ( $\mu$ Gy/image)		3.6	0.36
Phase 1		4f/s	4s
Phase2		1f/s	16s
Mask		30f/s	5s
Fill		30f/s	5s
Washout		0.5f/s	2s

**Figure 5. 4** Examination parameters between 2D radiography and 3D RA.

1	DSA	VAR TIME RT.ICA	13s	4F/s	22-Jun-15 10:01:59
B	79kV	175mA	40.5ms	100CL micro	0.0Cu 25cm 242.8mGymøø 17.6mGy 90RAD OCRA 25
2	DYNA	DYNAAUT 5s-1k DS	5s	30F/s	22-Jun-15 10:04:04
A	70kV	238mA	10.8ms	400CL small	0.0Cu 42cm 805.5mGymøø 33.7mGy 0LAD OCRA 126I

**Figure 5. 5** kVp, mAs, sequence time, frame rate and DAP of 2D radiography (1) and 3D RA (2).

Nikolaos A, et al. also reported no significantly difference between radiologist and fellows with years of experience. Similarly in this study, the experience of radiologist from two to more than ten years was no significant correlation with the effective dose. But difference from Bor D, et al. [41] studied, his study concluded that lack of sufficient technical knowledge regarding dose related equipment factors is one of the major reasons for the higher doses received by patients in interventional examinations carried out by junior radiologists.

In addition, the results from Xu G, et al. [42] showed the decreasing radiation doses in DSA consecutively performed by trainees shown insufficient catheter skill of trainees significant during the first 20 procedures, after that the dose decrease because of learning effect.

## 5.2 Conclusion

### 5.2.1 Patient radiation dose from CTA examination

From 30 patients who underwent CTA of the brain examination, the mean DLP was 1948 mGy.cm, range 1484-2732 mGy.cm. The median and 3<sup>rd</sup> quartiles were 1831 and 2228 mGy.cm, respectively.

The mean effective dose was 3.7 mSv, range 2.82-5.19 mSv. The median and 3<sup>rd</sup> quartile were 3.48 and 4.23 mSv, respectively.

Patient characteristics (age, weight, height, and BMI) have been investigated in CTA examination. The results show strong correlation between the patient effective dose and weight, BMI, and height but weak correlation between the effective dose and patient age.

For scanning parameters of CTA examination, the strong correlation between the patient effective dose and parameters setting, tube current-time (mAs), tube voltage (kVp) and scan length were reported. So, we can conclude that increasing of scanning parameters, mAs, kVp and scan length result in increasing the effective dose from CTA examination of the brain.

### 5.2.2 Patient radiation dose from DSA procedure

The study in 30 patients from intracranial DSA procedure, the mean DAP was 68.25 Gy.cm<sup>2</sup>, range 138-115.7 Gy.cm<sup>2</sup>. The median and 3<sup>rd</sup> quartiles were 64.73 and 82.89 Gy.cm<sup>2</sup>, respectively. The mean effective dose was 5.94 mSv, range 3.30 - 10.06 mSv. The median and 3<sup>rd</sup> quartiles were 5.63 and 7.21 mSv, respectively.

Weak correlation between the effective dose and patient characteristics in DSA procedure is reported.

The results show strong correlation between the patient effective dose and a number of 2D radiography and the number of 3-Dimensional rotational angiography (3D RA). The number of vessels selective catheterization and fluoroscopic time were moderate correlation with the effective dose.

No relationship between the effective dose and experience of Radiologist for 2-28 year.

The mean effective dose from DSA procedure was 1.5 time of CTA examination of the brain.

## Summary

### CTA examination

- The mean effective dose was 3.70 (2.82-5.19) mSv.
- The factors affecting effective dose were patient weight, height, BMI, kVp, mAs and scan length.
- Patient age (23-89 year) not affect the effective dose.

### DSA examination

- The mean effective dose was 5.94 (3.30 - 10.06) mSv.
- The factors affecting effective dose were a number of 2D radiography, the number of 3D rotational angiography (3D RA), the number of vessels selective catheterization and fluoroscopic time.
- Experience of Radiologist is not affecting the effective dose.

**REFERENCES**



- [1] Mahesh M. Fluoroscopy: **Patient radiation exposure issues**. RadioGraphics. 21 (Jul-Aug2001):1033-45.
- [2] Mettler FA, Huda W, Yoshizumi TT and Mahesh M. **Effective Doses in Radiology and Diagnostic Nuclear Medicine: A catalog**. Radiol. 248 (Jul 2008): 254-63.
- [3] American Association of Physicists in Medicine (AAPM) report 96. **The Measurement Reporting and Management of Radiation Dose in CT**. New York: AAPM,2008.
- [4] Shrimpton PC, Wall BF, Jones DG, Fisher ES. **The measurement of energy imparted to patients during diagnostic x-ray examinations using the Diamentor exposure-area product meter**. Physics in Medicine and Biology. 1984;29(10):1199.
- [5] Kalender WA. **X-ray computed tomography. Physics in medicine and biology**.2006;51(13):R29-43.
- [6] The ImPACT Group. **Multi-slice CT scanners CEP08007**. Medical Physics Bence Jones Offices Perimeter Road Tooting London UK: impactscan.org, 2009.
- [7] Giancoli, Douglas C. (1998), **Physics: principles with applications (5th edition**, p. 784-787). Upper Saddle River, NJ: Prentice Hall.
- [8] **ACR–ASNR Practice guideline for the performance and interpretation of Cervicocerebral computed tomography angiography (CTA)**. Available from <http://www.asnr.org/sites/default/files/guidelines/CervicocerebralAngio.pdf>
- [9] Htyte N, Jenkins JS. **Diagnostic Cerebral and Peripheral Angiography**. 2014:1-55.
- [10] Nickoloff ED. **Survey of Modern Fluoroscopy Imaging: Flat-Panel Detectors versus Image Intensifiers and More**, RadioGraphics. 2011;31:591-602.
- [11] **ACR–ASNR–SIR–SNIS Practice parameter for the performance of diagnostic cervicocerebral catheter angiography in adults**. Available from <http://www.acr.org/~media/261A171F55D744439FAACD9C61B0D462.pdf>

- [12] Dendy PP, Heaton B., **Physics for diagnostic radiology (2nd edition p.145)**. Philadelphia: Institute of Physics publication;1990.
- [13] Martin CJ. **Effective dose: how should it be applied to medical exposures?** The British journal of radiology. 2007;80(956):639-47.
- [14] Klingebiel R, Kentenich M, Bauknecht HC, Masuhr F, Siebert E, Busch M et al.**Comparative evaluation of 64-slice CT angiography and digital subtractionangiography in assessing the cervicocranial vasculature**. Vascular Health and Risk Management 2008;4(4): 901-07.
- [15] Cohnen M, Wittsack HJ, Assadi S, Musakala K, Ringelstein A and Poll LW et al.**Radiation exposure of patients incomprehensive computed tomography of the head in acute stroke**.AJNRAmJNeuroradiol 2006; 27:1741–45.
- [16] Mnyusiwalla A, Aviv RI, Symons SP. **Radiation dose from multidetector row CT imaging for acute stroke**. Neuroradiology. 2009;51(10):635-40.
- [17] Manninen AL, Isokangas JM, Karttunen A, Siniluoto T and Nieminen MT. **A comparison of radiation exposure between diagnostic CTA and DSA examinations of cerebral and cervicocerebral vessels**. AJNR American journal of neuroradiology. 2012; 33(11): 2038-42.
- [18] Marshall NW, Noble J, Faulkner K. **Patient and staff dosimetry in neuroradiological procedures**. Br J Radiol. 1995;68:495–501.
- [19] Deak PD, Smal Y and Kalender WA. **Sex- and Age-Specific Conversion Factors for Effective Dose at CT**, Radiol.2010; 257: 158-66.
- [20] American Association of Physicist in Medicine. **Specification and acceptance testing of computed tomography scanners, report 39** (May 1993).
- [21] ImPACT. **ImPACT information leaflet 1: CT scanner acceptance testing**. Version 1.02 (2001): 1-8.
- [22] National Council on Radiation Protection and Measurements (NCRP) Report No. 160 –**Ionizing Radiation Exposure of the Population of the United States (2009)**. Availablefrom [https://rpop.iaea.org/RPOP/RPoP/Content/InformationFor/HealthProfessionals/4\\_InterventionalRadiology/patient-staff-dose-fluoroscopy.htm](https://rpop.iaea.org/RPOP/RPoP/Content/InformationFor/HealthProfessionals/4_InterventionalRadiology/patient-staff-dose-fluoroscopy.htm)

- [23] McCollough CH, Primak AN, Braun N, Kofler J, Yu L, Christner J. **Strategies for reducing radiation dose in CT**. Radiologic clinics of North America. 2009;47(1):27-40.
- [24] Diekmann S, Siebert E, Juran R, Roll M, Deeg W, Bauknecht HC, et al. **Dose exposure of patients undergoing comprehensive stroke imaging by multidetector-row CT: comparison of 320-detector row and 64-detector row CT scanners**. AJNR American journal of neuroradiology. 2010;31(6):1003-9.
- [25] Yamauchi-Kawara C, Fujii K, Aoyama T, Yamauchi M, Koyama S. **Radiation dose evaluation in multidetector-row CT imaging for acute stroke with an anthropomorphic phantom**. The British journal of radiology. 2010;83(996):1029-41.
- [26] Zheng P, Bhuta S. **CT brain perfusion radiation dosimetry on a 128 slice MDCT; What is all the hue cry about?** The royal Australian and new Zealand college of radiologists.RANZCR-AOCR2012. Available from [file:///C:/Users/user/Downloads/RANZCR-AOCR2012\\_R-0059.pdf](file:///C:/Users/user/Downloads/RANZCR-AOCR2012_R-0059.pdf).
- [27] Jessen KA, Shrimpton PC, Geleijns J et al (1999) **Dosimetry for optimization of patient protection in computed tomography**. Appl Radiat Isot 50:165–172.
- [28] Huda W, Ogden KM, Khorasani MR. **Converting Dose-Length Product to Effective Dose at CT**. Radiology. 2008;248(3):995-1003.
- [29] Huda W, Magill D, He W. **CT effective dose per dose length product using ICRP 103 weighting factors**. Medical Physics. 2011;38(3):1261.
- [30] Huda W, Lieberman KA, Chang J, et al. **Patient size and x-ray technique factors in head computed tomography examinations. I. Radiation doses**. Med Phys. 2004;31:588–94.
- [31] Kalender WA, Wolf H, Suess C, Gies M, Greess H, Bautz WA. **Dose reduction in CT by on-line tube current control: principles and validation on phantoms and cadavers**. EurRadiol 1999;9:323-8.
- [32] Greess H, Wolf H, Baum U, Lell M, Pirkl M, Kalender WA, et al. **Dose reduction in computed tomography by attenuation based on-line modulation of tube current: evaluation of six anatomical regions**. EurRadiol 2000;10:391-4.



- [33] Smith AB, Dillon WP, Gould R, Wintermark M. **Radiation dose-reduction strategies for neuroradiology CT protocols.** AJNR American journal of neuroradiology. 2007;28(9):1628-32.
- [34] Waaijer A, Prokop M, Velthuis BK, Bakker CJG, Kort GAP, Leeuwen MSV. **Circle of Willis at CT Angiography: Dose Reduction and Image Quality—Reducing Tube Voltage and Increasing Tube Current Settings.** Radiology. 2007;242(3):832-9.
- [35] Paterson A, Frush DP, Donnelly LF. **Helical CT of the body: are settings adjusted for pediatric patients?** Am. J. Roentgenol. 176, 297-301.
- [36] Feygelman VM, Huda W, Peters KR. **Effective dose equivalents to patient undergoing cerebral angiography.** AJNR American journal of neuroradiology. 1992;13(6):845-9.
- [37] McParland BJ. **A study of patient radiation doses in interventional radiology procedures.** The British Journal of Radiology. 1998;71:175-85.
- [38] Bergeron P, Carrier R, Roy D, Blais N, Raymond J. **Radiation doses to patients in neurointerventional procedures.** Am J Neuroradiol. 1994;15:1809–12.
- [39] International Atomic Energy Agency 2010. **Patient dose optimization in fluoroscopically guided interventional procedures: Final report of a coordinated research project – Vienna.** IAEA-TECDOC-1641. Available from [http://www-pub.iaea.org/MTCD/publications/PDF/te\\_1641\\_web.pdf](http://www-pub.iaea.org/MTCD/publications/PDF/te_1641_web.pdf).
- [40] Gkanatsios NA, Huda W, Peters KR. **Adult patient doses in interventional neuroradiology.** Medical physics. 2002;29(5):717-23.
- [41] Bor D, Sancak T, Toklu T, Olgar T, Ener S. **Effects of radiologists' skill and experience on patient doses in interventional examinations.** Radiation protection dosimetry. 2008;129(1-3):32-5.
- [42] Xu G, Zhao W, Zheng L, Fan X, Yin Q, Liu X. **Decreasing radiation doses in digital subtraction angiographies consecutively performed by trainees.** Radiation protection dosimetry. 2012;148(2):181-4.



## Appendix A: Case Record Form

### Case record form: CTA

Clinical data collection sheet for radiation dose from **computed tomography angiography (CTA)** of the brain at Prasat neurological institute.

Study Date	
Case study number	
Gender (M/F)	
Age (year)	
Height (cm)	
Body weight (kg)	
BMI (kg/cm <sup>2</sup> )	
kVp	
Total mAs	
Pitch	
Rotation time (s)	
Slice acquisition (mm)	
Slice collimation (mm)	
Total DLP (mGycm)	
Effective dose (mGy)	

### Case record form: DSA

Clinical data collection sheet for radiation dose from **digital subtraction angiography (DSA)** of the brain at Prasat neurological institute.

Study Date	
Case study number	
Gender (M/F)	
Age (year)	
Height (cm)	
Body weight (kg)	
BMI (kg/cm <sup>2</sup> )	
Fluoroscopic time (min.)	
Number of vessels	
Number of 2D radiography	
Number of 3D rotation angiography	
DAP (μGy.cm <sup>2</sup> )	
Radiologist experience (year)	
Effective dose (mSv)	

## Appendix B: Quality Control of research equipment

### Equipment performance for CT system

#### Report of CT system performance

Location	Prasat Neurological Institute, Bangkok, Thailand
Date	16 Jan 2016
Manufacturer	Siemens
Model	Somatom Definition AS 64
<b><u>Pass</u></b>	Scan Localization Light Accuracy
<b><u>Pass</u></b>	Alignment of Table to Gantry
<b><u>Pass</u></b>	Table Increment Accuracy
<b><u>Pass</u></b>	Slice Increment Accuracy
<b><u>Pass</u></b>	Gantry Angle Tilt
<b><u>Pass</u></b>	Position Dependence and SNR of CT Numbers
<b><u>Pass</u></b>	Reproducibility of CT Numbers
<b><u>Pass</u></b>	mAs Linearity
<b><u>Pass</u></b>	Linearity of CT Numbers
<b><u>Pass</u></b>	Accuracy of Distance Measurement
<b><u>Pass</u></b>	Image uniformity
<b><u>Pass</u></b>	High Contrast Resolution
<b><u>Pass</u></b>	Low Contrast Detectability
<b><u>Pass</u></b>	Radiation Profile width

### 1. Scan Localization Light Accuracy

**Purpose:** To test congruency of scan localization light and scan plane.

**Method:** Place the tape measurement vertically along the midline the couch aligned with its longitudinal axis. Raise the table to the head position. Turn the localization light. Set external light align with the reference point on the tape measurement. Set table position to zero. Move table by automatic positioning button to slide table from external to internal localization light. Measure and record deviation position.

**Tolerance:** The position on tape measurement between external and internal localization light should be less than 2 mm.

**Results:** Measured deviation < 1 mm.

**Comment:** Pass

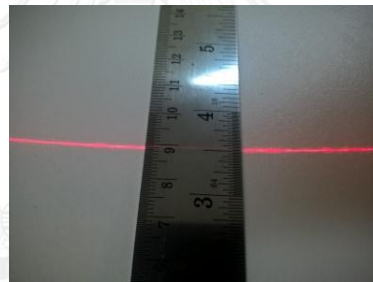


**Figure I** Scan localization light accuracy setting.

### 2. Alignment of Table to Gantry

**Purpose:** To ensure that long axis of the table is horizontally aligned with a vertical line passing through the rotational axis of the scanner.

**Method:** Locate the table midline using a ruler and mark it on a tape affixed to the table. With the gantry untilted, extend the table top into gantry to tape position. Measure the horizontal deviation between the gantry aperture centre and the table midline.

**Tolerance:** The deviation should be within 5 mm.

**Results:**

	<b>Table</b>	<b>Bore</b>
Distance from Right to Center	(mm) 226	402
Distance from Center to Left	(mm) 224	398
Measured Deviation*	(mm) 1	2

Note: Measured deviation = (Distance from right to center - Distance from center to left)/2

**Comment:** Pass

### 3. Table Increment Accuracy

**Purpose:** To determine accuracy and reproducibility of table longitudinal motion.

**Method:** Tape a measuring tape at the foot end of the table. Place a paper clip at the center of the tape to function as an indicator. Load the table uniformly with 150 lbs. From the initial position move the table 300, 400 and 500 mm into the gantry under software control. Record the relative displacement of the pointer on the ruler. Reverse the direction of motion and repeat. Repeat the measurements four times.

**Tolerance:** Positional errors should be less than 3 mm at 300 mm position.

**Results:**

Indicated (mm)	Measured (mm)	Deviation (mm)
500	500	0
400	400	0
300	299	0
-300	-300	0
-400	-400	0
-500	-500	0

Note: Deviation = | Indicated - Measured|

**Comment:** Pass

### 4. Slice Increment Accuracy

**Purpose:** To Determine the accuracy of the slice increment.

**Method:** Set up as you would for beam profile measurement. Select 120 kVp, 100 mAs, and smallest slit width. Perform several scans with different programmed slice separations under auto control. Scan the film with a densitometer and measure the distance between the peaks.

**Tolerance:** Position errors should be less than 3 mm at 300 mm position.

**Results:**

Slice Separation in mm	Measured Separation in mm	Deviation (mm)
20	20	0
30	30	0
50	50	0

Note: Deviation = |Slice separation - Measured separation|

**Comment:** Pass

### 5. Gantry Angle Tilt

**Purpose:** To determine the limit of gantry tilt and the accuracy of tilt angle indicator.

**Method:** Tape a localization film to the backing plate making sure that the edges of the film are parallel to the edges of the backing plate. Place the film vertically along the midline of the couch aligned with its longitudinal axis. Raise the table to the head position. Move the table into the gantry. Set center position to alignment light. Expose the film at inner light location using narrowest slit, 120-140 kVp, 50-100 mAs. Tilt the gantry to one extreme from the console. Record the indicated gantry angle. Expose the film using the above technique. Measure the clearance from the closest point of gantry to midline of the table. Tilt the gantry to its extreme in the opposite direction. Record clearance and repeat the exposure. Measure the tilt angles from the images on the film.

**Tolerance:** Deviation between indicated and measured tilt angles <30. Gantry clearance should be >30 cm.



**Results:**

	Away	Toward
Indicated Angle	30°	30°
Measured Angle	30°	30°
Deviation*	0	0

Note: Deviation = |Indicated angle - Measured angle|

**Comment:** Pass

### 6. Position Dependence of CT Numbers

**Method:** Position the water phantom centered in the gantry. Using 5 cm slice thickness, obtain one scan using typical head technique. Select a circular region of interest of approximately 400 sq. mm. and then record the mean C.T. number and standard deviation for each of the positions 1 through 5.

**Technique:** 120 kVp, 320 mA, 1 sec, slice collimation 5 mm. 200 mm FOV.

**Tolerance:** The coefficient of variation of mean CT numbers of the four scans should be less than 0.2.

**Results:**

Position	Mean C.T. #	S.D.	C.V.
1	-0.220	0.065	-0.295
2	-1.165	0.006	-0.005
3	-0.795	0.037	-0.047
4	-0.695	0.006	-0.008
5	-0.620	0.024	-0.040

Note: CV = Standard deviation/mean CT number



**Figure II** Position of ROI for CT number measurement.

**Comment:** Pass

### 7. Reproducibility of CT Numbers.

**Method:** Using the same set up and technique as position dependence, obtain three scans. Using the same ROI as position dependence in location 5, this is the center of the phantom obtain mean C.T. numbers for each of the four scans.

**Tolerance:** The coefficient of variation of mean CT numbers of the four scans should be less than 0.002.

**Results:**

Run Number	1	2	3	4
Mean CT Number (HU)	8.7	8.8	8.7	8.7
Mean Global C.T. Number	8.725			
Standard Deviation	0.005			
Coefficient of variation	0.001			

**Comment:** Pass

### 8. mAs Linearity

**Method:** Set up the same as position dependence and insert 10 cm long pencil chamber in the center slot of the C.T. dose head phantom. Select the same kVp and time as used for head scan. Obtain four scans in each of the mA stations normally used in the clinic. For each mA station record the exposure in mGy for each scan. Scans should be performed in the increasing order of mA. Compute mGy/mAs for each mA setting.

**Technique:** 120 kVp, 320 mA, 1 sec, 200 mmSFOV

**Results:**

mA	Exposure in mGy				mGy/mAs	C.V.
	1	2	3	4		
100	1.88	1.885	1.878	1.881	1.881	0.0188
200	3.746	3.755	3.749	3.756	3.7515	0.0188
250	5.618	5.621	5.637	5.633	5.62725	0.0188
300	7.501	7.496	7.488	7.484	7.49225	0.0187
400	9.351	9.338	9.37	9.37	9.35725	0.0187
500	12.45	12.45	12.45	12.44	12.4475	0.0207
700	14.45	14.49	14.47	14.5	14.4775	0.0207

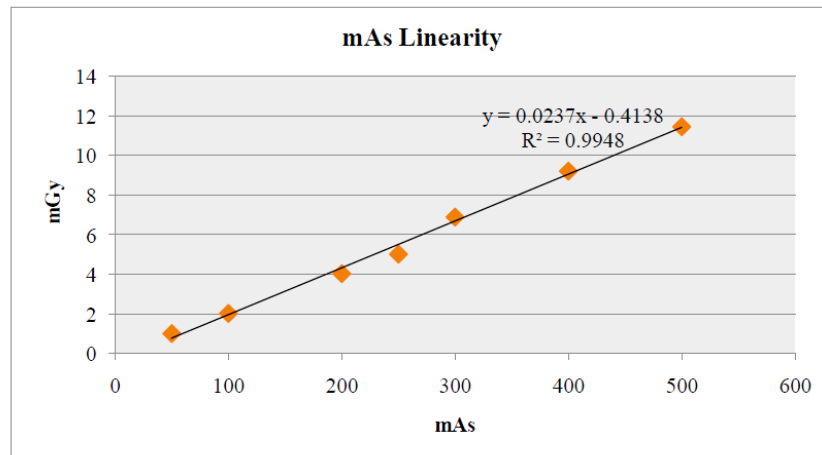


**Figure III** The relationship of mGy and mAs.

**Comment:** Pass

### 9. Linearity of CT Numbers

**Method:** Set up the catphan phantom as described in beam alignment. Select the section containing the test objects of different CT numbers. Select the head technique and perform a single transverse scan. Select a region of interest (ROI) of sufficient size to cover the test objects. Place the ROI in the middle of each test object and record the mean CT number.

**Technique:** 120 kVp, 320 mA, 1 sec, 200 mm SFOV, slice collimation 5 mm.

**Tolerance:** R-square between measured CT number and linear attenuation coefficient ( $\mu$ ) more than 0.9

**Results:**

Material	Expected CT no. (HU)	Measured CT no. (HU)	$\mu(\text{cm}^{-1})$
Air(inferior)	-1000	-952.9	0
Air(superior)	-1000	-957.3	0
Acrylic	120	124.1	0.184
Polystyrene	-35	-33.6	0.162
LDPE	-100	-90.4	0.151
PMP	-200	-181.3	0.136
Delrin	340	347	0.217
Teflon	990	941.3	0.305

**Note:** Expected CT numbers are either the predicted ones or the ones obtained during the previous annual measurement.

**Comment:** Pass

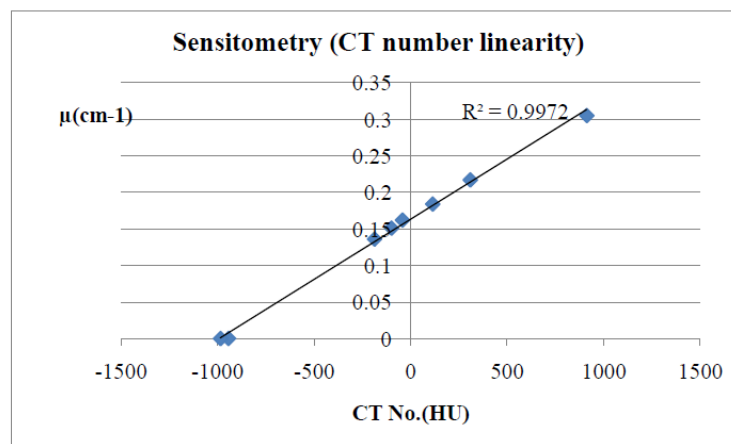


**Figure IV** Linearity of CT number.

## 10. Accuracy of Distance Measurement

**Purpose:** To test accuracy of Distance Measurement and for circular symmetry of the CT image.

**Method:** Set up the catphan phantom as described in beam alignment. Select the section containing the test accuracy of distance measurement. Select the head technique and perform a single transverse scan. Measured object in x and y axes.

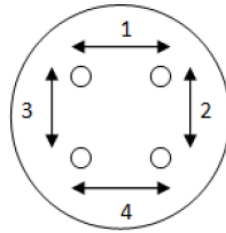


**Figure V** Accuracy measurement.

**Results:**

Position	Indicate (mm)	Measured (mm)	Different (mm)
1	50	50.1	0.1
2	50	49.9	0.1
3	50	49.9	0.1
4	50	50.1	0.1

**Comment:** Pass

### 11. Image uniformity

**Method:** Set up the catphan phantom as described in beam alignment. Select the section containing the image uniformity module. Select the head technique. Perform a single transverse scan. Measure the mean value and the corresponding standard deviations in CT numbers within a region of interest (ROI). These measurements are taken from different locations within the scan field.

**Technique:** 120 kVp, 320 mA, 1.0 sec, 200 mm FOV.

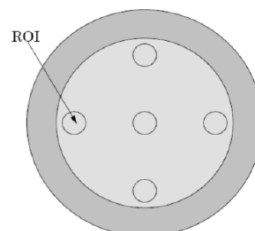


**Figure VI** Image Uniformity.

**Tolerance:** 5 HU.

**Results:**

Position	CT number (HU)	SD	Different (HU)
Center	2.85	3.02	0
3 o'clock	3.57	2.24	0.72
6 o'clock	2.82	2.53	0.03
9 o'clock	3.55	2.37	0.70
12 o'clock	4.30	2.35	1.45

**Note:** Different = |CT number center - CT number peripheral|

**Comment:** Pass

## 12. High Contrast Resolution

**Method:** Set up the catphan phantom as described in beam alignment. Select the section containing the high resolution test objects. Select the head technique. Perform a single transverse scan. Select the area containing the high resolution test objects and zoom as necessary. Select appropriate window and level for the best visualization of the test objects. Record the smallest test object visualized on the film.

**Technique:** 120 kVp, 320 mA, 1.0 sec, 200 mm FOV.

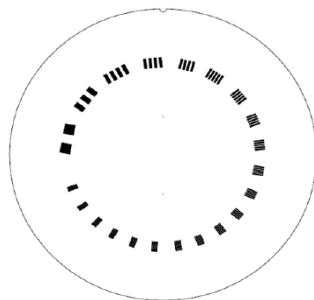


**Figure VII** High contrast resolution.

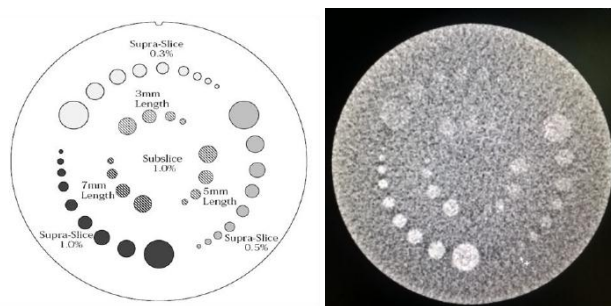
**Results:**

Slice Thickness in mm	Resolution
5	11 lp/cm (0.045 mm)

**Comment:** Pass**13. Low Contrast Detectability**

**Method:** Select the section containing the low resolution test objects in the mini phantom. Perform a single transverse scan utilizing the same technique as high resolution.

**Technique:** 120 kVp, 320 mA, 1.0 sec, 200 mm FOV, slice collimation 5 mm.



จุฬาลงกรณ์มหาวิทยาลัย  
CHULALONGKORN UNIVERSITY

**Figure VIII** Low contrast detectability.**Results:**

Supra-slice	Nominal target contrast levels	Hole	%Contrast
	0.30%	6	1.5
	0.50%	8	1.5
	1%	9	2
Sub-slice	Nominal target contrast levels	Hole	%Contrast
	3 mm Length	4	3
	5 mm Length	4	5
	7 mm Length	4	7

**Comment:** Pass



#### 14. Radiation Profile width

**Purpose:** To Determine the accuracy of the slice thickness.

**Method:** Set up the catphan phantom as described in beam alignment. Select the section containing the accuracy of the slice thickness test objects. Select the head technique. Perform scan following catphan manual in each slice collimation. Calculate the real slice thickness.

**Technique:** 120 kVp, 320 mA, 1.0 sec.

**Tolerance:** The different of the radiation profile width center and collimation setting should less than  $\pm 1$  mm.

**Results:**

Collimation setting (mm)	Measured (mm)	Deviation (mm)
5.0 (5×1)	4.6	0.4
10.0 (10×1)	9.5	0.6

**Comment:** Pass

#### 15. Verification of Computed Tomography Dose Index (CTDI)

**Purpose:** To verify CTDI of scanner to published values of ImPACT.

**Method:** Recorded the CTDI using head protocol and scan parameter were 100 mA tube current, 1 sec scan time and kilovoltage setting of 80, 100, 120 and 140 kVp. The displayed CTDI on CT monitor were compared with CTDI from ImPACTSCAN for each kVP.

**Technique:** 120 kVp, 100 mA, 1.0 sec, 10 mm collimation.

**Tolerance:** The percent difference between the displayed CTDI on CT monitor and CTDI from ImPACTSCAN should less the than 10%.

**Results:**

kVp	CTDI (mGy) in head protocol		
	Displayed	ImPACTSCAN	% difference
80	4.91	5.70	9.76
100	9.83	10.45	5.93
120	16.22	16.94	4.25
140	24.12	24.32	0.82

**Comment:** Pass

### 16. Verification of Dose Length Product (DLP)

**Purpose:** To verify displayed DLP of scanner to the measured DLP from dosimeter.

**Method:** The DLP in head phantom was determined by using a 100 mm pencil ionization chamber and 16 cm diameter PMMA phantom placed at the isocenter of the CT bore. The scan parameters were 100 mA, 1 sec scan time, 200 mm FOV and 10x1 mm collimation setting for all measurements at each kVp setting of 80, 100, 120 and 140. The displayed DLP on CT monitor were recorded to compare percentage difference with the DLP measured values by dosimeter for each kVp.

**Technique:** 120 kVp, 100 mA, 1.0 sec, 10 mm collimation.

**Tolerance:** The percent difference between the displayed DLP on CT monitor and measured DLP should less the than 10%.

**Results:**

DLP from head protocol			
kVp	Displayed	Measured	% difference
80	9.4	9.8	4.08
100	18.9	19.5	3.08
120	31.1	32.0	2.81
140	46.3	46.6	0.64

**Comment:** Pass

**Equipment performance for DSA system**  
**Report of DSA system performance**

<b>Hospital :</b>	Prasat Neurological Institute
<b>Room :</b>	DSA
<b>Date :</b>	17 Jan 2016
<b>X-ray unit :</b>	Siemens Axiom Artis
<b>Report Number :</b>	1
<b>Test performed by :</b>	Yutthana Netwong

Bi plane

Rotating Anode, Pulse Fluoroscopy 0.5, 1, 2, 3, 4, 7.5, 15, 30 p/s

Small focal spot: 0.3 mm, Large focal spot: 0.6, 1 mm

Anode heat storage capacity 2.4 HU

Filter 0.8, 1 mmAl, 0.2, 0.3, 0.4 mmCu

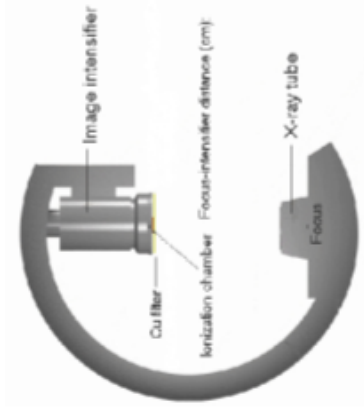
Rectangular Collimator |

Cesium Iodine Scintillator use amorphous silicon array max FOV 30x30 cm.

Carbon fiber table minimum height adjust 28 cm, minimum weight 250 kg+ CPR 50 kg.

Table at 0 position, minimum distance from Focus to table 76.2 cm, focus to detector face 116 cm and to detector 120 cm.

Manufactured 2007



**DOSE ASSESSMENT (Plane A)**

Focus –Intensifier distance (cm)

**Set**  
100

**Measure**  
100

60 cm

**Error**  
0%

Patient dose measurement: Focus-Ionization chamber distance

Entrance II dose measurement: II-Ion Ionization chamber distance 40 cm

Mode	Submode/ Image quality	Pulse rate (pulses/s)	Automatic added filtration (mm Cu)	Field size (cm)	kV	mA	Added Filtration (mm Cu)	(Patient entrance surface air kerma) Copper filter entrance air kerma (mGy/min)	Patient entrance surface air kerma at 60 cm (including backscatter (1.3) (mGy/min)	Phantom
Fluoroscopy	High	30.0	0.1 mmCu + 1.0 mmAl	48.0	80.0	37.2	0.3	12.20	15.9	2 mm Cu sheet
				42.0	80.0	36.3	0.3	11.82	15.4	
				32.0	80.0	46.3	0.3	16.12	21.0	
				22.0	80.0	60.4	0.3	23.19	30.1	
				16.0	80.0	113.1	0.3	57.40	74.6	
				11.0	86.6	115.0	0.2	72.54	94.3	

Mode	Submode/ Image quality	Pulse rate (pulses/s)	Automat ic added filtration (mm Cu)	Field size (cm)	kV	mA	Added Filtration (mm Cu)	(Patient entrance surface air kerma) Copper filter entrance air kerma (mGy/min)	Patient entrance surface air kerma at 60 cm (including backscatter (1.3) (mGy/min)	Phanto m	
				48.0	80.0	36.2	0.3	5.89	7.7	2 mmCu sheet	
	High	15.0	0.2	42.0	80.0	35.8	0.3	5.82	7.6		
				32.0	80.0	45.8	0.3	8.11	10.5		
				22.0	80.0	58.0	0.3	11.40	14.8		
				16.0	80.0	105.4	0.3	28.71	37.3		
				11.0	80.0	140.0	0.3	43.94	57.1		
				48.0	80.0	40.8	0.3	3.90	5.1		
				42.0	80.0	39.9	0.3	3.85	5.0		
				32.0	80.0	50.6	0.3	5.40	7.0		
	High	10.0	0.2	22.0	80.0	62.9	0.3	7.63	9.9		
				16.0	80.0	109.9	0.3	19.03	24.7		
				11.0	80.0	142.9	0.3	29.50	38.4		

Mode	Submode/ Image quality	Pulse rate (pulses/s)	Automatic filtration (mm Cu)	Field size (cm)	kV	mA	Added Filtration (mm Cu)	(Patient entrance surface air kerma) Copper filter entrance air kerma (mGy/min)	Patient entrance surface air kerma at 60 cm (including backscatter (1.3) (mGy/min)	Phantom
Fluoroscopy	High	7.5	0.2	48.0	80.0	36.9	0.3	3.06	4.0	2 mm Cu sheet
				42.0	80.0	35.7	0.3	2.90	3.8	
				32.0	80.0	46.5	0.3	4.22	5.5	
				22.0	80.0	58.0	0.3	5.81	7.6	
				16.0	80.0	106.7	0.3	14.86	19.3	
				11.0	80.0	141.9	0.3	23.02	29.9	

Mode	Submode/ Image quality	Pulse rate (pulses/s)	Automatic added filtration (mm Cu)	Field size (cm)	kV	mA	Added Filtratio n (mm Cu)	(Patient entrance surface air kerma) Copper filter entrance air kerma (mGy/min)	Patient entrance surface air kerma at 60 cm (including backscatter (1.3) (mGy/min)	Phantom
Fluoroscop y	Medium	30.0	0.2	48.0	80.0	68.0	127.7	0.6	19.0	2 mm Cu sheet
				42.0	80.0	68.0	120.8	0.6	17.3	
				32.0	80.0	68.5	145.6	0.6	23.2	
				22.0	80.0	71.1	140.6	0.6	26.5	
				16.0	80.0	78.0	103.5	0.3	60.1	
				11.0	86.6	80.4	124.0	0.2	94.3	
	Medium	15.0	0.2	48.0	80.0	68.0	71.7	0.6	6.94	2 mm Cu sheet
				42.0	80.0	68.0	70.5	0.6	6.37	
				32.0	80.0	68.0	83.7	0.6	9.54	
				22.0	80.0	68.0	100.5	0.6	13.81	
				16.0	80.0	78.0	61.5	0.3	23.76	
				11.0	80.0	78.0	75.9	0.3	36.15	



Mode	Submode/ Image quality	Pulse rate (pulses/s)	Automatic filtration (mm Cu)	Field size (cm)	kV	mA	Added Filtration (mm Cu)	(Patient entrance surface air kerma) Copper filter entrance air kerma (mGy/min)	Patient entrance surface air kerma at 60 cm (including backscatter (1.3) (mGy/min)	Phantom
				48.0	80.0	36.2	0.3	5.89	7.7	2 mmCu sheet
				42.0	80.0	35.8	0.3	5.82	7.6	
	High	15.0	0.2	32.0	80.0	45.8	0.3	8.11	10.5	
				22.0	80.0	58.0	0.3	11.40	14.8	
				16.0	80.0	105.4	0.3	28.71	37.3	
				11.0	80.0	140.0	0.3	43.94	57.1	
				48.0	80.0	40.8	0.3	3.90	5.1	2 mmCu sheet
				42.0	80.0	39.9	0.3	3.85	5.0	
	High	10.0	0.2	32.0	80.0	50.6	0.3	5.40	7.0	
				22.0	80.0	62.9	0.3	7.63	9.9	
				16.0	80.0	109.9	0.3	19.03	24.7	
				11.0	80.0	142.9	0.3	29.50	38.4	

Mode	Submode/ Image quality	Pulse rate (pulses/s)	Automatic filtration (mm Cu)	Field size (cm)	kV	mA	Added Filtration (mm Cu)	(Patient entrance surface air kerma) Copper filter entrance air kerma (mGy/min)	Patient entrance surface air kerma at 60 cm (including backscatter (1.3) (mGy/min)	Phantom
Fluoroscopy	High	7.5	0.2	48.0	80.0	36.9	0.3	3.06	4.0	2 mm Cu sheet
				42.0	80.0	35.7	0.3	2.90	3.8	
				32.0	80.0	46.5	0.3	4.22	5.5	
				22.0	80.0	58.0	0.3	5.81	7.6	
				16.0	80.0	106.7	0.3	14.86	19.3	
				11.0	80.0	141.9	0.3	23.02	29.9	

Mode	Submode/ Image quality	Pulse rate (pulses/s)	Automatic added filtration (mm Cu)	Field size (cm)	kV	mA	Added Filtratio n (mm Cu)	(Patient entrance surface air kerma) Copper filter entrance air kerma (mGy/min)	Patient entrance surface air kerma at 60 cm (including backscatter (1.3) (mGy/min)	Phantom
Fluoroscop y	Medium	30.0	0.2	48.0	80.0	68.0	127.7	0.6	19.0	2 mm Cu sheet
				42.0	80.0	68.0	120.8	0.6	17.3	
				32.0	80.0	68.5	145.6	0.6	23.2	
				22.0	80.0	71.1	140.6	0.6	26.5	
				16.0	80.0	78.0	103.5	0.3	60.1	
				11.0	86.6	80.4	124.0	0.2	94.3	
				48.0	80.0	68.0	71.7	0.6	6.94	
	42.0	80.0	68.0	70.5	0.6	6.37				
	32.0	80.0	68.0	83.7	0.6	9.54				
	22.0	80.0	68.0	100.5	0.6	13.81				
	16.0	80.0	78.0	61.5	0.3	23.76				
	11.0	80.0	78.0	75.9	0.3	36.15				
	Medium	15.0	0.2	16.0	80.0	78.0	61.5	0.3	23.76	2 mm Cu sheet
	11.0	80.0	78.0	75.9	0.3	36.15				

Mode	Submode/ Image quality	Pulse rate (pulses/s)	Automatic added filtration (mm Cu)	Field size (cm)	kV	mA	Added Filtratio n (mm Cu)	(Patient entrance surface air kerma) Copper filter entrance air kerma (mGy/min)	Patient entrance surface air kerma at 60 cm (including backscatter (1.3) (mGy/min)	Phantom
Fluorosc opy	Medium	10.0	0.2	48.0	84.3	0.6	4.22	68.0	5.5	2 mm Cu sheet
				42.0	82.2	0.6	4.21	68.0	5.5	
				32.0	97.1	0.6	6.17	68.0	8.0	
				22.0	115.7	0.6	8.85	68.0	11.5	
				16.0	146.3	0.6	19.96	70.7	25.9	
				11.0	89.9	0.3	25.22	78.0	32.8	
				48.0	99.2	0.6	3.62	68.0	4.7	
	Medium	7.5	0.2	42.0	96.2	0.6	3.41	68.0	6.6	2 mm Cu sheet
				32.0	121.5	0.6	5.09	68.0	9.0	
				22.0	148.6	0.6	6.95	68.0	15.5	
				16.0	93.5	0.3	11.92	78.0	24.2	
				11.0	124.6	0.3	18.62	78.0		

Mode	Submode/ Image quality	Pulse rate (pulses/s)	Automatic added filtration (mm Cu)	Field size (cm)	kV	mA	Added Filtratio n (mm Cu)	(Patient entrance surface air kerma) Copper filter entrance air kerma (mGy/min)	Patient entrance surface air kerma at 60 cm (including backscatter (1.3) (mGy/min)	Phantom
Fluorosc opy	Low	30.0	0.2	48.0	68.0	103.3	0.6	10.51	13.7	Phantom
				42.0	68.0	98.5	0.6	9.75	12.7	
				32.0	68.0	123.3	0.6	13.63	17.7	
				22.0	78.0	44.8	0.3	13.79	17.9	
				16.0	78.0	84.3	0.3	34.00	44.2	
				11.0	78.0	114.0	0.3	52.05	67.7	
	Low	15.0	0.2	48.0	68.0	61.8	0.6	5.01	6.5	2 mm Cu sheet
				42.0	68.0	95.7	0.6	4.06	5.3	
				32.0	68.0	71.7	0.6	6.81	8.9	
				22.0	68.0	84.9	0.6	9.61	12.5	
				16.0	70.8	105.0	0.6	19.80	25.7	
				11.0	78.0	65.2	0.3	25.89	33.7	

Mode	Submode/ Image quality	Pulse rate (pulses/s )	Automatic added filtration (mm Cu)	Field size (cm)	kV	mA	Added Filtratio n (mm Cu)	(Patient entrance surface air kerma) Copper filter entrance air kerma (mGy/min)	Patient entrance surface air kerma at 60 cm (including backscatter (1.3) (mGy/min)	Phantom
Fluorosc opy	Low	10.0	0.2	48.0	68.0	72.3	0.6	2.91	3.8	2 mm Cu sheet
				42.0	68.0	71.4	0.6	3.09	4.0	
				32.0	68.0	84.5	0.6	4.44	5.8	
				22.0	68.0	98.9	0.6	6.15	8.0	
				16.0	68.6	151.2	0.6	17.43	22.7	
				11.0	71.2	144.3	0.6	20.17	26.2	
				48.0	68.0	81.5	0.6	2.58	3.4	
	42.0	68.0	79.8	0.6	2.44	3.2	2 mm Cu sheet			
	32.0	68.0	99.1	0.6	3.53	4.6				
	22.0	68.0	121.9	0.6	5.04	6.6				
	16.0	78.0	77.8	0.3	8.70	11.3				
	11.0	78.0	100.7	0.3	13.23	17.2				

## DOSE ASSESSMENT (Plane B)

	Set	Measure	Error							
Focus –Intensifier distance (cm)	100	100	0%							
Patient dose measurement: Focus-Ionization chamber distance		60 cm								
Entrance II dose measurement: II-Ion Ionization chamber distance		40 cm								
Mode	Submode/ Image quality	Pulse rate (pulses/s)	Automatic added filtration (mm Cu)	Field size (cm)	kV	mA	Added Filtrati on (mm Cu)	(Patient entrance surface air kerma) Copper filter entrance air kerma (mGy/min)	Patient entrance surface air kerma at 60 cm (including backscatter (1.3) (mGy/min)	Phantom
Fluorosc opy	High	30.0	0.2	25.0	80.0	90.8	0.3	49.3	64.0	2 mm Cu sheet
				20.0	80.0	110.7	0.3	65.4	85.0	
				16.0	85.0	99.8	0.2	80.2	104.2	
				10.0	97.3	102.1	0.2	94.6	122.9	
				25.0	80.0	85.9	0.3	25.260	32.8	
	High	15.0	0.2	20.0	80.0	102.3	0.3	33.120	43.1	2 mm Cu sheet
				16.0	80.0	122.7	0.3	43.710	56.8	
				10.0	83.5	162.8	0.3	75.870	98.6	

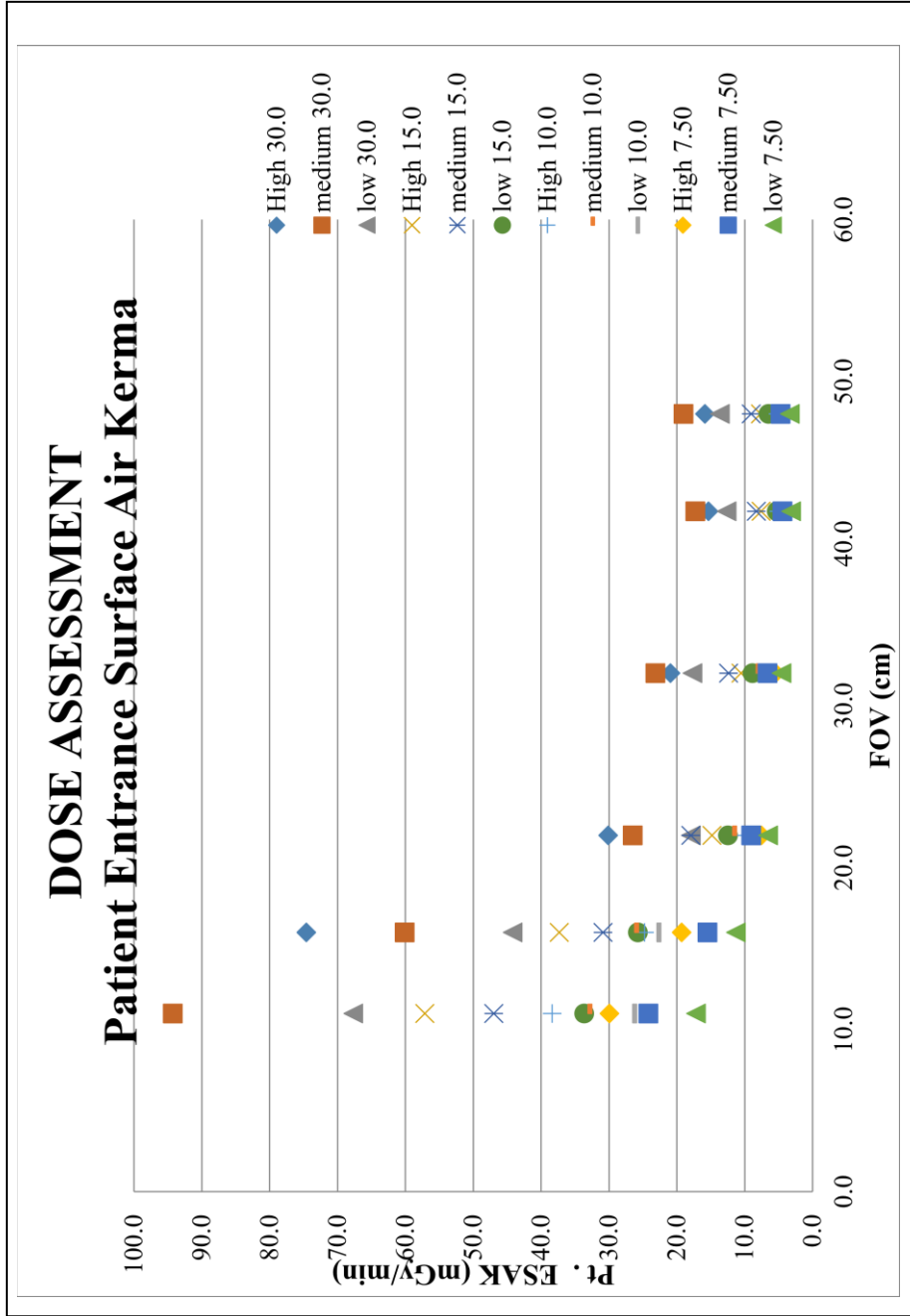
Mode	Submode/ Image quality	Pulse rate (pulses/s)	Automatic added filtration (mm Cu)	Field size (cm)	kV	mA	Added Filtrati on (mm Cu)	(Patient entrance surface air kerma) Copper filter entrance air kerma (mGy/min)	Patient entrance surface air kerma at 60 cm (including backscatter (1.3) (mGy/min)	Phantom
Fluorosc opy	High	10.0	0.2	25.0	80.0	91.2	0.3	17.2	22.3	2 mm Cu sheet
				20.0	80.0	107.2	0.3	22.5	29.3	
				16.0	80.0	127.4	0.3	30.0	39.0	
				10.0	85.0	137.1	0.2	57.6	74.9	
	High	7.5	0.2	25.0	80.0	86.7	0.3	7.5	9.8	2 mm Cu sheet
				20.0	80.0	103.5	0.3	17.0	22.2	
				16.0	80.0	124.7	0.3	22.8	29.6	
				10.0	85.0	155.2	0.2	44.7	58.1	



Mode	Submode/ Image quality	Pulse rate (pulses/s)	Automatic added filtration (mm Cu)	Field size (cm)	kV	mA	Added Filtration (mm Cu)	(Patient entrance surface air kerma) Copper filter entrance air kerma (mGy/min)	Patient entrance surface air kerma at 60 cm (including backscatter (1.3) (mGy/min)	Phantom
Fluoroscopy	Medium	30.0	0.2	25.0	78.0	84.4	0.3	39.7	51.7	Phantom
				20.0	78.0	101.4	0.3	51.9	67.5	
				16.0	78.0	123.9	0.3	69.0	89.8	
				10.0	89.0	111.1	0.2	91.9	119.5	
				25.0	71.1	105.7	0.6	23.5	30.6	
	Medium	15.0	0.2	20.0	78.0	60.7	0.3	26.0	33.9	2 mm Cu sheet
				16.0	78.0	69.3	0.3	34.7	45.1	
				10.0	78.8	95.1	0.3	71.2	92.5	

Mode	Submode/ Image quality	Pulse rate (pulses/s)	Automatic added filtration (mm Cu)	Field size (cm)	kV	mA	Added Filtrati on (mm Cu)	(Patient entrance surface air kerma) Copper filter entrance air kerma (mGy/min)	Patient entrance surface air kerma at 60 cm (including backscatter (1.3) (mGy/min)	Phanto m
Fluorosc opy	Medium	10.0	0.2	25.0	80.0	91.2	0.3	17.2	22.3	2 mm Cu sheet
				20.0	80.0	107.2	0.3	22.5	29.3	
				16.0	80.0	127.4	0.3	30.0	39.0	
				10.0	85.0	137.1	0.2	57.6	74.9	
				25.0	78.0	77.1	0.3	10.5	13.7	
	Medium	7.5	0.2	20.0	78.0	90.6	0.3	13.8	17.9	2 mm Cu sheet
				16.0	78.0	109.9	0.3	18.5	24.1	
				10.0	80.0	157.0	0.2	44.5	57.8	
				25.0	78.0	68.4	0.4	28.8	37.5	
				20.0	78.0	83.0	0.3	38.6	50.2	
Fluorosc opy	Low	30.0	0.2	16.0	78.0	100.5	0.3	51.1	66.4	2 mm Cu sheet
				10.0	83.7	118.3	0.2	91.6	26.7	
				25.0	69.1	10.9	0.6	20.5	30.1	
				20.0	70.9	106.2	0.6	23.0	32.7	
				16.0	78.0	59.8	0.3	25.1	71.2	
				10.0	78.0	85.1	0.3	54.7	26.7	

Mode	Submode/ Image quality	Pulse rate (pulses/s)	Automatic filtration (mm Cu)	Field size (cm)	kV	mA	Added Filtratio n (mm Cu)	(Patient entrance surface air kerma) Copper filter entrance air kerma (mGy/min)	Patient entrance surface air kerma at 60 cm (including backscatter (1.3) (mGy/min)	Phantom
Fluoroscop y	Low	10.0	0.2	25.0	68.0	137.7	0.6	15.3	19.9	2 mm Cu sheet
				20.0	68.8	151.9	0.6	19.5	25.4	
				16.0	70.2	149.2	0.6	21.6	28.0	
				10.0	78.0	100.5	0.3	36.9	47.9	
				25.0	78.0	63.1	0.3	7.7	10.0	
				20.0	78.0	75.5	0.3	10.1	13.1	
	Low	7.5	0.2	16.0	78.0	88.9	0.3	13.2	17.2	2 mm Cu sheet
				10.0	78.0	146.2	0.5	29.3	38.1	



**AUTOMATIC BRIGHTNESS CONTROL TEST (Plane A)**

Mode	Submode/ Image quality	Pulse rate (pulses/s)	Automatic added filtration (mm Cu)	Field size (cm)	Automatic added filtration (mm Cu)	kV	mA	Patient entrance surface air kerma (mGy/min)
Fluoroscopy	Medium	10.0	0.6	48.0	0.0	61.2	24.3	0.47
				42.0		58.0	51.3	0.47
				32.0		58.0	63.3	0.47
				22.0		58.0	79.7	0.59
				16.0		58.0	161.1	1.27
				11.0		60.0	165.4	1.90
Fluoroscopy	Medium	10.0	0.6	48.0	1.0	68.0	40.7	0.99
				42.0		58.7	167.9	1.56
				32.0		68.0	48.4	1.33
				22.0		68.0	57.3	1.9
				16.0		68.0	96.5	5.8
				11.0		68.0	119.1	9.1

**AUTOMATIC BRIGHTNESS CONTROL TEST (Plane A)**

Mode	Submode/ Image quality	Pulse rate (pulses/s)	Automatic added filtration (mm Cu)	Field size (cm)	Automatic added filtration (mm Cu)	kV	mA	Patient entrance surface air kerma (mGy/min)
Fluoroscopy	Medium	10.0	0.6	48.0	2.0	68.0	84.3	4.22
				42.0		68.0	82.2	4.21
				32.0		68.0	97.1	6.17
				22.0		68.0	115.7	8.85
				16.0		70.7	146.3	19.96
				11.0		78.0	89.9	25.22
Fluoroscopy	Medium	10.0	0.6	48.0	3.0	69.6	150.2	17.0
				42.0		68.2	152.4	17.7
				32.0		69.8	147.5	17.9
				22.0		78.0	76.7	25.3
				16.0		78.0	116.0	42.4
				11.0		80.0	125.9	66.3

**AUTOMATIC BRIGHTNESS CONTROL TEST (Plane A)**

Mode	Submode/ Image quality	Pulse rate (pulses/s)	Automatic added filtration (mm Cu)	Field size (cm)	Automatic added filtration (mm Cu)	kV	mA	Patient entrance surface air kerma (mGy/min)
Fluoroscopy	Medium	10.0	0.6	48.0	2.0	68.0	84.3	4.22
			0.9	42.0		68.0	82.2	4.21
			0.6	32.0		68.0	97.1	6.17
			0.6	22.0		68.0	115.7	8.85
			0.6	16.0		70.7	146.3	19.96
			0.6	11.0		78.0	89.9	25.22
Fluoroscopy	Medium	10.0	0.6	48.0	3.0	69.6	150.2	17.0
			0.3	42.0		68.2	152.4	17.7
			0.6	32.0		69.8	147.5	17.9
			0.3	22.0		78.0	76.7	25.3
			0.3	16.0		78.0	116.0	42.4
			0.2	11.0		80.0	125.9	66.3

**AUTOMATIC BRIGHTNESS CONTROL TEST (Plane B)**

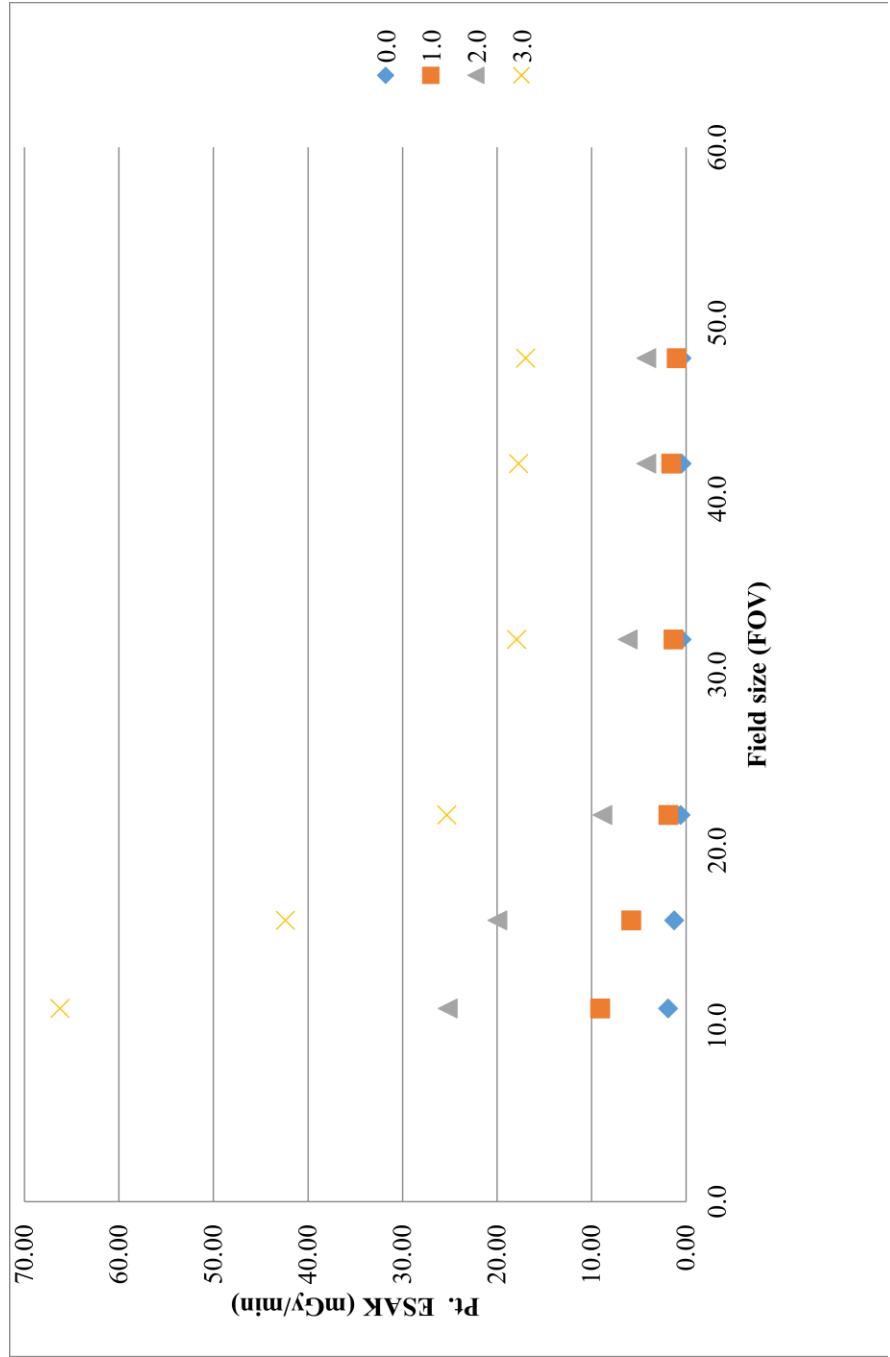
Mode	Submode/ Image quality	Pulse rate (pulse/s)	Automatic added filtration (mm Cu)	Field size (cm)	Automatic added filtration (mm Cu)	kV	mA	Patient entrance surface air kerma (mGy/min)
Fluoroscopy	Medium	10.0	0.6	25.0	0.0	68.0	39.7	1.172
			0.9	20.0		58.0	131.2	1.710
			0.9	16.0		58.0	156.0	2.355
			0.9	10.0		68.0	82.6	4.854
Fluoroscopy	Medium	10.0	0.6	25.0	1.0	68.0	83.4	5.195
			0.9	20.0		68.0	96.4	7.111
			0.6	16.0		68.0	113.0	9.793
			0.6	10.0		69.4	150.7	20.460



**AUTOMATIC BRIGHTNESS CONTROL TEST (Plane B)**

Mode	Submode/ Image quality	Pulse rate (pulse/s)	Automatic added filtration (mm Cu)	Field size (cm)	Automatic added filtration (mm Cu)	kV	mA	Patient entrance surface air kerma (mGy/min)
Fluoroscopy	Medium	10.0	0.6	25.0	2.0	69.0	151.5	19.9
				20.0		70.3	148.9	21.9
				16.0		78.0	82.0	23.5
				10.0		78.0	115.9	50.9
Fluoroscopy	Medium	10.0	0.6	25.0	3.0	78.0	98.9	35.630
				20.0		78.0	112.2	47.340
				16.0		78.0	127.1	61.240
				10.0		83.9	122.7	88.7

**AUTOMATIC BRIGHTNESS CONTROL TEST**



**MAXIMUM DOSE RATE ASSESSMENT**

SID 100 cm, 3.0 mmAl, Chamber to focus distance 47.5 cm

\*\*Measure dose rate for all modes and FOVs, dosimeter on the table and table at the lowest position Absorber: 2 mm of lead on the image intensifier (or equivalent attenuation with a folded lead apron)

**Plane A**

Mode	Submode/ Image quality	Field of view (cm)	Doserate (mGy/min)	Phantom
Fluoroscopy High	10.0 p/s	48.0	257.60	2 mmCu+ 2mm Pb
		42.0	257.50	
		32.0	255.50	
		22.0	255.70	
		16.0	251.70	
		11.0	248.50	
		8.0	119.60	
Fluoroscopy Medium	10.0 p/s	42.0	121.50	
		32.0	125.20	
		22.0	125.10	
		16.0	123.20	
		11.0	121.50	

**Plane B**

Mode	Submode/ Image quality	Field of view (cm)	Doserate (mGy/min)	Phantom
Fluoroscopy High	10.0 p/s	25.0	294.40	2 mmCu+ 2mm Pb
		20.0	293.00	
		16.0	296.90	
		10.0	295.50	
Fluoroscopy Medium	10.0 p/s	25.0	145.80	
		20.0	139.40	
		16.0	139.30	
		10.0	138.10	

**Plane A**

<b>Mode</b>	<b>Submode/ Image quality</b>	<b>Field of view (cm)</b>	<b>Doserate (mGy/min)</b>	<b>Phantom</b>
Fluoroscopy Low	10.0 p/s	48.0	62.81	2 mmCu+ 2mm Pb
		42.0	62.59	
		32.0	62.65	
		22.0	62.67	
		16.0	61.70	
		11.0	60.86	

**Plane B**

<b>Mode</b>	<b>Submode/ Image quality</b>	<b>Field of view (cm)</b>	<b>Doserate (mGy/min)</b>	<b>Phantom</b>
Fluoroscopy Low	10.0 p/s	25.0	73.21	2 mmCu+ 2mm Pb
		20.0	74.77	
		16.0	74.25	
		10.0	73.88	

**TABLE ATTENUATION**

Mode	Submode/ Image quality	Doserate ( $\mu\text{Gy}/\text{min}$ )	Table attenuation (%)	Absorber
C-arm at $0^\circ$	Medium	8.277	3.1	2mm Cu
C-arm at $90^\circ$	Medium	8.541		

**Note:** Measurement of doserate in fluoro for the same mode and field size

**HALF VALUE LAYER ASSESSMENT**

Al attenuator (mm)	Submode / Image quality	Doserate (mGy/min)	HVL (mm)
0.0	Medium mode 80 kVp FOV 48 cm 60 cm STD	5.901	6.32
1.0		5.100	
2.0		4.820	
3.0		4.370	
4.0		4.017	
5.0		3.650	
6.0		3.087	
7.0		2.886	

**Note:** Make measurement in fluoroscopic mode; add attenuator (copper sheets) on I.I. to drive kV to 80 kV

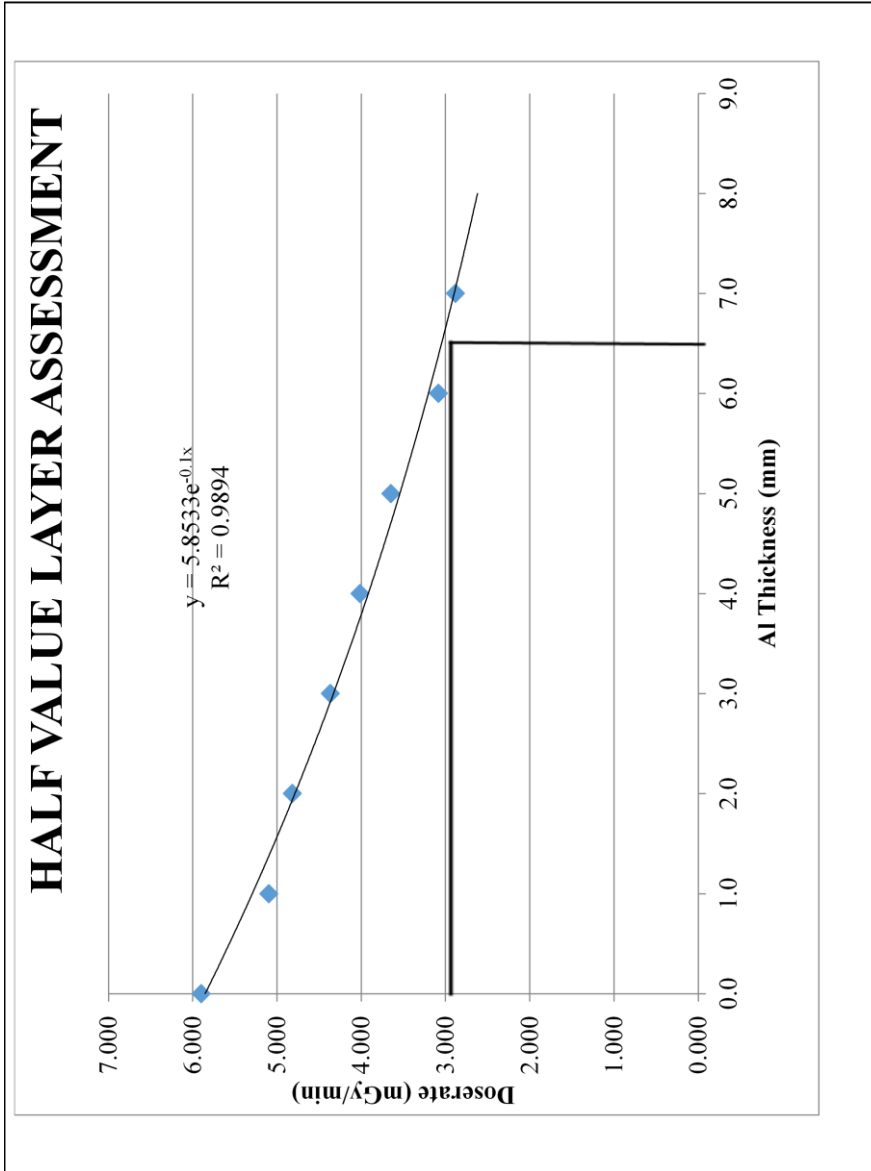


### IMAGE QUALITY ASSESSMENT

Resolution should be assessed in the usual illumination conditions and from the operator's position. Leeds Test placed on Image-Intensifier detector entrance surface with grid. All modes (fluoroscopy and image acquisition) and image qualities and FOVs.

Focus-Image Intensifier distance 100 cm, TO 10 phantoms.

#### Plane A

Mode	Submode/ Image quality	Focus (S/L)	Automatic added filtration (mm Cu)	Field size (cm)	kV	mA	Live image			
							No. of groups	High contrast resolution (lp/mm)	No. of disc	Low contrast (%/contrast)
Fluoroscopy High	10.0 p/s	Large					6	0.9	3	12.80
							7	1.0	4	10.90
							8	1.12	4	10.90
							8	1.12	4	10.90
							8	1.12	4	10.90
							8	1.12	4	10.90

## Plane A

Mode	Submode/ Image quality	Focus (S/L)	Automatic added filtration (mm Cu)	Field size (cm)	kV	mA	Live image			
							No. of groups	High contrast resolution (lp/mm)	No. of disc	Low contrast (%contrast)
Fluoroscopy Medium	10.0 p/s	Large	0.6	48.0	68.0	60.3	5	0.8	3	12.80
							5	0.8	3	12.80
							6	0.9	3	12.80
							6	0.9	4	10.90
							7	1.0	4	10.90
							7	1.0	4	10.90



Plane A

Mode	Submode/ Image quality	Focus (S/L)	Automatic added filtration (mm Cu)	Field size (cm)	kV	mA	Live image											
							No. of groups	High contrast resolution (lp/mm)	No. of disc	Low contrast %contrast								
Fluoroscopy Low	10.0 p/s	Large	0.6	48.0	68.0	53.9	4	0.71	3	12.80								
											0.6	42.0	68.0	53.3	4	0.71	3	12.80
											0.6	32.0	68.0	60.7	5	0.8	3	12.80
											0.6	22.0	68.0	71.4	5	0.8	3	12.80
											0.6	16.0	68.0	82.8	5	0.8	3	12.80
											0.6	11.0	68.0	98.6	6	0.9	4	10.90
Single shot 4 f/s	4 f/s	Large	0.6	48.0	70.0	8.6	6	0.9	6	7.50								
											0.6	42.0	70.0	8.7	7	1.0	8	4.50
											0.6	32.0	70.0	12.4	8	1.12	8	4.50
											0.6	22.0	70.4	1.6	9	1.25	8	4.50
											0.6	16.0	70.0	25.4	11	1.6	8	4.50
											0.6	11.0	70.1	36.2	14	2.24	8	4.50

### IMAGE QUALITY ASSESSMENT

Resolution should be assessed in the usual illumination conditions and from the operator's position. Leads Test placed on Image-Intensifier detector entrance surface with grid. All modes (fluoroscopy and image acquisition) and image qualities and FOVs.

Focus-Image Intensifier distance 100 cm, TO 10 phantoms.

#### Plane B

Mode	Submode/ Image quality	Focus (S/L)	Automatic added filtration (mm Cu)	Field size (cm)	kV	mA	Live image			
							No. of groups	High contrast resolution (lp/mm)	No. of disc	Low contrast (%contrast)
Fluoroscopy High	10.0 p/s	Large	0.3	25.0	80.0	40.7	0.8	3	12.80	0.8
							0.8	3	12.80	0.8
							0.8	3	12.80	0.8
							0.9	4	10.90	0.9

Plane B

Mode	Submode/ Image quality	Focus (S/L)	Automatic added filtration (mm Cu)	Field size (cm)	kV	mA	Live image			
							No. of groups	High contrast resolution (lp/mm)	No. of disc	Low contrast (%contrast)
Fluoroscopy Medium	10.0 p/s	Large	0.6	25.0	68.0	79.4	8	1.12	8	4.50
							9	1.25	8	4.50
							11	1.6	8	4.50
							14	2.24	8	4.50

Plane B

Mode	Submode/ Image quality	Focus (S/L)	Automatic added filtration (mm Cu)	Field size (cm)	kV	mA	Live image			
							No. of groups	High contrast resolution (lp/mm)	No. of disc	Low contrast (%contrast)
Fluoroscopy Low	10.0 p/s	Large	0.3	25.0	68.0	68.2	5	0.8	3	12.80
							5	0.8	3	12.80
							5	0.8	3	12.80
							6	0.9	4	10.90
Single shot 4f/s	4f/s	Large	0.6	25.0	68.0	60.3	8	1.12	8	4.50
							9	1.25	8	4.50
							11	1.6	8	4.50
							14	2.24	8	4.50

**VITA**

Name: Mr. Yutthana Netwong

Sex: Male

Nationality: Thai

Date of birth: July 13, 1982

Place of birth: Phayao, Thailand

Home Address: 99/102, Athichetthani village, Chiang Rak Yai sub-district, Sam Kok district, Pathumthani province, Thailand 12160

Qualification: Bachelor of Science (Radiological Technology), Naresuan University, 2005

Work experiences: 2005 - 2006: Radiologic technologist of Department of Radiotherapy, Lopburi cancer center, Lopburi 2006 – Present: Radiologic technologist of Department of Neuroradiology, Prasat Neurological Institute

E-mail Address: yutthana\_net@hotmail.com

